UNIVERSITY OF LIVERPOOL

High Efficiency Antenna Designs for Wearable Applications

Thesis submitted in accordance with the requirements of the

University of Liverpool

for the degree of Doctor in Philosophy

by

Rui Pei

March 2021

I would like to dedicate this thesis to my parents and my girlfriend.

Declaration

I hereby declare that except where specific reference is made to the work of others, the contents of this dissertation are original and have not been submitted in whole or in part for consideration for any other degree or qualification in this, or any other University. This dissertation is the result of my own work and includes nothing which is the outcome of work done in collaboration, except where specifically indicated in the text.

Rui Pei

Abstract

Wearable antennas have attracted more attention due to the increasing popularity of wearable electronics over the last decade. These antennas situated on the human body, in the clothing or on daily accessories help form the wireless channel required in a Wireless Body Area Networks (WBAN). The wearable antennas designs face a series of challenges due to its working environment. Frequency shifting, efficiency degradation and radiation distortion will be induced by the human body tissue. More importantly, a level of radiation shielding into the body should be provided to meet the Specific Absorption Rate (SAR) requirement.

In this study, the aim is to design a type of antennas which are suitable for on-body applications over a long period of time. The proposed antennas should have the following properties: (1) being conformal and ergonomic to avoid any discomfort; (2) minimizing the radiation into the human body for safety concerns and also ensuring a high on-body radiation efficiency; (3) utilizing reasonable materials and manufacturing process to limit the overall cost and maintaining a certain level of robustness. To achieve these properties, the belt buckle was chosen to be the platform for the proposed antenna designs. The belt buckle, with rigid metallic nature, enabled the designs to be efficient and robust.

In this thesis, two types of novel belt antennas will be presented. The first one, based on a pin-buckle type design and the second one is based on a single tongue buckle. An in-house reverberation chamber is designed and installed to accurately measure the on-body radiation efficiency of the proposed antennas. Textile electromagnetic bandgap materials are studied and applied with the second belt antenna, to raise the on-body radiation efficiency of the antenna from around 40% to a level over 70%.

Key Words: wearable antennas, Artificial magnetic conductor (AMC), belt antenna, characteristic mode analysis (CMA), electromagnetic band gap (EBG) materials, metamaterial, specific absorption rate (SAR), reverberation chamber.

Acknowledgements

Thinking back of the past four years of my PhD life, I could not have come through without the guidance and support from all the great people around me. First and most importantly, I would like to give my most sincere gratitude to my primary supervisor, Dr. Mark Leach. He has been an incredible mentor to me, in terms of both academic study and attitude towards life. It is him who inspired me to start my career as a lecturer in a University. Dr. Mark Leach has always managed to deliver well-designed, substantial contents in a casual atmosphere. It has magical effects among the undergraduates in his class, and also, it helped me well throughout my PhD study.

Secondly, I would like to thank Prof. Yi Huang. Prof. Huang provided me with the direction of my study when I felt confused and lost in Liverpool. The group meetings and one-to-one discussions were encouraging and enlightening. My life in Liverpool high frequency group was productive and enjoyable.

I would also like to give my sincere appreciation to Prof. Eng Gee lim and Dr. Zhao Wang. As a tightly connected group, they have provided my with valuable guidance in research, academic writing and also support regarding to the equipment.

I would also like to thank Dr. Jiafeng Zhou for his valuable insights in both group meetings and my annual reviews.

I would like to give special thanks to Dr. Jingchen Wang, Dr. Chaoyun Song and Dr. Qian Xu. They have provided me with countless valuable advice. I am really lucky to meet predecessors as them. Dr. Qian Xu has offered tremendous help with the designing and the building of the reverberation chamber. The testing of the on-body antenna efficiency would not be possible without him.

I would like to thank all my friends from EE414, Room 220 and EE511. All these friends made my PhD journey enjoyable.

I would like to save special thanks to my parents. They have offered tremendous

support to me during my study.

Last, but not least, the department of Electrical Engineering and Electronics of the University of Liverpool and the department of Electrical and Electronic Engineering of Xi'an Jiaotong-Liverpool University are gratefully acknowledged for their support.

Publications

Journal Publications

[1] **R. Pei**, M. P. Leach, E. G. Lim, Z. Wang, C. Song, J. Wang, W. Zhang, Z. Jiang and Y. Huang, "Wearable EBG-Backed Belt Antenna for Smart On-Body Applications," *IEEE Transactions on Industrial Informatics*, vol. 16, no. 11, pp. 7177-7189, 2020.

[2] **R. Pei**, M. P. Leach, E. G. Lim, Z. Wang, J. Wang, Y. Wang, Z. Jiang and Y. Huang, "Wearable Belt Antenna for Body Communication Networks," *IEEE Antennas and Wireless Propagation Letters*, pp. 1-1, 2020.

[3] C. Song, E. L. Bennett, J. Xiao, T. Jia, **R. Pei**, K. Luk, and Y. Huang, "Passive Beam-Steering Gravitational Liquid Antennas" *IEEE Transactions on Antennas and Propagation*, vol. 68, no. 4, pp. 3207-3212, 2020.

[4] Z. Jiang, Z. Wang, M. Leach, E. G. Lim, H. Zhang, **R. Pei**, and Y. Huang, "Symbol-Splitting-Based Simultaneous Wireless Information and Power Transfer System for WPAN Applications," *IEEE Microwave and Wireless Components Letters*, vol. 30, no. 7, pp. 713-716, 2020.

[5] W. Zhang, C. Song, **R. Pei**, Y. Huang, and J. Zhou, "Broadband Metasurface Antenna Using Hexagonal Loop-Shaped Unit Cells," *IEEE Access*, vol. 8, pp. 223797-223805, 2020.

[6] J. Wang, M. P. Leach, E. G. Lim, Z. Wang, Z. Jiang, **R. Pei**, and Y. Huang, "A Conformal Split-ring Loop as a Self-resonator for Wireless Power Transfer," *IEEE Access*, pp. 1-1, 2019.

[7] Z. Jiang, Z. Wang, M. Leach, Y. Huang, E. G. Lim, J. Wang, and **R. Pei**, "Wideband Loop Antenna with Split-Ring Resonators for Wireless Medical Telemetry," *IEEE Antennas and Wireless Propagation Letters,* vol. 18, no. 7,

pp. 1415-1419, 2019.

[8] J. Wang, M. Leach, E. G. Lim, Z. Wang, **R. Pei**, and Y. Huang, "An Implantable and Conformal Antenna for Wireless Capsule Endoscopy," *IEEE Antennas and Wireless Propagation Letters*, vol. 17, no. 7, pp. 1153-1157, 2018.

Conference Publications

[1] **R. Pei**, M. Leach, E. G. Lim, Z. Wang, J. Wang, and Y. Huang, "A Belt Antenna Design with Textile Aritificial Magnetic Conductor Reflector," *in 2019 IEEE MTT-S International Wireless Symposium (IWS)*, 2019, pp. 1-3.

[2] **R. Pei**, J. Wang, M. Leach, Z. Wang, S. Lee, and E. G. Lim, "Wearable antenna design for bioinformation," *in 2016 IEEE Conference on Computational Intelligence in Bioinformatics and Computational Biology (CIBCB)*, 5-7 Oct. 2016, pp. 1-4.

[3] J. Wang, E. G. Lim, M. Leach, Z. Wang, **R. Pei**, and Z. Jiang, "Design of an Implantable Antenna for Wireless Communication of Ingestible Capsule Endoscope," in *2019 International Symposium on Antennas and Propagation (ISAP)*, 2019, pp. 1-3.

Contents

List of Abbreviations

ABS	Acrylonitrile Butadiene Styrene
AUT	Antenna Under Test
EBG	Electromagnetic Band Gap
EM	Electromagnetic
EMC	Electromagnetic Compatibility
FU	Field Uniformity
HIS	High Impedance Surface
IEC	International Electrotechnical Commission
IEEE	Institute of Electrical and Electronics Engineers
ISM	Industrial Scientific Medical
LUF	Lowest Usable Frequency
PCB	Printed Circuit Board
PDMS	Polydimethylsiloxane
PEC	Perfect Electric Conductor
PRS	Partial Reflective Surface
REF	Reference
RF	Radio Frequency
Rx	Receiving
SAR	Specific Absorption Rate

TL	Transmission Line
Tx	Transmitting
UHF	Ultra High Frequency
UoL	The University of Liverpool
VNA	Vector Network Analyzer
WBAN	Wireless Body Area Network
XJTLU	Xi'an jiaotong-Liverpool University

List of Figures

List of Tables

Chapter 1 Introduction

This thesis presents a study on high-efficiency wearable antenna designs, starting from the conception and justification of the research, through background investigation and theoretical development, to design, manufacture, test and evaluation of the novel ideas and processes cultivated. In this chapter, an introduction to the development of wireless communications and antennas is provided. In specific, wearable antenna designs are highlighted because the challenges of designing wearable antennas with high on-body radiation efficiency lead to the motivation of this project. The detailed research focus and objectives are further discussed and a brief overview of this thesis is provided at the end of this chapter.

1.1 Background

In 1864 a set of equations, which later became known as Maxwell's Equations, were summarised and established by James Clark Maxwell [1]. These equations characterised the properties of electromagnetic waves and laid the foundations for wireless communications. For years, scientists and engineers have devoted themselves to the development of communication systems without physical wires radically changing the way in which the world functions and operates for the betterment of humankind. This journey began in 1886 when German physicist Heinrich Hertz proved the existence of the electromagnetic waves predicted by Maxwell's Equations with an experiment involving two resonating metal rings [2]. These rings can be considered the world's first loop antennas.

Antennas are essential components of all wireless communications systems. They are responsible for converting guided waves on transmission lines into freely propagating electromagnetic waves. Various types of antenna have been designed to

meet the specific or desirable requirements of a communication system, e.g., band of radiation, size, shape, ability to direct energy and efficiency. In 1901, electrical dipole antennas were developed and used to conduct the first wireless communications across the ocean [3]. Yagi-Uda antennas were invented in 1926 and were later widely applied in television broadcasting and shortwave communication [4]. Modern horn antennas were invented in 1938, and their properties made them suitable for point-to-point communications and as feeds for radar antennas and satellite dishes [4]. The popularisation of printed circuit board (PCB) technology in the 1960's gave rise to the development of low-profile planar antennas such as the microstrip patch [5]. These so-called patch antennas consist of a metallic patch as top layer, a dielectric substrate layer and a metallic ground plane as bottom layer. They could be directly integrated with printed circuits and it was relatively easy to manufacture these with different shapes and properties, so that antennas could be rapidly designed to meet specific system requirements. Examples of the aforementioned antennas are shown in Figure 1-1.

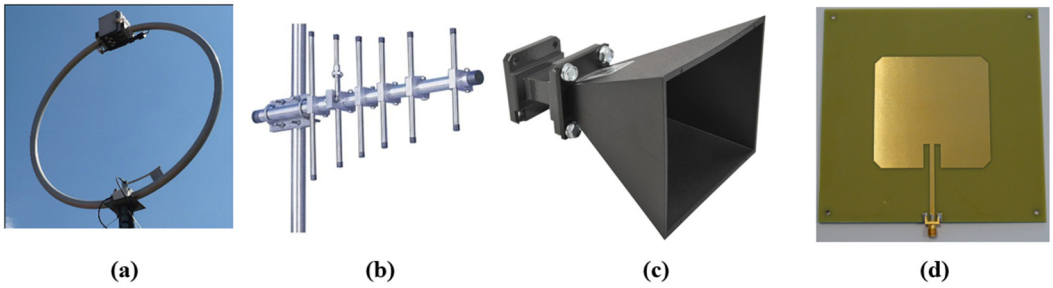

Figure 1-1：Examples of different antenna types: (a) Loop antenna. (b) Yagi-Uda antenna. (c) Horn antenna. (d) Microstrip patch antenna [6]-[9].

Recently there has been a boom in the use of wirelessly connected wearable electronics, which has led to the need for antennas to be designed to work in a body-centric environment. Such antennas that are specifically designed to function well in a complicated near-body environment are referred to by the general terminology wearable antennas. Generally speaking, wearable antennas are antennas designed to operate while being worn. Examples of wearable antennas can be seen in smartwatches, wristbands, glasses (Google Glass) and motion cameras (GoPro). These devices usually operate via Wi-Fi or Bluetooth at 2.45 GHz and 5.8 GHz. The close presence of the

human body to the antenna in such devices results in a number of special design challenges for wearable antenna designers, including, user safety, overcoming efficiency obstacles and maintaining desirable radiating characteristics whilst being ergonomic and fit for purpose.

1.2 Research Motivation

For modern wearable applications, ergonomic design requirements limit the shape and size of antenna designs. The typically limited battery capacity in wearable electronic devices brings about the need for an energy-efficient wireless communication link that reduces power consumption. For antenna engineers, this means designing an antenna with high radiation efficiency, which radiates into an appropriate half-space and that is conformal to the wearable accessory is desired.

To develop such an antenna suitable for wearable applications, the following factors and issues are taken into consideration:

1. Material selection – The material properties are imperative to the performance of an antenna. Metal would be an ideal choice for the resonating element as this should be a low loss, highly conductive material, but the shape and size of accessories to accommodate metallic antennas are quite limited. Other deformable materials commonly seen on daily clothing have issues regarding conductivity, dielectric loss and robustness. The analysis and selection of the material is a crucial factor for the antenna design to meet the efficiency target.

2. Antenna structure design – The structural design of wearable antennas requires special consideration. For metallic structures, the shape and size should be similar to those of daily accessories so that they can be situated in everyday life without causing discomfort and inconvenience. For designs based on deformable materials like conductive fibres, the effect of bending, crumpling and other deformations must be taken into consideration in the design process to ensure stable performance.

3. Safety issues – The radio frequency waves utilised in the common types of modern communication systems found in wearable applications are classified as forms of non-ionizing radiation making them relatively safe for use close to the human body. However, there are still safety regulations imposed, designed to prevent hazardous heating of body tissues. Specific Absorption Rate (SAR), is used to quantify the heating of body tissues due to radio frequency waves and has a unit in Watts per Kilogram (W/Kg). The International Commission on Non-Ionizing Radiation Protection (ICNIRP) requires a maximal SAR value of 2 W/kg averaged over every 10 g of tissue [10]. This standard is widely applied in the EU and China. In the United States, the Federal Communications Commission (FCC) restricts SAR over 1 g of tissue to below 1.6 Watts per Kilogram [11]. Wearable devices by their nature pose potential SAR risks, particularly due to the locality of the antenna to the human body and so antenna designs which limit the radiation directed into the human body are preferrable. It will be seen later that this can be challenging for planar antennas.

4. Measurement of the on/off-body efficiency – To accurately measure the on-body radiation efficiency of an antenna is a challenging task. Since many of the materials used for wearable applications tend to be lossy and non-uniform as they are integrated with items worn by the user on a daily basis e.g. textile. The ability to measure the radiation efficiency of the antenna can help determine the quality and consistency of the dielectric material used and the quality of the fabrication. Moreover, the ability to measure the on-body radiation efficiency with an actual human test subject provides a reliable validation of the proposed design. Determination of methods for practically achieving such measurements is an important challenge to be addressed.

1.3 Aims and Objectives

The main aim of this study is to propose wearable antenna designs with high on-body radiation efficiency. This main target can be divided into the following objectives, which also illustrates the research focus at different stages of this PhD study.

1. To explore the possibility of designing high-efficiency antennas based on daily clothing accessories. The challenge here lies in two aspects: first, to determine the properties of the materials to be used in the antenna design and evaluate material losses; second is to obtain enough isolation to the human body so that the antenna can maintain relatively high on-body radiation efficiency when applied on the human body.

2. Design and construct a reverberation chamber along with a measurement methodology which can be used to measure the on-body radiation efficiency of the wearable antenna designs created. This will allow the effectiveness of the antenna designs to be physically evaluated and provide a general set of guidelines on the method required for such measurements.

3. To explore the possibility of providing sufficient shielding between the wearable antenna and the body through the application of conductive textile materials to significantly improve device performance and reduce SAR. The selection of the material, the effect of bending and overall performance evaluation are key factors in determining performance improvement.

1.4 Overview of the Thesis

It is found in this research that using metallic and rigid structures to comprise the radiating element of a wearable antenna to the fullest extent is critical to ensuring stable and high efficiency radiating properties for wearable antennas. The metallic belt buckle structure is chosen as the platform for the proposed wearable belt antenna designs in

this study. The designed belt buckle antennas are targeted for use in the industrial, scientific and medical (ISM) band (at 2.45 GHz and 5.8 GHz) as components in Wi-Fi and Bluetooth applications. The concept of the smart belt is also proposed, along with a prototype.

This thesis contains seven chapters covering basics on antennas, a review on wearable antennas, background on reverberation chambers and relevant details relating to the design, construction and commissioning a reverb for this work, characteristic mode analysis, electromagnetic band gap materials, and most importantly, two wearable belt antenna designs.

In detail, this thesis is organised as follows:

In chapter 1, an introduction to the project is provided. Information on wireless communications and antennas is discussed and the motivations for this research are presented together with the thesis aims and objectives.

In chapter 2, a general review of the research area, wearable antennas, is provided. The review classifies wearable antennas into two types: textile-based antennas and accessory-like antennas. Example antennas from both categories are studied and the advantages and challenges for each antenna type are discussed in this section.

In chapter 3, an overview of the reverberation chamber and the design and commissioning of the in-house reverberation chamber used in this study is presented. The measurements in the reverberation chamber with a human test subject are key for this study.

Chapter 4 presents the first proposed belt buckle antenna design. This belt buckle antenna design has a similar structure to a patch antenna and follows the quasi-TM_{30} mode. Despite not using the commonly applied low-loss dielectric materials designed for RF applications, the antenna is able to achieve a higher on-body radiation efficiency and realised gain than reported in other studies. The effect of different voxel human body models is also studied.

In chapter 5, a second belt buckle antenna, based on a loop design, is developed with the aid of characteristic mode analysis (CMA). The antenna is analysed with various voxel human body models and shows significant advantages for use in wearable applications over existing designs.

In chapter 6, a textile-based electromagnetic band gap ground plane is proposed for application together with the belt buckle antenna. The ground plane, when applied closely with the antenna, can increase the radiation efficiency and the realised gain of the antenna. Also, the isolation provided by the ground plane brings a significant drop in SAR value. The presented designs can all be considered safe under the regulations stated in [10] and [11]. A prototype of a smart belt system is proposed for proof of concept in this chapter and sample functions have been achieved.

Chapter 7 is the final chapter in which conclusions are drawn and the key contributions summarised. Some promising future directions are also discussed in this section.

1.5 References

[1] J. C. Maxwell, “A dynamical theory of the electromagnetic field”, Philosophical Transactions, Volume 155, Dec 1865.

[2] H. R. Hertz, “Ueber einen Einfluss des ultravioletten Lichtes auf die electrische Entladung”, Annalen der Physik, 1887.

[3] G. C. Corazza, "Marconi's history [radiocommunication]," *Proceedings of the IEEE*, vol. 86, no. 7, pp. 1307-1311, 1998.

[4] Y. Huang and K. Boyle, *Antennas: from theory to practice*. John Wiley & Sons, 2008.

[5] Balanis, C. A., *Antenna Theory: Analysis and Design Third Edition*, WILEY-INIERSCIENCE, 2005.

[6] Trixt. *A shortwave loop antenna*. Available: https://simple.wikipedia.org/wiki/Loop_antenna#/media/File:Loop_antenna.jpg

[7] T. T. Solutions. (2013). *Yagi Antenna*. Available: Available: https://www.indiamart.com /proddetail/yagi-antenna-18692155788.html

[8] Festo. (2015). *Horn Antenna, Large Aperture, Model 9550*. Available: https://www.labvolt.com/solutions/9_telecommunications/60_955000_horn_antenna_large_aperture

[9] Saturn. PCB. (2021). *915MHz Patch Antenna*. Available: https://saturnpcb.com

/pa915/

[10] International Commission on Non-Ionizing Radiation Protection, "Guidelines for limiting exposure to time-varying electric, magnetic, and electromagnetic fields (up to 300 GHz)," *Health Phys.*, vol. 74, pp. 494–522, Apr. 1998.

[11] Federal Communications Commission, "Specific absorption rate (SAR) for cellular telephones," 2016. [Online]. Available: https://www.fcc.gov/general/specific-absorption-rate-sar-cellular-telephones.

Chapter 2 Wearable Antennas

This chapter provides a review of wearable antennas, including some related antennas theory, historical discussion on the development of wearable antennas and some cutting-edge design concepts. Discussions are made with a focus on the design challenges addressed during this study.

2.1 Antenna Theory

A number of parameters are used to describe the performance of an antenna. Some of these parameters: *S*-parameters, radiation pattern and radiation efficiency, will be discussed briefly with special consideration in regards to wearable antenna designs.

Scattering parameters, commonly referred to as *S*-parameters in RF engineering, describe the reflection and transmission relationships between incident waves and reflected or transmitted waves from a network. For an RF signal incident at one port of a multi-port system, a portion of the signal gets reflected from the incident port, while the remainder gets transmitted to, or 'scatters' to, some or all the other ports. *S*-parameters quantify this process. *S*-parameters are normally analysed over a frequency range. For antenna measurements, a two-port network model is commonly used. Port 1 in the system denotes the feed port of the antenna under test (AUT) and S_{11} represents the ratio of the voltage reflected at that port (2-1),

$$S_{11}=\frac{V_{reflected\ at\ port\ 1}}{V_{toward\ port\ 1}}=\frac{Z_{input}-Z_0}{Z_{input}+Z_0} \tag{2-1}$$

V=voltage, Z_{input} *=input impedance*, Z_0*=characteristic impedance.*

The parameter S_{11} is used in evaluating the impedance matching between the antenna and its feeding network. In practice, the ratio of the voltage reflected from the

antenna feed to the incident voltage is a major concern as this represents power being reflected and hence lost in the system. Reflected power results in low power efficiency and can cause problems to the feeding circuit. S_{11} is often represented in dB (2-2),

$$S_{11}(dB) = 10 \log S_{11}^{2} = 20 \log S_{11} \quad (2\text{-}2)$$

This coincides with the data provided by the main simulation software package used throughout this work, CST Microwave Studio, and is also common practice in the research community and industry.

For a typical antenna, the frequency range with S_{11} of lower than -10 dB (indicating power lost to reflection of less than 10%) is considered as the usable bandwidth. This bandwidth is sometimes referred to as the impedance bandwidth, as it evaluates the impedance match of the antenna and the feeding network. An example of the simulated return loss for a microstrip patch antenna (S_{11} in dB) is provided in Figure 2-1

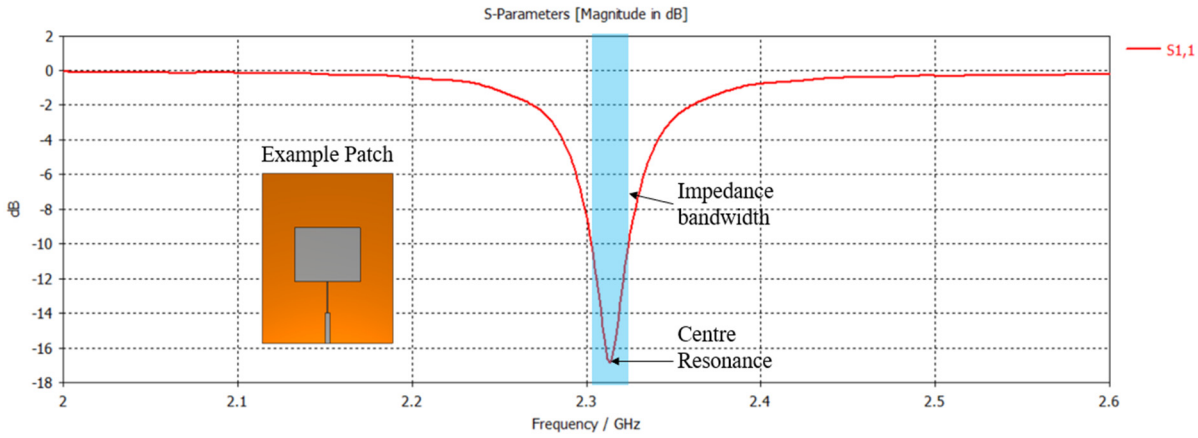

Figure 2-1：S_{11}-parameter of a microstrip patch antenna.

The impedance bandwidth for an S_{11} of less than -10 dB is labelled blue in Figure 2-1. The situation is considered differently when an antenna is applied in close proximity to the human body. Human body tissues are generally quite lossy in the frequency band ranging from 10 Hz to 10 GHz and therefore a large portion of power radiated close to the human body will be absorbed by the body tissues. The dielectric properties of the body tissue have a significant impact on antenna performance. These

properties are normally frequency dependant. As an example, the pertinent properties of muscle and blood over the frequency range from 2 GHz to 10 GHz are provided in Table 2-1, which shows that the relative permittivity of these two tissue types ranges between 40 and 60. This relatively large permittivity could cause a frequency shift to an antenna in close proximity. It can also be seen that at RF frequencies, the dielectric loss tends to increase with frequency while relative permittivity tends to decrease. The body tissues are very lossy when compared to other materials dedicated for circuits and RF applications (e.g., FR-4 with a loss tangent of 0.017 to 0.025, which is already considered lossy for some RF applications).

Table 2-1: Dielectric properties for body tissues (from IFAC-CNR) [1]

Frequency (GHz)	Relativity Permitivity		Loss tangent	
Tissue Type	Blood	Muscle	Blood	Muscle
2	59.022	53.290	0.33290	0.24520
4	55.677	50.821	0.33364	0.26665
6	52.184	48.217	0.39010	0.32321
8	48.610	45.497	0.45628	0.38511
10	45.109	42.764	0.52326	0.44666

When an antenna is analysed along with the human body (either using a voxel human model in simulation software or testing including human presence), a significant drop in S_{11} could be seen. This drop would be even more significant if the antenna were implanted into the body rather than worn close to or stuck on the body surface. The reduction in S_{11} would cover a wide frequency range hence a wider impedance bandwidth would be apparent. The wearable designs in this work focus on the band ranging from 2 GHz to 6 GHz. At this target band, the relative permittivity and loss tangent of blood and muscle are much higher than the substrate material used for antenna design. These body tissues will introduce significant frequency shifting and efficiency degrading to antennas in close proximity. The increased impedance bandwidth does not necessarily mean a wider useful bandwidth therefore other parameters, including the gain and radiation efficiency, become more important when analysing the performance of the antenna.

Antenna gain is a measure of how well an antenna transmits (or receives) electromagnetic energy in a given direction. The antenna gain is usually measured with the unit dBi, referring to ratio of the power radiated by the antenna to the power that would be radiated by an ideal isotropic antenna. An isotropic antenna is a hypothetical antenna that radiates the same amount of energy in all directions. The dBi unit is used throughout this thesis in the analysis of antenna designs.

Gain measurements in this work are performed using a gain-comparison method. This requires the use of a standard gain antenna as a reference. The two most-widely used reference antenna types are the half-wavelength dipole and the pyramidal horn. In this thesis, measurements of antenna gain are performed inside an in-house anechoic chamber with a set of standard gain horn antennas. Two sets of measurements are performed for each antenna gain measurement. For the first part, the antenna under test was paired with a standard gain horn antenna and viewed as a receiving terminal. A single-axis rotary table located in the anechoic chamber enables one-dimensional 360° cuts to be measured. The largest received power is recorded and denoted as P_1. Then the AUT is replaced with another standard gain horn antenna and the horns are aligned along the direction of their maximal gain. A measurement with the same input power level is then performed and the received power is denoted as P_2.

The calculation process then follows the equation,

$$G_{AUT} = G_{ref} + 10 \log_{10} \frac{P_1}{P_2} \tag{2-3}$$

G_{AUT}=gain of the antenna under test, G_{ref}= gain of the reference antenna, P_1=received power from the first measurement; P_2=received power from the second measurement.

It should also be noted that the term realised gain is commonly used. This term specifically refers to the gain value when all losses (mismatch loss, conduction and dielectric loss) are considered. In this study, when antennas are analysed along with the human body model, it is the realised gain which includes losses from the human body that is considered.

Aside from gain, another very important parameter that this study focuses on is antenna efficiency. Generally speaking, antenna efficiency is the ratio of radiated power to the power fed to the antenna by the source. Antenna efficiency can be further categorized into two values: radiation efficiency and total efficiency.

The radiation efficiency is the ratio of the power radiated to the power accepted at the antenna input terminal. This efficiency includes conduction and dielectric losses. Total efficiency is the ratio of the radiated power to the power from the feeding source. This includes one more potential loss: the mismatch loss due to the reflection between the antenna port and the feeding network. For a well-matched design, the term antenna efficiency usually refers to the radiation efficiency.

For designs in this thesis, the primary target efficiency is the on-body efficiency, which is the antenna total efficiency when applied to a lossy human body. The significant dielectric loss of the human body is considered throughout the design process. To achieve on-body efficiency in simulation, the CST voxel family model is used. To accurately measure the on-body efficiency, a reverberation chamber is designed and constructed. Details about the reverberation chamber and the measurement process will be discussed in Chapter 3.

2.2 Overview of Wearable Antenna Designs

The wearable consumer electronic market has seen a boom in recent years with the advent of products including smartwatches, fitness bands and augmented reality glasses. To improve user experience many of these wearable products operate in a wireless mode and hence to facilitate this, wearable antennas are required. For this reason, wearable antenna designs have received a significant amount of attention from the research community in recent years.

Wearable antennas are required to operate close to the human body, and often over relatively long time periods. Thus, special requirements for the antenna design exist

depending on the specific working environment of the device. Typically, for these applications, traditional antennas on PCB board, small dielectric resonator antennas or antennas on metal frames are used [2]-[5]. Recently some state-of-the-art designs have used transparent conducting material to form transparent antennas on glass [6]-[7].

For applications in the health and rescue areas, including protective garments and life jackets, antennas embedded in the specialised items of clothing are commonly used [8]-[9]. These designs are usually planar and low-profile, and are likely to undergo a certain level of deformability and stretchability during use.

Some wearable antenna designs have utilised structures that allow them to be integrated with daily accessories, making use of their natural materials and size to achieve better antenna performance. Examples of this include button antennas, watch strap antennas, shoelace antennas, zipper antennas and belt antennas [10]-[17].

A special circumstance is encountered for applications requiring an antenna to be implanted or ingested into the human body. An example of this is found in a wireless capsule endoscope, which uses an antenna to broadcast real-time images from inside the body to a receiver on the outside. This kind of application normally requires an omnidirectional radiation pattern. The key issue for the design is to determine the properties of the tissues and contents surrounding the antenna and then evaluate the radiation efficiency. Commonly, conformal loops or meander lines are applied for this kind of application [18]-[19].

Throughout the literature review phase of this project, it is found that the designs of wearable antennas can be divided into two groups: soft-substrate based antennas and accessory-like antennas. Soft-substrate antennas are planar antennas with deformable substrates and conductive layers. Accessory-like antennas are antennas designed in accordance with the shape and size of common wearable accessories. Antenna designs in both categories are discussed in this chapter.

2.3 Soft-substrate Antenna Designs

Soft-substrate antennas are generally meant to be integrated into a garment of clothing to be worn. The challenges of designing such antennas mainly fall into two areas: the material selection and the fabrication techniques used. In the following sections, some published studies are provided with an emphasis on how they meet these challenges.

2.3.1 Conductive material selection

Conductive and dielectric materials are required to form a planar, layered antenna structure, normally seen in wearable antenna designs.

For conductive materials, high conductivity, and stable performance under deformation (bending, stretching, crumpling, etc.) are the two most critical factors to ensuring stable, high-efficiency antenna performance. Electro-textiles provide one solution to meet the conductivity requirements. Conductive fabrics used to have poor conductivity and high losses resulting in reduced antenna efficiency and gain [20]. However, recent advances in the fabrication of conductive fabrics have led to improved efficiencies for embroidered antennas and circuits. Electro-textiles are commonly created using metal-plated thread. Silver-plated thread is widely applied due to its high conductivity and nickel is sometimes added to increase the thread's corrosion resistance [20]. Silver-plated threads have been used with various substrates to form planar antennas [21]-[25]. An example of a planar spiral antenna sewn with such threads is shown in Figure 2-2. In a state-of-the-art work, improved embroidery techniques allow conductive fibres made with silver-plated threads to be used to fabricate antennas and circuits which meet the high-efficiency, low-loss requirements. An application of this has been made in an RF energy harvesting system [25]. In the energy harvesting system, the conductive fibre antennas can achieve a radiation efficiency of 77.3% at 2.45 GHz while the rectifying circuit can achieve an efficiency over 70% in the same operation

band. The efficiency improvement presented in [25] is based on prior studies on the loss characterization of embroidered conductive textiles [24], in which a transmission line method was used to characterize the loss of the fibres in RF band.

Figure 2-2：Example planar antenna fabricated with conductive threads [21].

Due to the complexity of thread composition and alignments, the conductivity of a single thread cannot directly reflect the loss of the conductive textile structure in the RF band. Thus, it is difficult to quantify the loss theoretically. By fabricating a transmission line using the thread and fabrication technique to be tested and then measuring the transmission coefficient of that transmission line, the loss of the conductive fibre can be quantified. In [24], three transmission lines were fabricated and tested as shown in Figure 2-1. These three transmission lines use the same Polydimethylsiloxane (PDMS) substrate material. The difference between them is the conductive material. Sample A in Figure 2-3 uses conductive E-fibre for both the transmission line top layer and the ground plane. Sample B uses conductive E-fibre for the top layer and copper as the ground plane. Sample C, as a conventional comparison, uses copper for both the top layer and the ground plane.

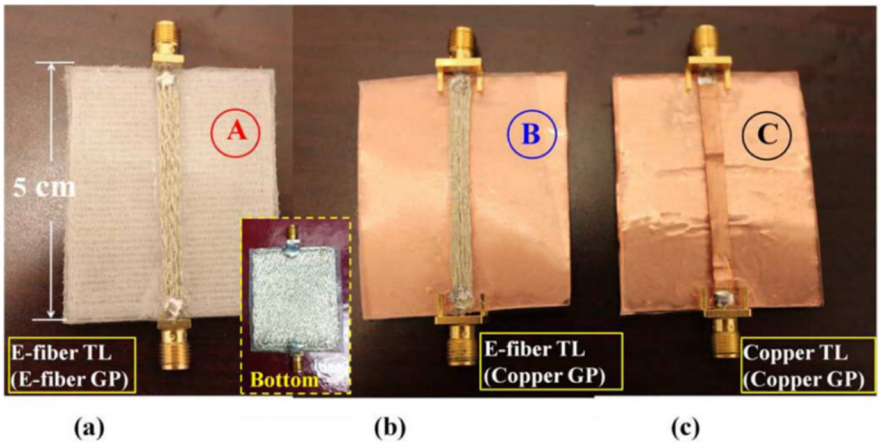

Figure 2-3：Three transmission line (TL) samples. (a) E-fibre TL with E-fibre ground plane, (b) E-fibre TL with a copper ground plane, and (c) copper TL with copper ground plane [24].

The transmission loss per unit length for the three transmission lines are compared. The transmission loss per centimetre in dB for case A, B and C are 0.21 dB/cm, 0.17 dB/cm and 0.14 dB/cm. Patch antenna fabricated with E-fibres in this study can achieve a realised gain of 5.6 dBi, which is only 0.3 dB lower than the copper patch used as comparison.

In addition to conductive fibres, other conductive materials including graphene and conductive ink have been applied in antenna designs [26]-[33]. These materials can also achieve desirable conductivity. For example, a low-cost dipole antenna was manufactured achieving a radiation efficiency of 32 % using graphene on a paper substrate [29]. An example of how graphene ink can be applied to a substrate and an antenna fabricated using that process is shown in Figure 2-4 [26]. The application of graphene or conductive ink usually requires a flat, stable, and homogeneous substrate. Such requirements on the substrate could be a problem for wearable applications.

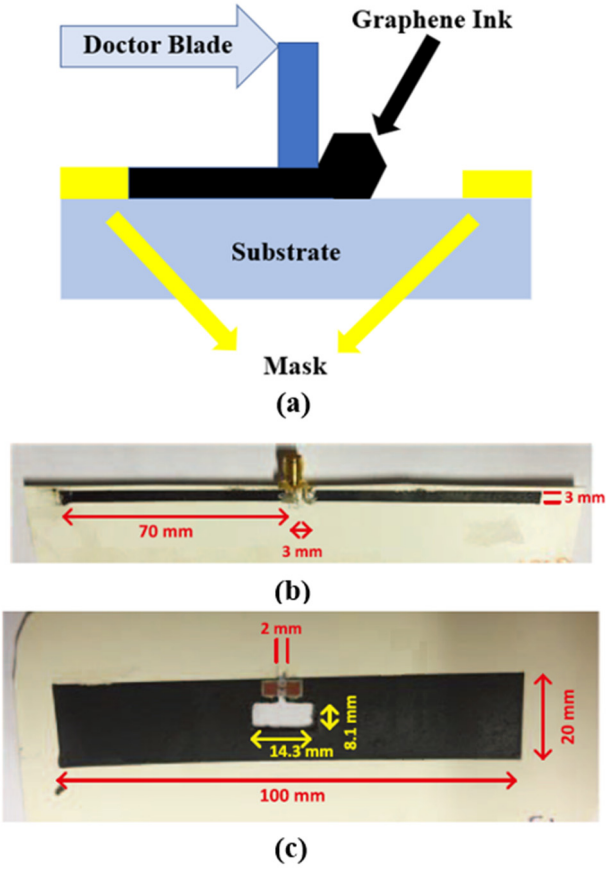

Figure 2-4：Low-cost graphene antenna made with doctor blade technique. (a) The process of fabrication. (b) Side view of the finished antenna with dimensions. (c) Top view of the finished antenna with dimensions [26].

2.3.2 Substrate material selection

The dielectric substrate material is important in determining an antennas' performance, the two most important properties in affecting antenna performance are the dielectric constant and the loss tangent of the substrate. A high dielectric constant would result in a smaller size antenna, which is obviously good for convenience in wearable applications, but also tends to result in a small operational bandwidth which may not be application friendly. The dielectric loss of the substrate will directly affect the efficiency of the antenna and so should be minimised. Therefore, ideally, the soft substrate used would have a tuneable dielectric constant and low loss tangent, allowing a tradeoff between bandwidth and size whilst maintaining high radiation efficiency.

Textile materials are a common choice as the wearable substrate allowing antennas to be fabricated directly onto items of clothing. Felt, fleece, Cordura and spacer fabric are some examples chosen in previously published research. The dielectric properties of some materials are summarised in [33]. Normal fabrics reported in [33] have a relative permittivity ranging from 1.3 to 1.95 and a loss tangent ranging from 0.0004 to 0.0400. It should be noted that these dielectric properties are only indicative for the textile materials as actual values depend on thickness, weave, any applied dye and natural properties of the thread. Therefore, measurements of textile material properties should always be performed prior to simulation and fabrication.

Polymer-based substrates have recently attracted attention due to their flexibility and stretchability. Polydimethylsiloxane (PDMS) is one promising example of poly-based substrate material. Figure 2-5 shows an example of a PDMS-embedded conductive fibric antenna and indicates its flexibility.

Figure 2-5：Fabricated PDMS-embedded conductive fabric antenna. (a) Top view. (b) Bottom View. (c) Side view. (d) Bent view [35].

For PDMS, doping with various powders can change its dielectric properties and hence make the material adjustable for different applications. Examples of this dielectric constant tuning by mixing in ceramic powders can be seen in [22] and [35]. With ceramic composite added, the relative permittivity of the PDMS substrate was around 6 (stable over a frequency range between 0.5 GHz to 5 GHz), with a loss tangent lower than 0.05 [35]. PDMS deposited around conductive rubber can be an ideal substrate for stretchable wearable antennas [36]. Generally, the PDMS substrates used for wearable applications have a relative permittivity between 2.8 to 6. This value is considerably larger than normal fabrics ranging from 1.3 to 1.95. Therefore, the overall

antenna size achievable using PDMS substrate can be smaller than that using other textile fabric substrates.

2.3.3 Fabrication techniques

The fabrication techniques used to manufacture soft-substrate wearable antennas tend to be those general techniques already commonly associated with the type of substrate material selected. These include techniques such as screen-printing, inkjet printing and embroidery.

The embroidery method is commonly applied with antennas using conductive thread and textile materials as the substrate. A typical process to fabricate an embroidered antenna is shown in Figure 2-6. Fabrication parameters including the number of threads per centimetre, alignment of the threads and the embroidery tension will affect the performance of the fabricated antenna [24]. These parameters can be adjusted with an automated embroidery machine.

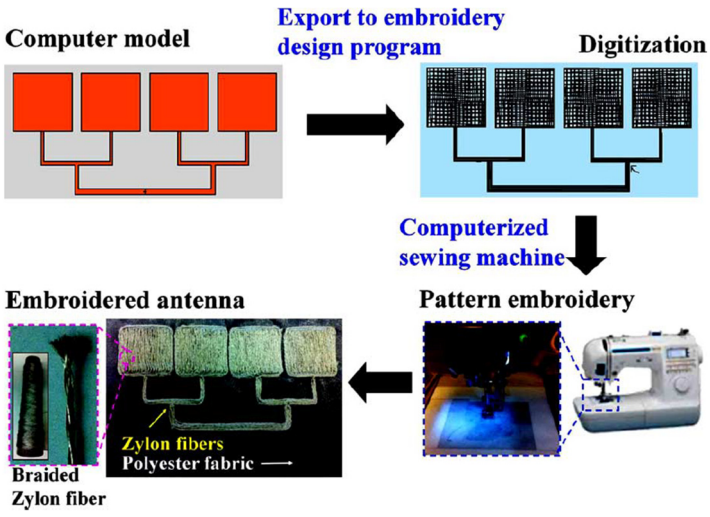

Figure 2-6：Embroidery process of the E-fibres to create RF designs on polyester fabrics [22].

An alternative example is provided in Figure 2-7, where conductive fibres are attached onto a PDMS substrate. With this manufacturing process, the antenna design can enjoy the benefit of a tuneable substrate dielectric constant and a high conductivity

at the same time.

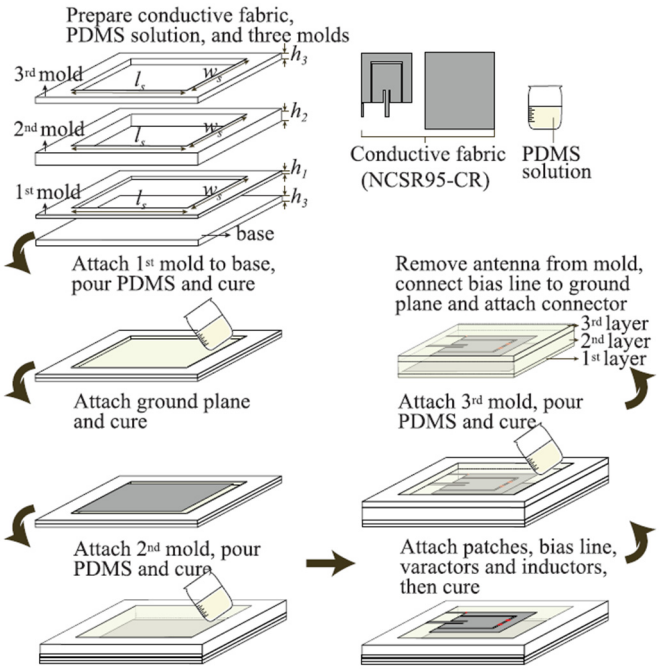

Figure 2-7：Manufacturing process flow for polymer-embedded conductive fabric antennas [22].

The screen-printing method has also been shown to be a viable process for wearable antenna fabrication. The screen used in this method is made of a mesh of fabric thread with non-image area blocked by a stencil and the image (antenna pattern) area left open. The printing is performed by pressing a conductive ink (typically silver based) onto the substrate through the screen. Successful fabrication of an E-shape patch antenna on a multi-layered polyester fabric has been demonstrated in [37]. A picture of the screen-printed antenna is shown in Figure 2-8. The polyester fabric has a water-resistant characteristic and can stand severe bending conditions. The screen-printing method has also been applied to materials including PDMS and graphene [38].

Figure 2-8：Screen printed antenna on polyester fabric [37].

Ink-jet printing utilizes a specialized printer to spread conductive ink particles onto the surface of substrates. Similar to conventional printing, paper has been used as a substrate and good performance has been achieved in 1.8 GHz, 2.4 GHz and 3.5 GHz bands [31]-[32]. This method has also been used on leather to achieve a wearable wideband antenna [33].

2.4 Accessory-like Antenna Designs

For accessory-like antennas, the general idea is to utilise the rigid metallic structures of typical daily accessories as the main radiating element of the antenna. A good example of this is the handbag zipper antenna [15]. A gain of 5 dBi at 2.44 GHz was achieved owing to the shape, size, and metallic nature of the zipper. The detailed design of the antenna is shown in Figure 2-9.

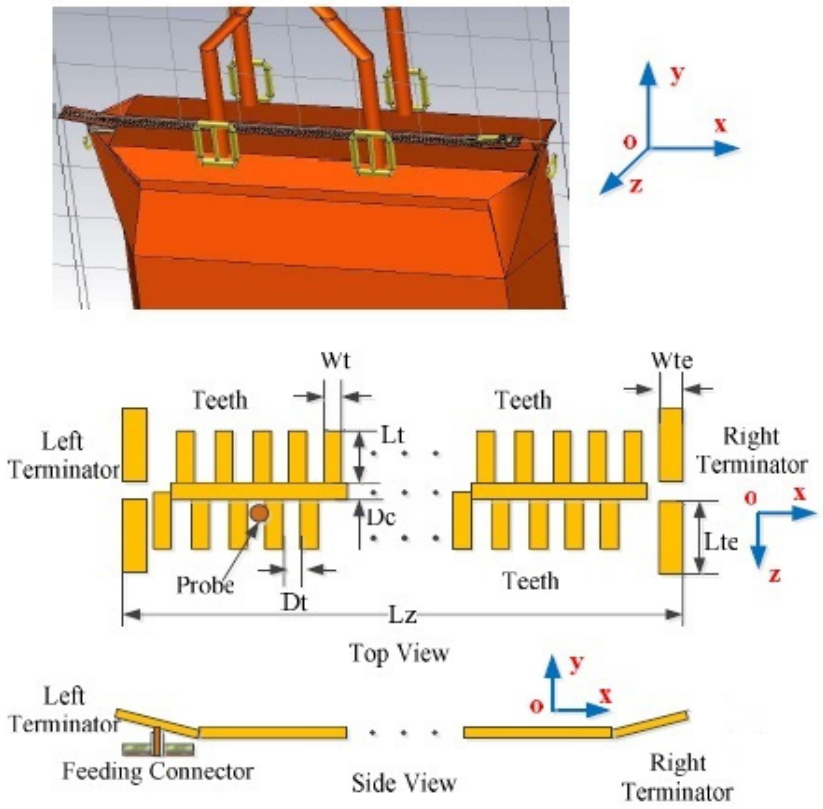

Figure 2-9：Geometry of the handbag zipper antenna [15].

The design of the zipper antenna reveals a major limitation for metallic accessory antennas. The shape and size of the antenna structure should be very similar to the original accessory to maintain its functionality. In this case, the shape of the zipper teeth and handle, along with the overall length of the zipper are unchanged from the original handbag design. The proposed zipper antenna achieved a realised gain of about 5 dBi at 2.45 GHz.

Another good example of an accessory antenna is the button antenna [10]-[13]. Buttons are one of the most rigid items found on daily clothing. The special shapes possible with buttons enables the antenna to be slightly high profile. The co-design of a textile substrate or a conductive textile ground plane also becomes possible. A maximal on-body radiation efficiency of 72% at 2.45 GHz was achieved by the button design proposed in [13].

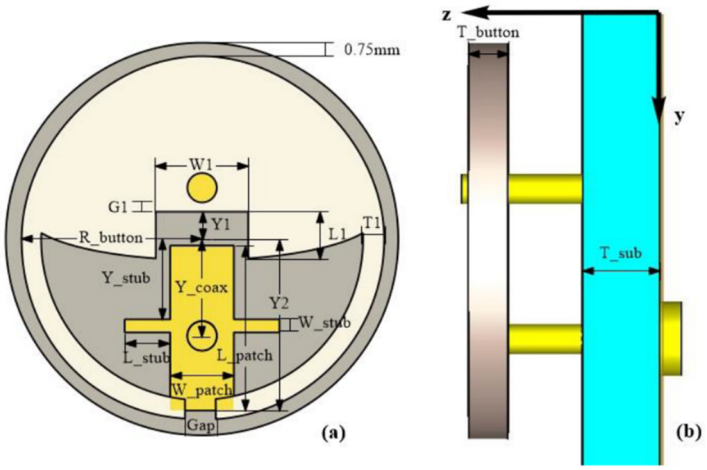

Figure 2-10：Geometry of a proposed button antenna. (a) Top view. (b) Side view [11].

The first belt buckle antenna found in published literature was seen in 2008 [16]. The design is shown in Figure 2-11. This belt buckle antenna design uses a single tongue buckle type of belt to create an antenna using a principle similar to a regular loop antenna. The antenna achieved a measured gain of over 1 dBi in the 2.45 GHz and 5.25 GHz bands.

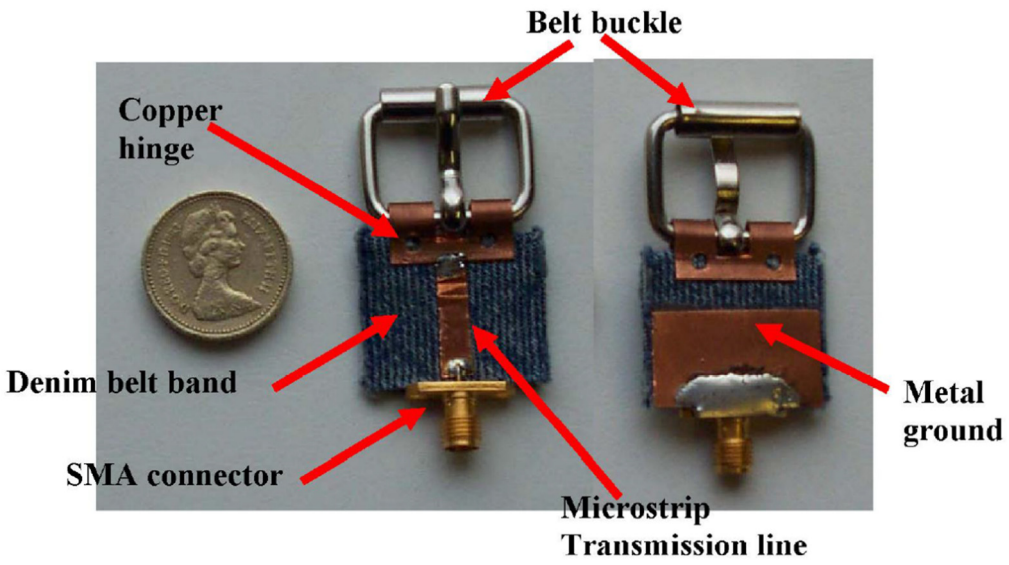

Figure 2-11：The first proposed belt antenna [16].

2.5 Textile Shield/Reflector Structures with EBG

Aside from the aforementioned wearable antenna designs, a special structure called an electromagnetic band gap (EBG) structure has been proven desirable in wearable antenna designs to provide antenna isolation for the body [41]-[43]. This type of structure is applied in this project to reduce the power from the antenna that radiates towards the human body and to improve antenna gain performance.

The special wave propagation properties of EBGs have been used in various antenna designs. One common application is to use the structure as a high impedance surface (HIS) to improve radiation performance for low profile antennas [39]. It should be noted that the EBG structures in this study have been denoted as high impedance surfaces (HIS) or artificial magnetic conductors (AMC) in other literature [40]-[42]. The textile EBG structure was first applied with a planar textile antenna to improve antenna performance in [43].

Generally, EBG structures have two main desired properties for RF applications. The first one is an in-phase reflector designed to function as such over specific frequency bands. A properly designed EBG surface can have a property similar to a

perfect magnetic conductor (PMC), with a reflection phase of 0° for normal incident waves. In contrast, a perfect electric conductor would have a reflection phase of 180° under the same condition. The possible in-phase reflection property allows for constructive reflections to be formed when the reflecting plane is located in close proximity to the radiating element.

The second use of an EBG is for surface wave suppression. EBG structures can block the propagation of surface waves over their designed working frequency bands. This feature allows the suspended transmission line method, which will be discussed in Chapter 6, to be used to evaluate the performance of the EBG surface.

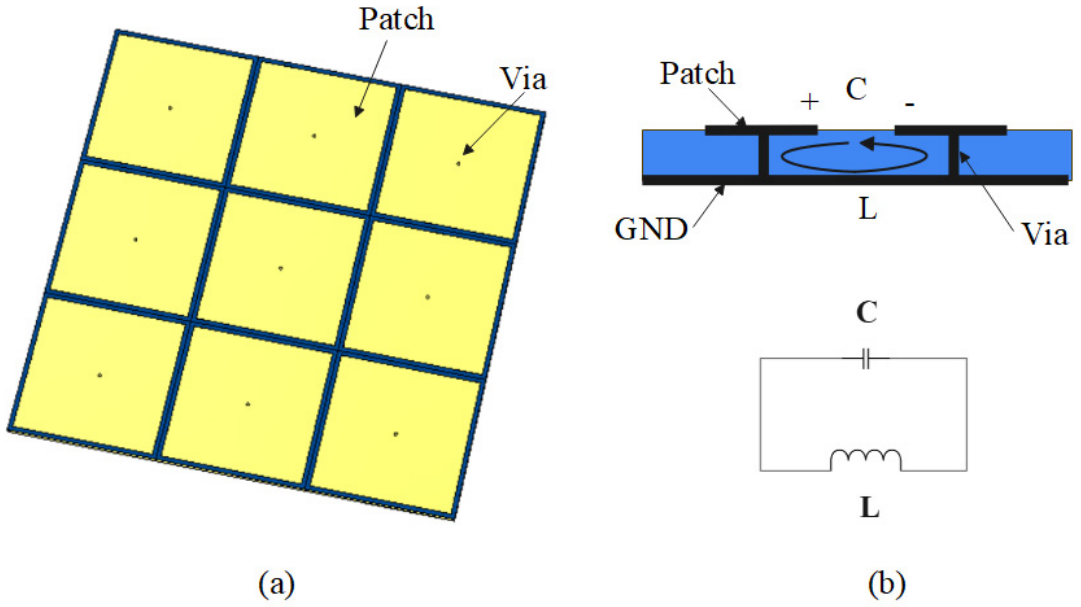

Figure 2-12：The mushroom EBG structure. (a) Overview of the structure. (b) Side view and LC model of the structure [44].

A very popular EBG structure is the mushroom structure, as shown in Figure 2-12 (a). The side view of the structure is provided in Figure 2-12 (b). A via is used to connect each unit cell patch to the ground plane. An L-C resonance model can be used to characterize each unit cell structure. This structure is evaluated in detail in Chapter 6 for the textile EBG design in this study.

The reflected phase in this study is obtained using the frequency domain solver with periodic unit cell boundary condition in CST Microwave studio. An incident plane

wave labelled in Figure 2-13 (a) is sent towards the EBG unit cell and the phase of the reflected wave is evaluated. The point of 0° reflected phase is considered as the centre of the response. Generally, a frequency band with reflected phase ranging from -90° to 90° is considered the band gap of the EBG structure and is the usable band when the EBG is acting as a reflecting plane.

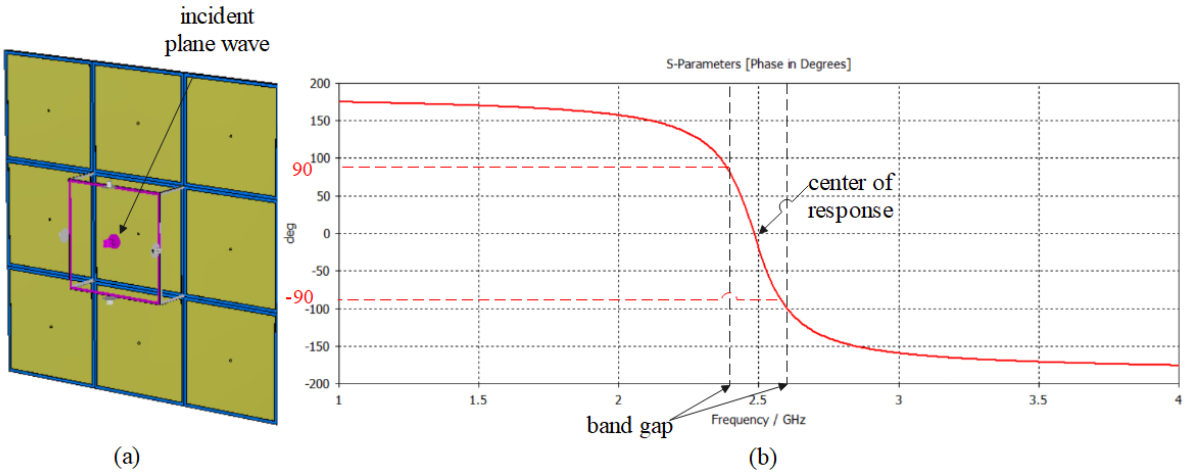

Figure 2-13： EBG (a) unit cell simulation environment and (b) reflected phase.

2.6 Antenna Design Challenges

The general design challenges for wearable antennas are summarised in this section and some antenna model ideas are proposed. The challenges can be categorised into the following three aspects:

1. Maintaining stable performance with non-standard RF materials. For wearable antenna designs, materials ranging from leather, to wool, to PDMS and metal can be found. The determination of accurate material properties for these materials and the specific use of the materials is crucial to developing high-efficiency antennas. Moreover, the mechanical effects of bending and crumpling on the RF performance of the material should be taken into consideration.

2. Minimising the effect of the human body on antenna performance. Wearable antenna designs may not provide enough isolation to the human body. This lack of

isolation could result in an undesired frequency shift, degraded efficiency, and result in SAR safety related issues.

3. For accessory-like antennas, designing the antenna to fit within or following the shape and size of a wearable accessory is difficult. Accessories-like antenna designs should share the shape and size of the original accessories to meet ergonomic requirements. Designing a high-performance antenna of limited shape and size is a challenging task.

This thesis seeks to design high-efficiency wearable antennas and therefore based on the previous discussions; accessory type antennas are the most appropriate choice. They allow for a rigid metal structure that is not necessarily dependent on the use of an RF inappropriate or deformable substrate material. Considering the various types of accessory available, the belt buckle is the most suitable choice. It is a popular accessory item, used daily by consumers. It can be made from conductive material and can be of a size suitable to operating in the frequency bands of interest in wearable applications e.g. Bluetooth and Wi-Fi, and finally its overall shape is designable.

The general structure of a belt buckle gives rise to two basic antenna types, the loop antenna, and the aperture (patch type) antenna, dependent on the buckle type. In either case, these antennas are bi-directional and as they lie flat on the body will direct a significant amount of EM radiation into the body, decreasing performance and leading to potential safety issues. An EBG ground plane can be used in conjunction with the antenna to control EM radiation into the body and simultaneously improve antenna radiation efficiency and gain.

A loop antenna is a wire-type antenna. Figure 2-14 shows a circular shaped loop antenna. Loop antennas can have a variety of configurations including circular, rectangular, elliptical, and other shapes.

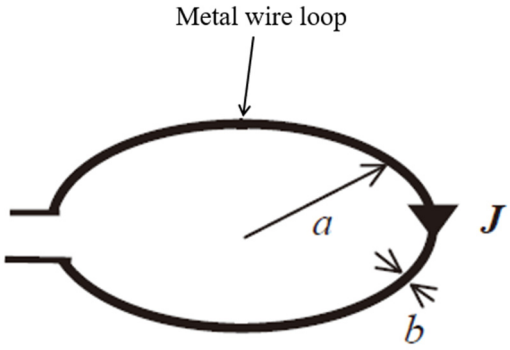

Figure 2-14：Loop antenna structure and its magnetic current form [45].

The parameters *a* and *b* in Figure 2-14 are important for loop antennas as the radius *a* determines the overall length and hence the resonant frequency of the loop. The value of *b*, which is the diameter of the loop metal, is closely related to the impedance of the antenna. The symbol ***J*** denotes the current flow in the loop. The analysis of the current flow in the loop is useful in loop-type antenna designs and is used in Chapter 5 for the loop belt buckle antenna structure design.

Considering the shape and configuration for regular belt buckles, the aperture type belt antenna in this study shares similar principle with that of a planar microstrip patch antenna. For the thoroughness of the thesis, microstrip patch antenna is also introduced here.

A typical planar patch antenna consists of a metal patch, a substrate layer (dielectric material with permittivity ε_r and thickness *d* and a metal ground plane, as shown in Figure 2-15. At resonance, the length *L* for the patch should be around half of the wavelength so that the antenna can be considered as a half wavelength transmission line resonant cavity with two open ends. The two open ends, labelled as radiating slots in Figure 2-15, create fringing field and are the main reason for the radiation.

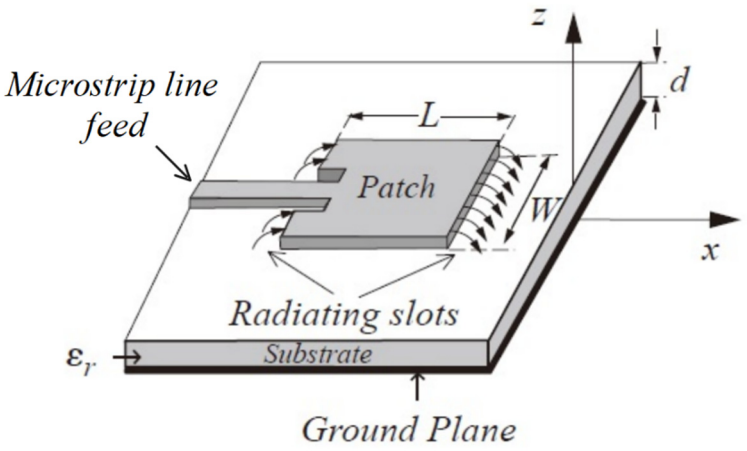

Figure 2-15：Structure for a planar patch antenna [45].

As a resonant cavity, there are many possible modes in a patch antenna depending on the frequency. The fundamental and dominant mode is TM_{100} mode. The term TM here represents a magnetic field distribution. The magnetic field between the patch and the ground, as denoted with black arrows in Figure 2-16, is transverse to the *z*-axis. The three numbers in the term TM_{100} represents the number of half wave changes (field direction changes along a distance of half a wavelength) along the *x*, *y* and *z*-axis. The third zero, which is the one with respect to the *z*-axis, is usually dropped as the magnetic field in this type of patch antenna is transverse to the *z*-axis. With the TM mode setup, the patch antenna can be characterised with three field components: the electric field in the *z*-direction and the magnetic field in the magnetic field components in the *x* and *y* directions. In practice, the electric field in the *z*-direction is commonly used to determine the TM mode for a patch antenna. Figure 2-16 illustrates a typical electric field distribution for a patch antenna with a TM_{10} mode. One field direction change can be seen over a span of half a wavelength, hence the subscript notation of 10 is used.

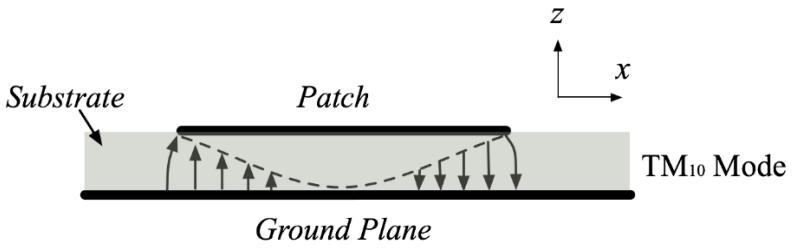

Figure 2-16：An illustration of a patch antenna TM_{10} mode.

Similar TM mode characterisation is used in Chapter 4 for the proposed patch type belt buckle antenna design.

2.7 Summary

In this chapter, basic antenna theory and a review for wearable antenna designs are included. The wearable antennas included in this chapter are categorised into two groups: soft substrate antenna designs and accessory-like designs. The challenges in material selection, fabrication techniques and structural designs are addressed. For the thoroughness of this thesis, basic information on textile electromagnetic band gap (EBG) materials, loop antennas and patch antennas are included.

2.8 Reference

[1] Obtained from the website of the Italian National Research Council: http://niremf.ifac.cnr.it/tissprop/

[2] P. Dempsey, "The teardown: Apple Watch," *Engineering & Technology*, vol. 10, no. 6, pp. 88-89, 2015.

[3] J. R. Lyons, T. P. Register, T. C. Wilcher, J. R. Simpson, and D. L. Dorris, "Watch with bezel antenna configuration," ed: Google Patents, 2015.

[4] S. Su and Y. Hsieh, "Integrated Metal-Frame Antenna for Smartwatch Wearable Device," *IEEE Transactions on Antennas and Propagation*, vol. 63, no. 7, pp. 3301-

3305, 2015.

[5] M. Ferreira, C. Oliveira, F. Cardoso, and L. M. Correia, "SAR assessment of google glasses at cellular wireless frequency bands," in *2016 10th European Conference on Antennas and Propagation (EuCAP)*, 2016, pp. 1-4.

[6] M. Stanley, Y. Huang, H. Wang, H. Zhou, A. Alieldin, and S. Joseph, "A Transparent Dual-Polarized Antenna Array for 5G Smartphone Applications," in *2018 IEEE International Symposium on Antennas and Propagation & USNC/URSI National Radio Science Meeting*, 2018, pp. 635-636.

[7] S. Hong, S. H. Kang, Y. Kim, and C. W. Jung, "Transparent and Flexible Antenna for Wearable Glasses Applications," IEEE Transactions on Antennas and Propagation, vol. 64, no. 7, pp. 2797-2804, 2016.

[8] A. A. Serra, P. Nepa, and G. Manara, "A Wearable Two-Antenna System on a Life Jacket for Cospas-Sarsat Personal Locator Beacons," *IEEE Transactions on Antennas and Propagation*, vol. 60, no. 2, pp. 1035-1042, 2012.

[9] L. Vallozzi, P. V. Torre, C. Hertleer, H. Rogier, M. Moeneclaey, and J. Verhaevert, "Wireless Communication for Firefighters Using Dual-Polarized Textile Antennas Integrated in Their Garment," *IEEE Transactions on Antennas and Propagation*, vol. 58, no. 4, pp. 1357-1368, 2010.

[10] X. Y. Zhang, H. Wong, T. Mo, and Y. F. Cao, "Dual-Band Dual-Mode Button Antenna for On-Body and Off-Body Communications," *IEEE Transactions on Biomedical Circuits and Systems*, vol. 11, pp. 933-941, 2017.

[11] H. Xiaomu, S. Yan, and G. A. E. Vandenbosch, "Wearable Button Antenna for Dual-Band WLAN Applications With Combined on and off-Body Radiation Patterns," *IEEE Transactions on Antennas and Propagation*, vol. 65, pp. 1384-1387, 2017.

[12] B. Sanz-Izquierdo, J. C. Batchelor, and M. I. Sobhy, "Button antenna on textiles for wireless local area network on body applications," *IET Microwaves, Antennas &*

Propagation, vol. 4, pp. 1980-1987, 2010.

[13] S. Yan and G. A. E. Vandenbosch, "Design of Wideband Button Antenna Based on Characteristic Mode Theory," *IEEE Trans. on Biomed. Circuits Sys.,* vol. 12, no, 6, pp. 1383-1391, Dec. 2018.

[14] G. Li, G. Gao, J. Bao, B. Yi, C. Song, and L. Bian, "A Watch Strap Antenna for the Applications of Wearable Systems," *IEEE Access*, vol. 5, pp. 10332-10338, 2017.

[15] G. Li, Y. Huang, G. Gao, X. Wei, Z. Tian, and L. Bian, "A Handbag Zipper Antenna for the Applications of Body-Centric Wireless Communications and Internet of Things," *IEEE Transactions on Antennas and Propagation*, vol. 65, pp. 5137-5146, 2017.

[16] B. Sanz-Izquierdo and J. C. Batchelor, "A Dual Band Belt Antenna," in *2008 International Workshop on Antenna Technology: Small Antennas and Novel Metamaterials*, pp. 374-377, 2008.

[17] D. Gaspar and A. A. Moreira, "Belt antenna for wearable applications," in *2009 IEEE Antennas and Propagation Society International Symposium*, pp. 1-4, 2009.

[18] J. Wang, M. Leach, E. G. Lim, Z. Wang, R. Pei, and Y. Huang, "An Implantable and Conformal Antenna for Wireless Capsule Endoscopy," *IEEE Antennas and Wireless Propagation Letters*, vol. 17, no. 7, pp. 1153-1157, 2018.

[19] Z. Jiang, Z. Wang, M. Leach, Y. Huang, E. G. Lim, J. Wang, and R. Pei, "Wideband Loop Antenna with Split-Ring Resonators for Wireless Medical Telemetry," *IEEE Antennas and Wireless Propagation Letters*, vol. 18, no. 7, pp. 1415-1419, 2019.

[20] K. N. Paracha, S. K. A. Rahim, P. J. Soh, and M. Khalily, "Wearable Antennas: A Review of Materials, Structures, and Innovative Features for Autonomous Communication and Sensing," *IEEE Access*, vol. 7, pp. 56694-56712, 2019.

[21] J. Zhong, A. Kiourti, T. Sebastian, Y. Bayram, and J. L. Volakis, "Conformal

Load-Bearing Spiral Antenna on Conductive Textile Threads," *IEEE Antennas and Wireless Propagation Letters*, vol. 16, pp. 230-233, 2017.

[22] Z. Wang, L. Zhang, Y. Bayram, and J. L. Volakis, "Embroidered Conductive Fibers on Polymer Composite for Conformal Antennas," *IEEE Transactions on Antennas and Propagation*, vol. 60, no. 9, pp. 4141-4147, 2012.

[23] A. Kiourti, C. Lee, and J. L. Volakis, "Fabrication of Textile Antennas and Circuits With 0.1 mm Precision," *IEEE Antennas and Wireless Propagation Letters*, vol. 15, pp. 151-153, 2016.

[24] D. Vital, J. Zhong, S. Bhardwaj, and J. L. Volakis, "Loss-Characterization and Guidelines for Embroidery of Conductive Textiles," in *2018 IEEE International Symposium on Antennas and Propagation & USNC/URSI National Radio Science Meeting*, 2018, pp. 1301-1302.

[25] D. Vital, S. Bhardwaj, and J. L. Volakis, "Textile-Based Large Area RF-Power Harvesting System for Wearable Applications," *IEEE Transactions on Antennas and Propagation*, vol. 68, no. 3, pp. 2323-2331, 2020.

[26] M. Akbari, M. W. A. Khan, M. Hasani, T. Björninen, L. Sydänheimo, and L. Ukkonen, "Fabrication and Characterization of Graphene Antenna for Low-Cost and Environmentally Friendly RFID Tags," *IEEE Antennas and Wireless Propagation Letters*, vol. 15, pp. 1569-1572, 2016.

[27] C. Fan, B. Wu, Y. Hu, Y. Zhao, and T. Su, "Millimeter-Wave Pattern Reconfigurable Vivaldi Antenna Using Tunable Resistor Based on Graphene," *IEEE Transactions on Antennas and Propagation*, vol. 68, no. 6, pp. 4939-4943, 2020.

[28] M. Yasir, P. Savi, S. Bistarelli, A. Cataldo, M. Bozzi, L. Perregrini, and S. Bellucci, "A Planar Antenna With Voltage-Controlled Frequency Tuning Based on Few-Layer Graphene," *IEEE Antennas and Wireless Propagation Letters*, vol. 16, pp. 2380-2383, 2017.

[29] T. Leng, X. Huang, K. Chang, J. Chen, M. A. Abdalla, and Z. Hu, "Graphene Nanoflakes Printed Flexible Meandered-Line Dipole Antenna on Paper Substrate for Low-Cost RFID and Sensing Applications," *IEEE Antennas and Wireless Propagation Letters*, vol. 15, pp. 1565-1568, 2016.

[30] E. Sipilä, J. Virkki, L. Sydänheimo, and L. Ukkonen, "Experimental Study on Brush-Painted Metallic Nanoparticle UHF RFID Tags on Wood Substrates," *IEEE Antennas and Wireless Propagation Letters*, vol. 14, pp. 301-304, 2015.

[31] H. A. Elmobarak, S. K. A. Rahim, M. Himdi, X. Castel, and T. A. Rahman, "Low cost instantly printed silver nano ink flexible dual-band antenna onto paper substrate," in *2017 11th European Conference on Antennas and Propagation (EUCAP)*, 2017, pp. 3061-3063.

[32] H. F. Abutarboush, M. F. Farooqui, and A. Shamim, "Inkjet-Printed Wideband Antenna on Resin-Coated Paper Substrate for Curved Wireless Devices," *IEEE Antennas and Wireless Propagation Letters*, vol. 15, pp. 20-23, 2016.

[33] M. F. Farooqui and A. Shamim, "Dual band inkjet printed bow-tie slot antenna on leather," in *2013 7th European Conference on Antennas and Propagation (EuCAP),* 2013, pp. 3287-3290.

[34] R. Salvado, C. Loss, R. Gonçalves, and P. Pinho, "Textile materials for the design of wearable antennas: A survey," *Sensors*, vol. 12, no. 11, pp. 15841_15857, 2012.

[35] R. B. V. B. Simorangkir, Y. Yang, R. M. Hashmi, T. Björninen, K. P. Esselle, and L. Ukkonen, "Polydimethylsiloxane-embedded conductive fabric: Characterization and application for realization of robust passive and active flexible wearable antennas," *IEEE Access*, vol. 6, pp. 48102_48112, 2018.

[36] R. A. Liyakath, A. Takshi, and G. Mumcu, "Multilayer stretchable conductors on polymer substrates for conformal and reconfigurable antennas," *IEEE Antennas Wireless Propag. Lett.*, vol. 12, no., pp. 603_606, 2013.

[37] S. B. Roshni, M. P. Jayakrishnan, P. Mohanan, and K. P. Surendran, "Design and fabrication of an E-shaped wearable textile antenna on PVB coated hydrophobic polyester fabric," *Smart Mater. Struct*., vol. 26, no. 10,

2017, Art. no. 105011.

[38] D. Xu, X. Tian, X. Guo, W. Jiang, W. Liu, and S. Xing, "Design and research of flexible wearable textile antenna based on GNPs/PANI/PDMS composites for 2.45 GHz," *Nanosci. Nanotechnol. Lett.*, vol. 9, no. 4, pp. 476-480, 2017.

[39] A. P. Feresidis, G. Goussetis, W. Shenhong, and J. C. Vardaxoglou, "Artificial magnetic conductor surfaces and their application to low-profile high-gain planar antennas," *IEEE Transactions on Antennas and Propagation,* vol. 53, no. 1, pp. 209-215, 2005.

[40] S. Yan, P. J. Soh, and G. A. E. Vandenbosch, "Low-Profile Dual-Band Textile Antenna With Artificial Magnetic Conductor Plane," *IEEE Transactions on Antennas and Propagation*, vol. 62, pp. 6487-6490, 2014.

[41] M. Wang, Z. Yang, J. Wu, J. Bao, J. Liu, L. Cai, et al., "Investigation of SAR Reduction Using Flexible Antenna With Metamaterial Structure in Wireless Body Area Network," *IEEE Transactions on Antennas and Propagation*, vol. 66, pp. 3076-3086, 2018.

[42] A. Alemaryeen and S. Noghanian, "On-Body Low-Profile Textile Antenna with Artificial Magnetic Conductor," *IEEE Transactions on Antennas and Propagation*, vol. 67, pp. 3649-3656, 2019.

[43] S. Zhu and R. Langley, "Dual-Band Wearable Textile Antenna on an EBG Substrate," *IEEE Transactions on Antennas and Propagation*, vol. 57, pp. 926-935, 2009.

[44] S. Zhu, "Wearable antennas for personal wireless networks", Ph.D. dissertation, University of Sheffield, 2008.

[45] Y. Huang and K. Boyle, *Antennas: from theory to practice*. John Wiley & Sons, 2008.

Chapter 3 Reverberation Chamber and On-body Efficiency Measurements

This chapter discusses the design and commission of a reverberation chamber vital to the completion of this work. In addition, detailed measurement processes are defined for the measurement of on-body antenna efficiency. The specifications and performance of the Xi'an Jiaotong-Liverpool University (XJTLU) in-house reverberation chamber are provided. Design of the chamber was completed in conjunction with Dr. Qian Xu. The concept and key definitions of parameters related to the reverberation chamber follow the textbook [1].

3.1 An Overview of the Reverberation Chamber

A reverberation chamber, also referred to as a reverberating chamber, mode-stirred chamber or mode tuned chamber, is a conducting-screened room with electrically large stirrers used to stir the EM field inside. An example of a reverberation chamber without two walls and the ceiling is shown in Figure 3-1. This structural design shown is used for the chamber developed for this study. In some of the following context, the name reverberation chamber is simplified to reverb for conciseness. The core objective for the reverb is to create a statistically uniform and isotropic EM field in the usable volume of the chamber. The metal walls of the chamber form an electrically large resonant cavity. The horizontal and vertical stirrers in the chamber can rotate stepwise and create different paths of reflection. With enough paths generated, a near-isotropic and mathematically uniform field distribution can be formed. In practice, aside from the change of stirrer positions, change of radiating source position and polarisation are also necessary to achieve the desired uniform distribution.

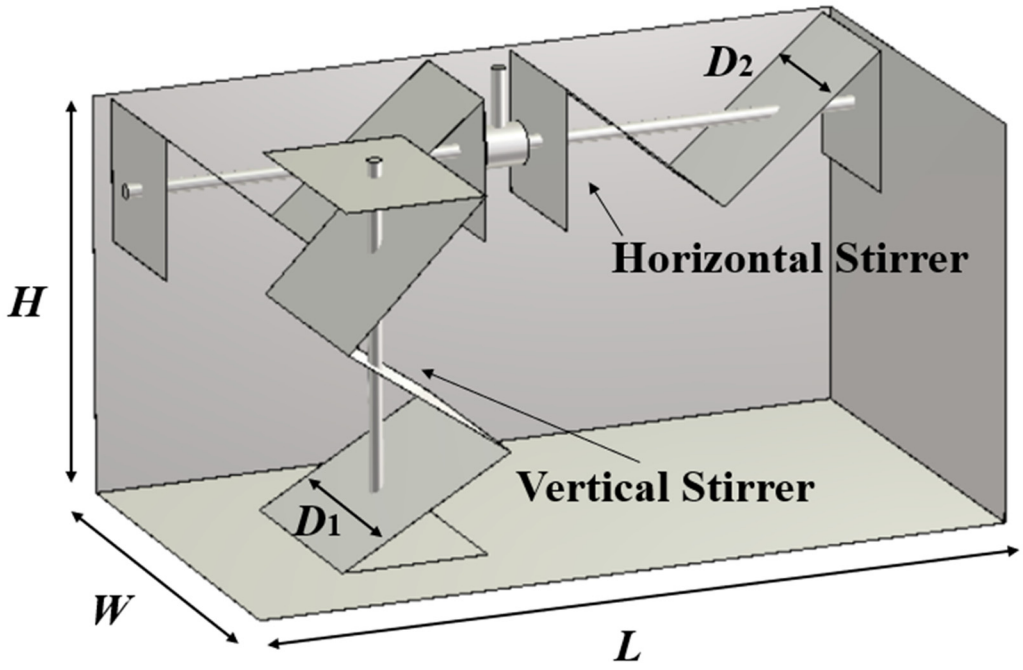

Figure 3-1：A model for the in-house reverberation chamber design.

As the reverb is normally considered as an electrically large resonant cavity, the resonant cavity model can be used for analysis. The cavity model states that the field in the cavity can be decomposed into the superposition of modes with different weights. Each mode is a distinct field distribution pattern in the cavity. When the field inside a reverb is stirred with the stirrers, the weighting coefficients for many modes are changed. In the practical design and application of a reverb, the mode number, rather than the detailed distribution of a single model is the main focus. With a determined chamber size, the mode number can be written as a function of the frequency, as defined in [1], is shown by the following function,

$$N_s(f)=\frac{8\pi \mathrm{HWL}f^3}{3c^3}-(H+W+L)\frac{f}{c}+\frac{1}{2} \tag{3-1}$$

where H, W and L are the height, width and length of the chamber. The variable f is the frequency and c is the speed of light in the cavity. It should be noted that the term $H\times W\times L$ represents the volume of the cavity, which will later be denoted by V.

Another important parameter, mode density, can be obtained by differentiating (3-1)

leading to:

$$D_s(f)=\lim_{\Delta f\to 0}\frac{\Delta N_s(f)}{\Delta f}=8\pi \mathrm{HWL}\frac{f^2}{c^3}-\frac{\mathrm{H+W+L}}{c}. \tag{3-2}$$

Mode density provides a measure of how many modes can be excited in a given bandwidth. If the mode density is low, a statistical nonuniformity could be present in the chamber modes.

Mode number and mode density are important parameters for the reverb because the lowest usable frequency (LUF) depends on them. Empirically, at the LUF, the mode number in the chamber should satisfy,

$$N_s(f)\sim\frac{8\pi Vf^3}{3c^3}\geqslant 60 \tag{3-3}$$

$$D_s(f)\sim 8\pi V\frac{f^2}{c^3}\geqslant 1.5 \text{ modes/MHz} \tag{3-4}$$

Mode number and mode density are analytical evaluations of the chamber performance without considering the stirring in the chamber. The performance of the reverb needs to be further analysed with the effect of stirring considered. The measurement in this case involves a pair of identical antennas with bandwidth covering the band of interest. In a reverb, three types of stirring are commonly used to create a statistically uniform field distribution in the chamber, these are mechanical stirring, source stirring and polarisation stirring. Mechanical stirring involves stepwise rotation of the stirrers in the chamber. S-parameters (especially S_{21}) between the two antennas are documented for each stirrer position. Source stirring involves moving one antenna (the one considered as the transmitting antenna). Source stirring could be achieved using a robotic arm or a moving platform. In this study, six fixed antenna positions are manually selected to perform source stirring due to the limitation in equipment. Polarisation stirring requires the polarisation of both the transmitting and receiving antennas to be changed. A complete test including all three stirring schemes will follow

these procedures:

1. Setting up a pair of antennas in one position and performing *S*-parameter measurements with a stepwise changed stirrer position (e.g., 360 data sets with a 1° step size for both horizontal and vertical stirrer rotations).

2. Changing the polarisation of both antennas and repeating step 1 again (720 data sets acquired at this stage).

3. Changing the transmitting antenna location and perform the previous two steps again. If six different transmitter positions are used, a full measurement set using all 3 stirring types generates 4320 datasets.

The ratio of the standard deviation and the mean value of the received power taken over different stirring positions(10log(Std/Mean)) is a measure of the field distribution in the chamber. Generally, if a random variable follows an exponential distribution, which is the ideal distribution for a reverb, the standard deviation should equal the mean value. This property provides a quick method to assess the performance of the reverb. In a measurement setup with vector network analyser (VNA) available (Agilent N5230C used in this study), the received power can be represented by measuring S_{21} and determining $|S_{21}|^2$. If the value of 10log(Std/Mean) is close to 0 dB (within a range of ±1 dB), the distribution of the received power is very close to an exponential distribution.

The field uniformity (FU) describes how uniform the field distribution is in a reverb. It is defined as the standard deviation from the normalised mean value of the normalised maximal values at each of the eight locations during one rotation of the stirrer [2]. The FU is quantified with standard deviation. In practice, there are two possible forms of FU. In one form, the maximal S_{21} values in all measurements with both mechanical and source stirring are taken as the reference value. The standard deviation over N antenna positions calculated with the maximal S_{21} obtained with one fixed position and the reference value, is as shown in formula (3-5).

$$Std_{max}=\sqrt{\frac{\sum_{p=1}^{N}(|S_{21}|^2_{max,p}-\langle|S_{21}|^2_{max}\rangle)^2}{N-1}} \tag{3-5}$$

In another form, the average S_{21} values in all measurements with both mechanical and source stirring are taken as the reference value. The standard deviation is calculated with the average values, as shown in formula (3-6).

$$Std_{avg}=\sqrt{\frac{\sum_{p=1}^{N}(|S_{21}|^2_{aver,p}-\langle|S_{21}|^2_{aver}\rangle)^2}{N-1}} \tag{3-6}$$

The FU in dB is defined as,

$$FU(dB)=10\log_{10}\frac{Std(linear)+Mean(linear)}{Mean(linear)} \tag{3-7}$$

The selection of the FU calculation method is dependent on the application of the chamber. If the testing of the maximum E-field is of interest, then the MaxE method should be selected. This is normally used when evaluating the ability to handle maximal E-field for a device under test in EMC testing. If the average E-field is of interest, then the MeanE method is the choice. This is normally used for long-term duration EMC tests.

A reverb has another pair of important and closely related parameters, the quality factor (Q) and the time constant τ. The quality factor shows the chamber's ability to store energy.

$$Q=\frac{16\pi^2 V}{\lambda^3}\times\frac{\langle P_r\rangle}{P_t} \tag{3-8}$$

The term P_r in formula (3-8) is the averaged received power in the chamber while the term P_t is the transmit power. The term λ is the wavelength. In practice, this quality can be measured in the frequency domain as the S_{21} between two antennas.

$$Q = \frac{16\pi^2 V}{\lambda^3 \eta_{Tx}\eta_{Rx}} \langle |S_{21}|^2 \rangle \tag{3-9}$$

The term η_{Tx} and η_{Rx} are the total efficiency of the two selected antennas for reverb testing.

It is also common practice to translate the frequency dependent quality factor into the time domain, where it becomes the reverb time constant τ.

$$\tau_{RC} = \frac{Q}{2\pi f} \tag{3-10}$$

3.2 The In-house Reverberation Chamber

A model for the reverberation chamber constructed for this study is shown in Figure 3-1. The chamber is a sealed metallic structure containing one vertical and one horizontal stirrer, a manual shielded door with shielding finger stripes and two waveguide windows for chamber ventilation. The chamber uses solid stirrers to ensure stability and reduce overall cost. It is acknowledged that cutting slots in the stirrers can improve the low frequency performance of the chamber, however this can also lead to mechanical instability. Also, the frequency range for which coverage is desired in this study is far above the lowest operating frequency covered by this chamber design. The specific dimensions of the chamber are provided in the following Table 3-2 and a photograph of the finished reverberation chamber is shown in Figure 3-2.

Table 3-2: The specifications of the reverberation chamber

Dimension	Value (m)
Length of the chamber L	5.4
Width of the chamber W	3.0
Height of the chamber H	2.8
Width of vertical stirrer D_1	1.5
Width of horizontal stirrer D_2	1.0

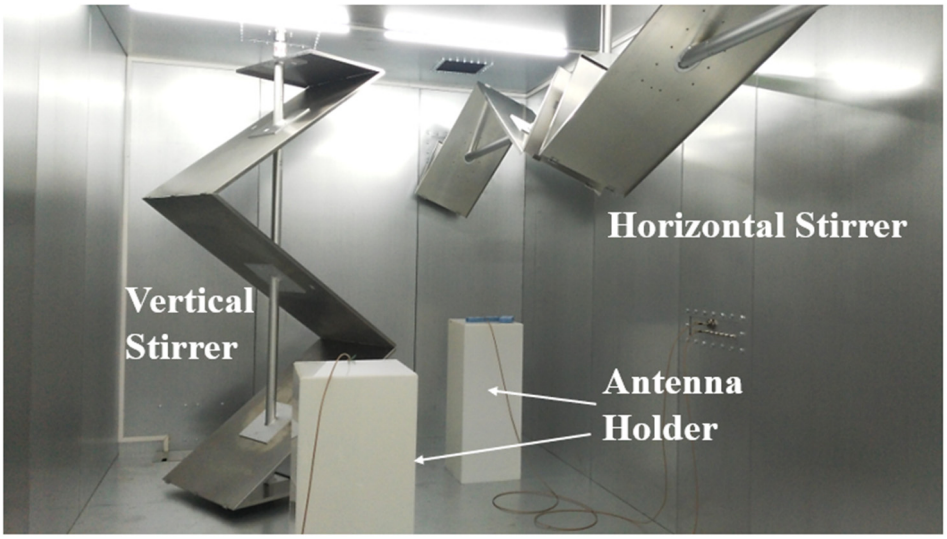

Figure 3-2：The finished in-house reverberation chamber.

Since this chamber is not a standard commercial product, characterisation is important. Two broadband Vivaldi antennas have been used to measure the chambers performance and the results (Std/Mean, field uniformity, time constant, etc.) will be discussed in the following.

The mode number versus frequency graph from equation (3-1) based on chamber size for the reverb built in this study is shown in Figure 3-3.

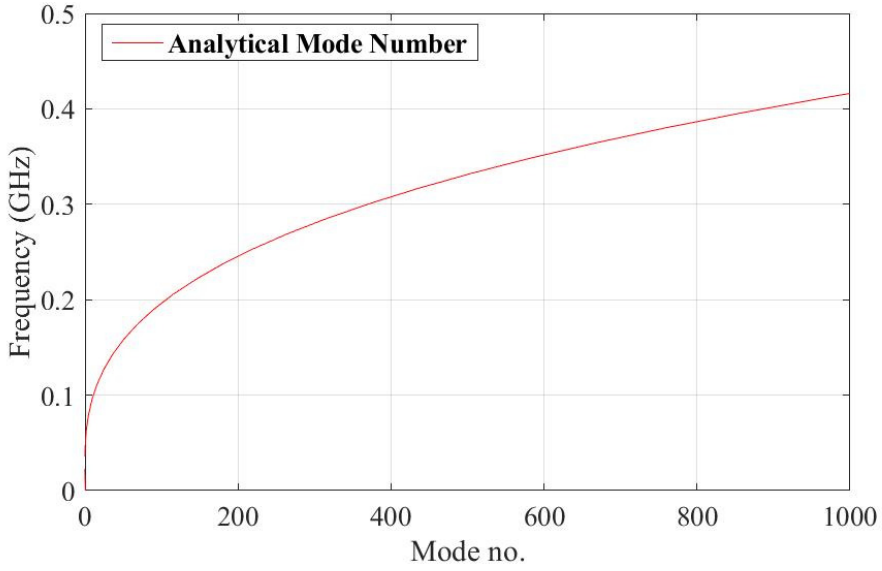

Figure 3-3：The mode number of the reverberation chamber.

The mode density of the reverb calculated with equation (3-2) in this study is provided in Figure 3-4.

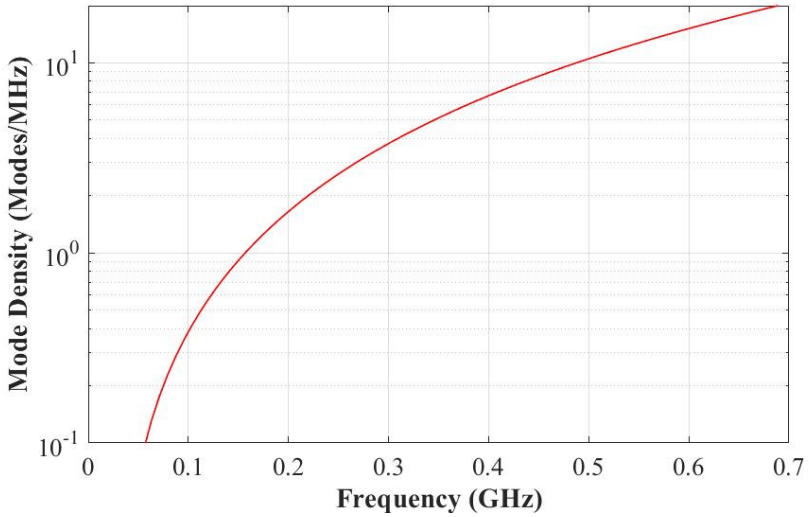

Figure 3-4：The mode density of the reverberation chamber.

The value of Std/Mean is measured with mechanical stirring and source stirring. With a 1° step size for both horizontal and vertical stirrers' rotation and six different antenna positions, a data set of 2160 S_{21} values were used to calculate the Std/Mean. The results are shown in Figure 3-5.

From the results on mode number, mode density and the Std/Mean value, it can be seen that the performance of the reverb is acceptable above 0.3 GHz, with a Std/Mean value range of ±1 dB.

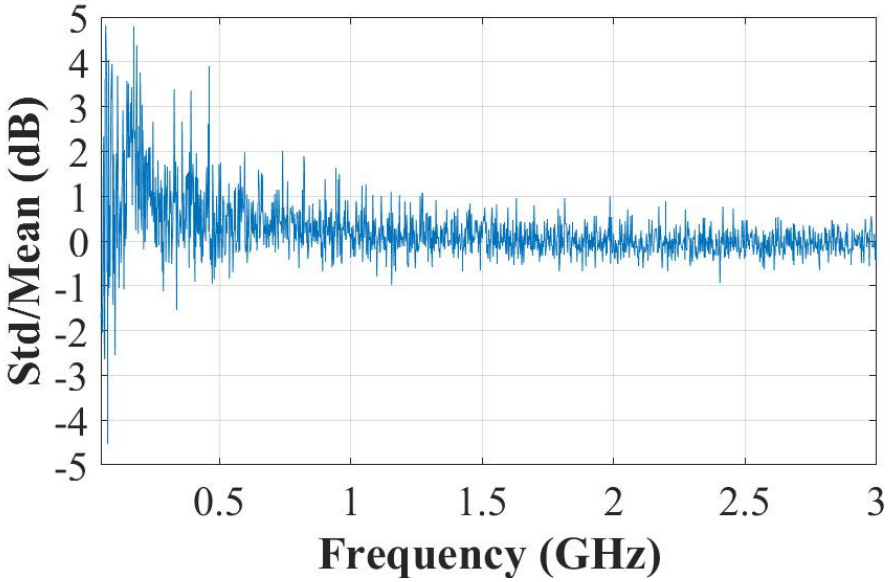

Figure 3-5：The Std/Mean value in dB of the reverberation chamber.

The FU with maximum E-field versus received power is shown in Figure 3-6. The red line here outlines the minimal FU tolerance given in [2]. When the FU level is below the limit, the chamber performance can be considered usable.

The FU with average E-field versus received power is shown in Figure 3-7.

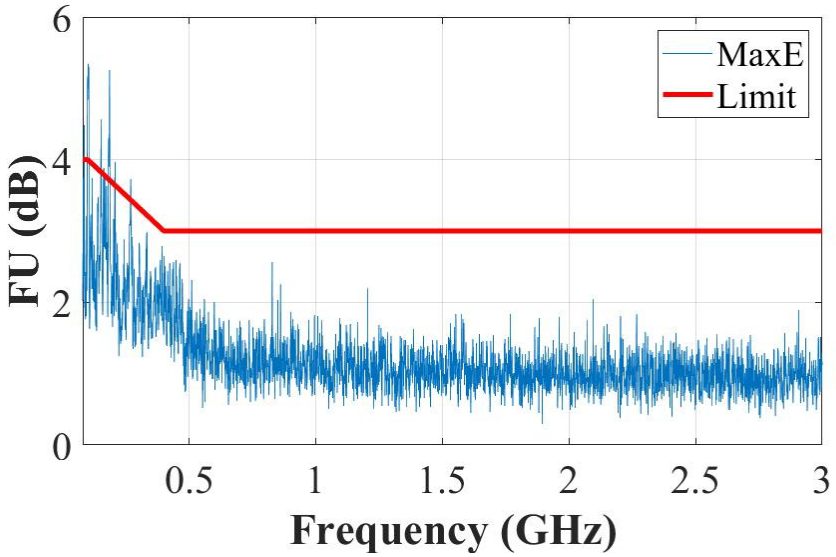

Figure 3-6：The field uniformity (FU) with MaxE in dB of the reverberation chamber.

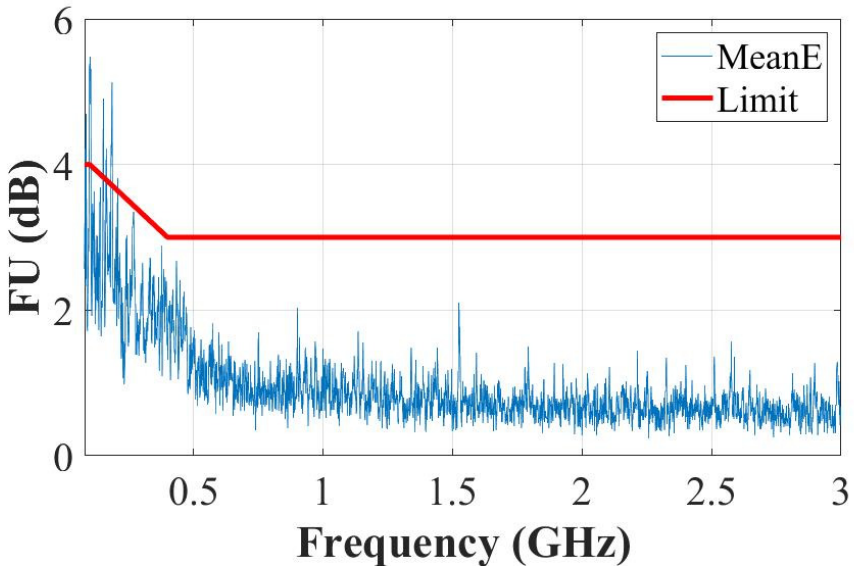

Figure 3-7：The field uniformity (FU) with MeanE in dB of the reverberation chamber.

The time constant of the chamber is shown in Figure 3-8.

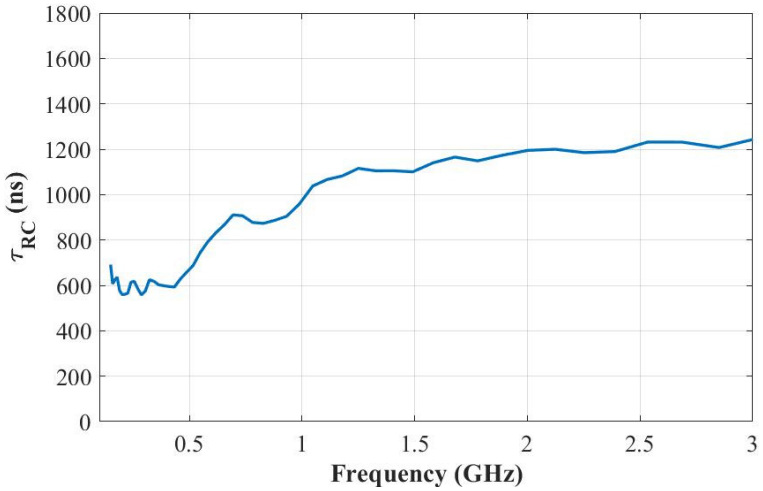

Figure 3-8：The time constant (τ) in ns of the reverberation chamber.

The maximal E-Field for an input power of 1 Watt against frequency are shown in Figure 3-9. The results are measured with Narda EP-601 E-field probes. The E-field values shown in the figure are maximal values obtained in horizontal with one fixed stirrer position (no stirring), with 15 stirrer positions over 360 degrees and 100 stirrer positions over 360 degrees. It can be seen that with more stirring positions sampled, it is possible to achieve a higher electric field intensity. This property can be used in EMC

testing to create a large E-field with limited input power. With an input power of 1 W, the E-field in the in-house chamber can achieve a level of over 60 V/m for frequencies over 1 GHz.

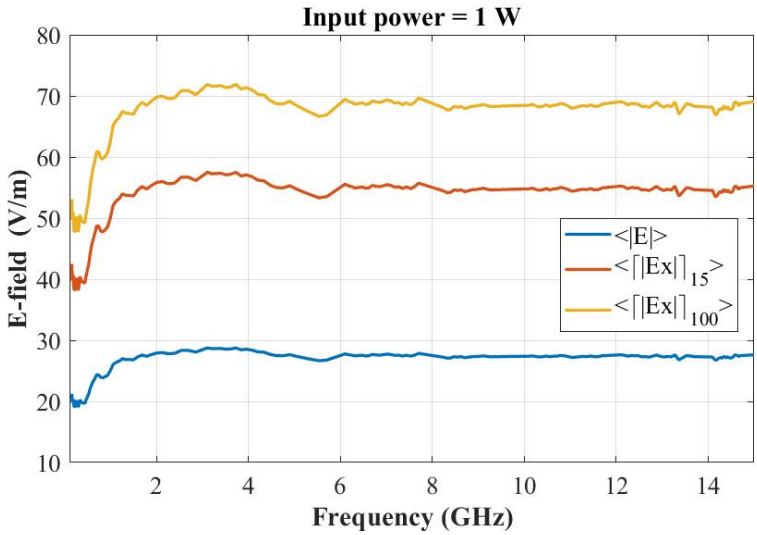

Figure 3-9：The E-field strength in V/m for the reverberation chamber.

With the previous measurements and characterisations, the performance of the in-house reverberation chamber is found to be acceptable for 300 MHz and above.

3.3 Measurement of Antenna On-body Efficiency in a Reverberation Chamber

The measurement of the on-body radiation efficiency for wearable antennas adapts the method proposed in [3]. The method requires one references antenna, one antenna undertest (AUT) and a VNA. The reference antenna is connected to port 1 of the VNA while the AUT is connected to port 2. The definition used for antenna efficiency measurement is as follows,

$$\eta_{RAD} = \left\{ \frac{\langle |S_{21AUT}|^2 \rangle}{\langle |S_{21REF}|^2 \rangle} \times \frac{1-|S_{22REF}|^2}{1-|S_{22AUT}|^2} \right\} \times \eta_{REF} \tag{3-11}$$

In this formula, <.> represents the averaging of the S parameter data set obtained with different stirring conditions. The term η_{RAD} is the radiation of the antenna under

test (AUT) and η_{REF} is the efficiency of the known reference antenna. It should be noted that for the total radiation efficiency the antenna mismatch loss, denoted as S_{22} in this case, can be measured in an anechoic chamber and the total efficiency can be calculated with the following formula,

$$\eta_{TOTAL} = \eta_{RAD} \times (1-(S_{22AUT})^2) \tag{3-12}$$

The measurement of wearable antenna efficiency generally follows the principle shown with equations (3-11) and (3-12). The main difference is that the human body dominates the losses in the chamber with its presence. The calibration of the chamber needs to be performed with the human body in the chamber as it has a severe loading effect on the chamber. The calibration is performed with two identical reference horn antennas and with the human body (including same clothing and pocket contents) in the chamber. The *S*-parameter datasets with the three types of stirring is documented as the reference value. The detailed measurement process is as follows,

1. Setting up the reference horn antennas in one position and performing *S*-parameter measurements with a stepwise changed stirrer position (180 data sets with a 2° step size for both horizontal and vertical stirrer rotations).

2. Changing the polarisation of both antennas and repeating step 1 again (360 data sets acquired at this stage).

3. Changing the transmitting antenna location and perform the previous two steps again. Four different transmitter positions are used in this case considering both the test subject's tolerance and the accuracy of the measurement.

The S parameter measured with two horns are the S_{21REF} and S_{22REF} values. One of the horns is then changed to the belt antenna attached to the test subject and the same process is repeated for one more time, obtaining S_{21AUT} and S_{22AUT}.

Enough data points must be selected to ensure sufficient modes in the chamber. The original work in [3] proposed use of a total of 710 sample points per frequency sample.

In the measurements in this study, a slightly different setting is used considering the different frequency range, equipment set up and the test subject's tolerance. The stirring sequence for the on-body measurement in this study includes mechanical stirring (2 degrees, 180 measurements), polarisation stirring (two orthogonal linear polarisations) and position stirring (4 receiver positions). A total of 1440 datasets are documented for each run to calculate the efficiency in this study. With the calibration run (two horns) and the measurement run (AUT on-body and one horn), 2880 datasets are used for the whole calculation process.

3.4 Summary

A reverberation chamber was designed constructed and characterised in XJTLU during this project. For wearable applications, the reverberation chamber enables researchers to test the antenna's on-body radiation efficiency with an actual human test subject. The reverberation chamber provides a high-accuracy and affordable solution for the assessment of the efficiency of wearable antenna designs.

3.5 Reference

[1] Q. Xu and Y. Huang, "Anechoic and Reverberation Chambers: Theory, Design, and Measurements," 2019.

[2] IEC 61000-4-21. "Electromagnetic compatibility (EMC) – Part 4–21: Testing and measurement techniques–Reverberation chamber test methods", 2.0e. *IEC Standard*, 2011.

[3] S. J. Boyes, P. J. Soh, Y. Huang, G. A. E. Vandenbosch, and N. Khiabani, "Measurement and Performance of Textile Antenna Efficiency on a Human Body in a Reverberation Chamber," *IEEE Trans. Antennas Propag.*, vol. 61, pp. 871-881, 2013.

Chapter 4 Dual-band Patch Style Belt Buckle Antenna Design

A dual-band high efficiency wearable belt buckle antenna design offering stable performance for both on and off body scenarios is presented. The proposed antenna is composed of a metal buckle affixed to a lossy leather substrate. A layer of conductive fibre is attached to the leather to provide isolation between the human body and the radiating element. A novel snap on button structure is used to feed the antenna. With the Bluetooth and Wi-Fi bands targeted, the antenna can achieve an on body realised gain of 5.10 dBi at 2.45 GHz, 4.05 dBi at 5.2 GHz and 3.31 dBi at 5.8 GHz. A simulated specific absorption rate of 0.87 W/kg is achieved which meets the SAR regulations. The on/off body radiation efficiency of the antenna is measured in a reverberation chamber. The antenna can operate in both on and off-body communication as the frequency shift induced by the human body tissue is not significant. The proposed belt antenna is a low-cost and reliable solution for smart on-body applications.

The work in this chapter is mainly based on the following publication:

R. Pei, M. P. Leach, E. G. Lim, Z. Wang, J. Wang, Y. Wang, Z. Jiang and Y. Huang, "Wearable Belt Antenna for Body Communication Networks," *IEEE Antennas and Wireless Propagation Letters*, pp. 1-1, 2020.

4.1 Motivation for the Belt Antenna Design

The increasing popularity of wearable electronic devices has brought more attention to wearable antenna designs. Wearable antenna designs must address the following three challenges during the design process, frequency shifting and radiation distortion due to the proximity of the body tissues, Specific Absorption Rate (SAR) limitations

and the ergonomics and robustness of the design. To contend with these challenges, previous studies have tried to exploit existing metal parts of personal accessories worn daily as the radiating element of the antenna. Examples of such designs include button antennas [1]-[4], watch strap antennas [5], watch frame antennas [6], zipper antennas [7], shoelace antennas and belt buckle antennas [8]-[10]. Each of these has restrictions in terms of their shape and size in order to maintain their function as daily accessories.

The belt buckle is an ideal platform for wearable antenna designs due to its solid metallic nature and relatively large size. Previous studies [9]-[10] have made use of single tongue buckles (as shown in Figure 4-1. (a) and (b)) as the main radiating element of the antenna, proving the feasibility of the structure. The loop style of these buckles results in a radiation pattern similar to a one wavelength loop antenna, which is omnidirectional in the vertical plane. The radiation pattern would mean that at least half of the energy radiated by the belt buckle would be directed into the human body, leading to low radiation efficiency and hence low realised gain. Tissue absorption would also raise concerns about SAR. These issues will be addressed through antenna system designs in Chapters 5 and 6.

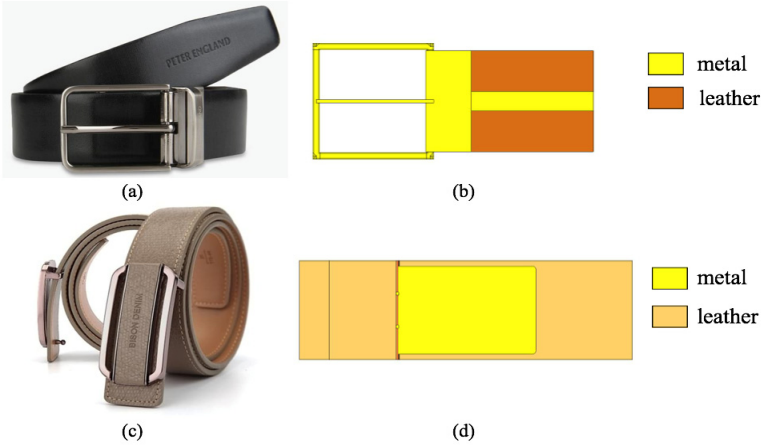

Figure 4-1：Types of belt buckle and corresponding antenna design. (a) Single tongue buckle [11]. (b) Single tongue antenna design as in [9] and [10]. (c) Pin buckle [11]. (d) Pin buckle antenna design proposed in this study.

In this section, a dual-band belt antenna aimed at Bluetooth (2.45 GHz) and Wi-Fi (2.45/5.2/5.8 GHz) applications based on a pin buckle, as shown in Figure 4-1 (c) and (d), is proposed. For this type of belt, there is a pin on the back of the buckle, which

hooks through a notch in the belt leather to hold the belt in position. In the proposed design, the buckle and the pin function as the radiating element. In addition, a layer of conductive fibre is attached to the leather to provide isolation to the human body and functions as a ground plane for the patch. A snap-on button structure, as shown in Figure 4-2, is used as the feed point as well as to hold the pin stable during use. Despite being quite lossy (a loss tangent of 0.08), leather is chosen to be the main material for the belt due to its popularity in the market.

The proposed antenna operates over bands around 2.4 GHz and 5 GHz. It has stable performance in both on-body and off-body situations. Without using any specific low loss materials for radio frequency applications, the designed antenna achieves desirable levels of on body radiation efficiency and realised gain.

4.2 Antenna Structure Design

The design is illustrated in Figure 4-2 with the key parameters detailed in Table 4-3. The metallic buckle and pin for this design are both made of brass. The snap-on button used here is a commercial one made of stainless steel. The ground layer is a conductive fibre glued to the leather belt. The conductive fibre is produced by the YGM company located in Foshan, China. The relative dielectric constant of the leather was measured to be 2.9 and the loss tangent was measured to be 0.08.

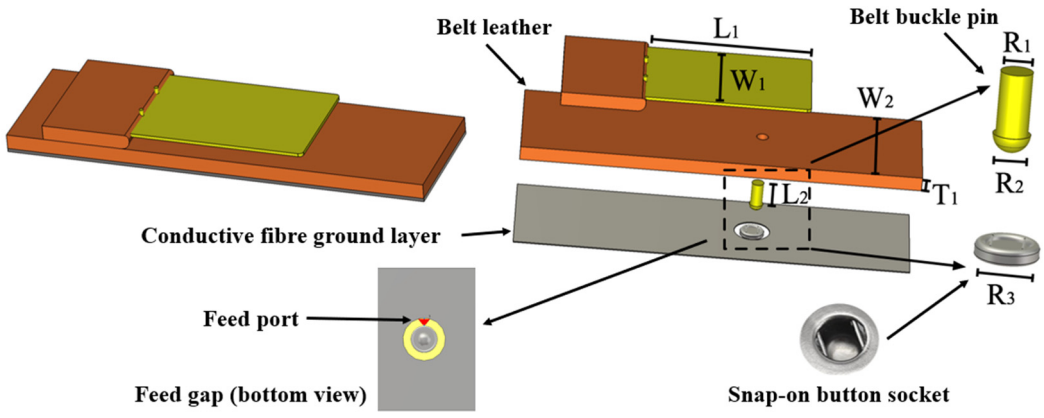

Figure 4-2：The structure of the proposed belt antenna and key parameters.

Table 4-3: Antenna Geometry Parameters

Symbol	Quantity	Value (mm)
W_1	width of the metal cap	25
W_2	width of the belt leather	30
L_1	length of the metal cap	42
L_2	length of the belt pin	7.7
R_1	radius of the belt pin	3
R_2	radius of the belt pin snap-on	3.5
R_3	radius of the snap-on button	6
T_1	thickness of the leather	3.6

Determination of the dielectric constant and loss tangent of the leather was made using a Keysight N1501A open-ended coaxial cable probe. Figure 4-3 shows the measurement apparatus.

Figure 4-3：The measurement setup for the electric properties of the leather.

Instead of a conventional holder, the human hand was used to press the open-ended testing probe firmly on the leather surface to avoid any air gaps. Low permittivity foam was placed beneath the leather to reduce any effects from the table on the measurement. Due to the limitations of the open-ended coaxial probe and measurement errors, the properties obtained have an error of approximately 15 %. A process of trial and error was used during the fabrication and measurement process of the belt buckle patch. The initial fabricated belt antenna has a frequency shift of 150 MHz. The reason of that is the measurement error of the leather permittivity. Further simulation was performed in accordance with the measured results to estimate the accurate permittivity (2.9 for the

leather used in this study). The design parameters for the belt buckle were revised and fabricated again.

At 2.45 GHz, the proposed belt antenna functions as an elevated patch antenna with a TM_{10} mode along the long side (L_1) of the buckle. The E-field distribution and a sketch of the TM_{10} mode are included in Figure 4-4. The 2D field cross-section was taken through the centre of the feeding pin to illustrate the effect of the pin on the electrical field distribution. In Figure 4-4 (a), a strong E-field distribution can be seen beneath the snap-on button, where the maximal SAR value is observed in the voxel human body analysis later.

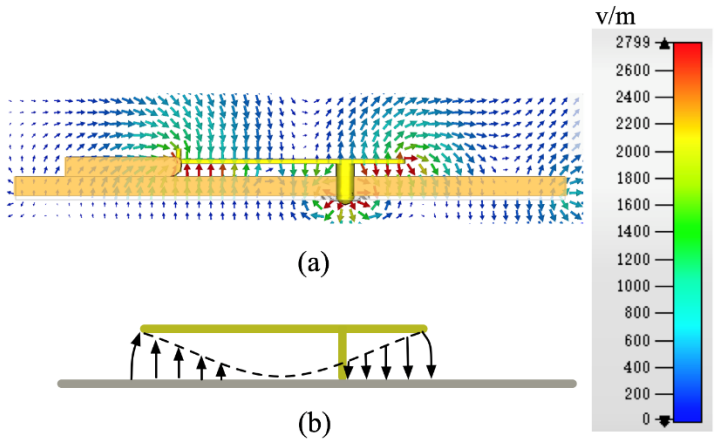

Figure 4-4：The E-field distribution of the proposed belt buckle at 2.45 GHz. (a) The simulated E-field distribution. (b) A sketch of the operation mechanism: a TM_{10} mode.

There are two reasons why the patch was designed to be elevated. The first is that the leather material selected in this design, which is widely used in belt manufacture, has a relatively large loss tangent and the elevation was found to reduce the loss and hence increase radiation efficiency in simulations. The second is that the presence of this small gap is common among pin buckle belts. In a number of belt designs studied during the research, the tip of the pin would hook to the leather and leave a gap between the metal cap and the leather. This is an ergonomic design and allows the buckle to accommodate belt leathers with slightly different thicknesses and curvatures.

The snap-on button structure was carefully designed to make sure the gap stays relatively stable when the antenna is in use. It has a locking structure, formed by two

metallic pins, to ensure solid contact between the original snap-on pin and the holder socket, as shown in Figure 4-5 (b). This structure also ensures a fixed distance between the ground plane and the radiating patch for our antenna design. The designed belt pin shares the same shape as the original snap-on button pin to ensure solid locking. Once the belt pin is locked and used on the human body, the tension would be mainly lateral to the body and hence would have little effect on the size of the gap to the underside of the buckle.

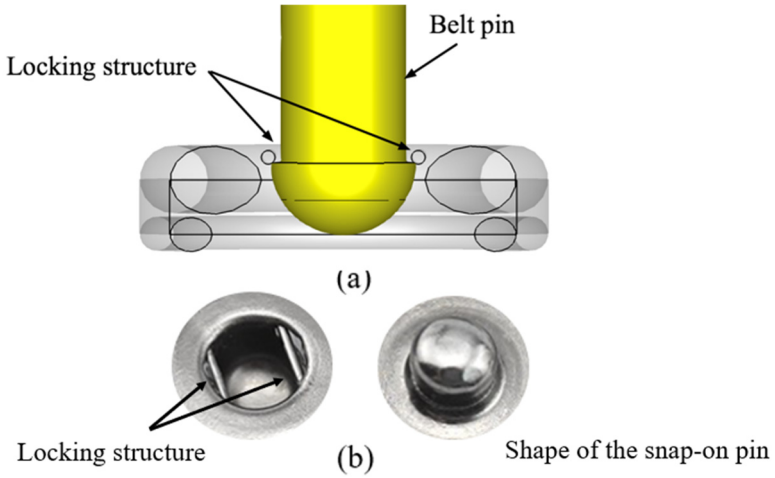

Figure 4-5：The snap-on button holding structure. (a) Crosssection view of the belt pin and the snap-on button holder. (b) The enlarged view of the snap-on holder (two holding bars) and the original snap-on pin structure.

In the 5 GHz band, the radiation follows a quasi-TM_{30} mode. The E-field distribution at 5.5 GHz is shown in Figure 4-6 (a) along with a magnified structure of the connection between the snap-on button and the belt pin. The cavity between the tip of the pin and the button sockets creates parallel capacitance, as shown in Figure 4-6 (a), which compensates for the inductance brought about by the long feeding pin. The size of the snap-on button affects the capacitance values and has to be carefully selected for impedance matching. The E-field distribution near the feeding pin does not coincide with the conventional TM_{30} mode as a transverse electrical field is present. Nonetheless, the field distribution elsewhere, especially at the radiation edge, still coincides with that of a TM_{30} mode.

The ground plane was made of conductive fibre adhered to the back of the leather.

It provided enough isolation between the radiating elements and the human body to achieve a low SAR value. A small gap is left between the conductive ground and the bottom of the snap-on button to place the feed.

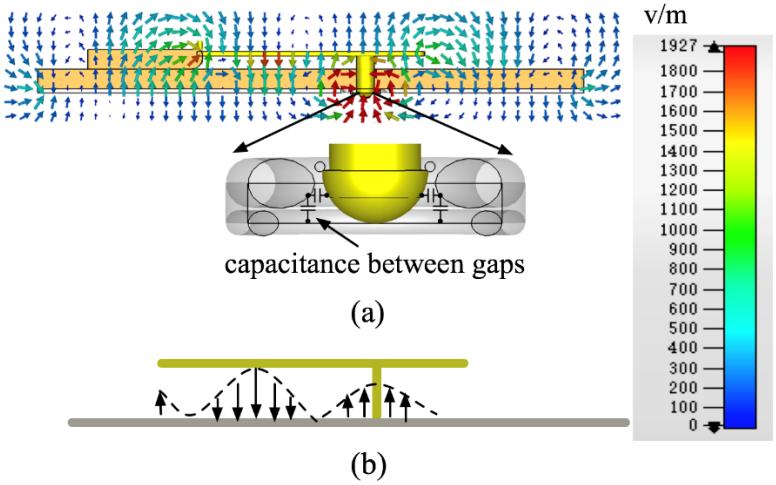

Figure 4-6：The E-field distribution of the proposed belt buckle at 5.5 GHz. (a) The simulated E-field distribution with the snap-on button structure enlarged. (b) A sketch of the operation mechanism: a quasi-TM_{30} mode.

4.3 Antenna Performance Analysis

Based on normal use the belt buckle antenna will function in close proximity to the human body and thus the effect of body tissues must be evaluated. The model Gustav (38-year-old male, 176 cm and 69 kg) from the CST voxel family was used to evaluate the effect of the human body on antenna performance. Two common postures, standing straight and sitting down were customised with CST poser and used in the analysis.

4.3.1 The effect of the standing/sitting human body.

The effects of the human body on the belt antenna performance include the following two aspects: frequency shifting due to the dielectric properties of the body tissue nearby and the reflection/absorption of the overall human body. The simulated *S*-parameters with the two human body postures are summarised in Figure 4-7 and Figure 4-8. With the isolation provided by the textile ground layer, the frequency shift

due to the human body tissue is not significant. The bandwidths for each posture, based on a -10 dB S_{11} criterion, are listed in Table 4-4. In terms of the reflection coefficient, the proposed antenna can achieve both on-body and off-body communication. In the 5 GHz band, the S_{11} value indicates a slight impedance mismatch.

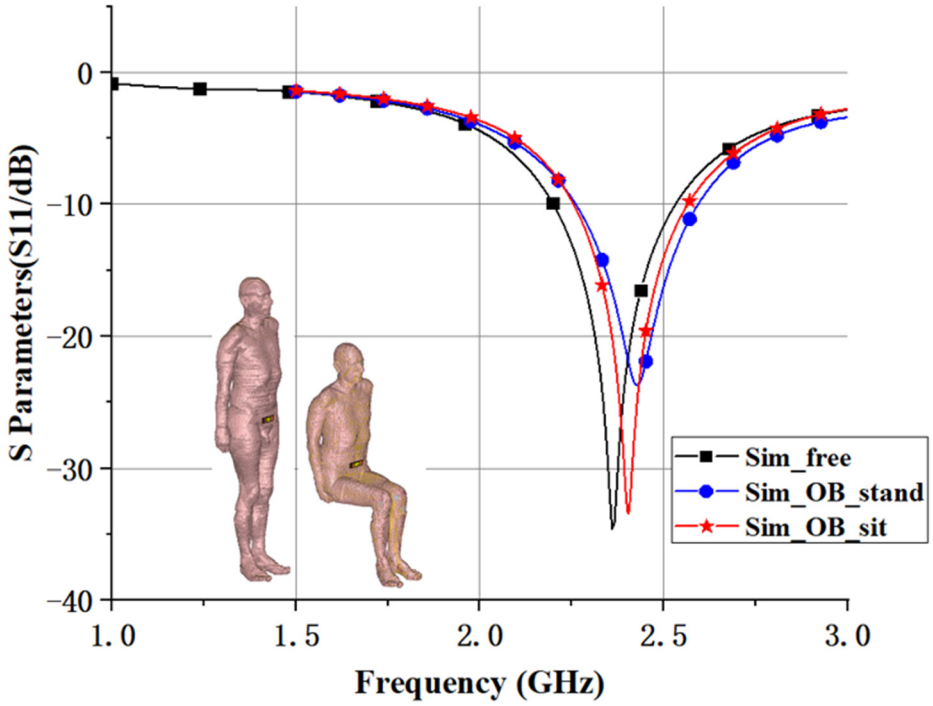

Figure 4-7：Simulated S_{11} for 2.45 GHz band with voxel models. (OB: on body).

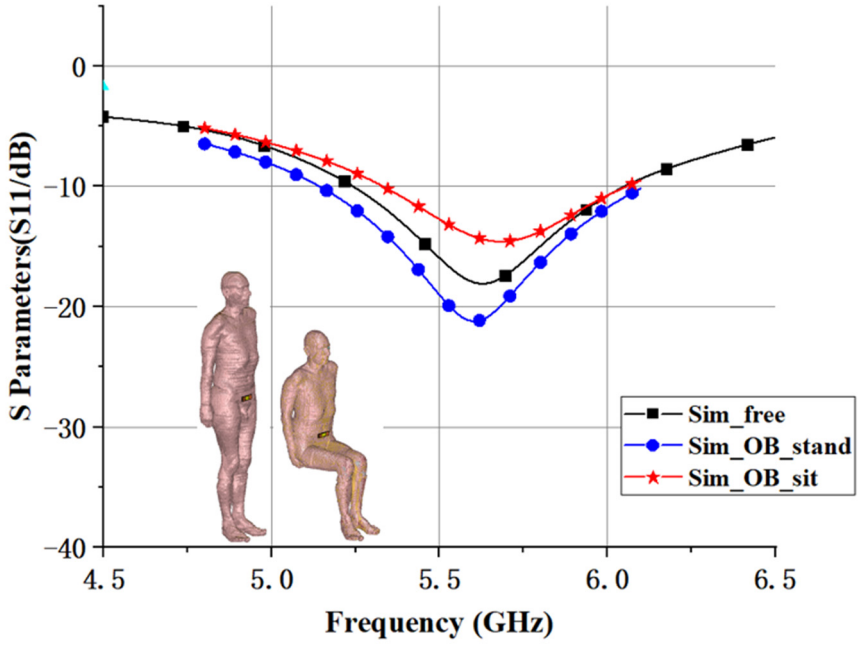

Figure 4-8：Simulated S_{11} for 5 GHz band with voxel models. (OB: on body).

4.3.2 The effect of different body composition.

Different body shapes present different material compositions. In terms of electromagnetics, this means that the dielectric properties close to the antenna are person dependent. Two additional CST voxel models have been used to analyse the performance of the antenna in this work as follows: Donna (40-year-old female, 176 cm, 79 kg, standing) and Child (7-year-old female, 115 cm, 21.7 kg, standing).

The antenna bandwidth and gain performances with different voxel models are summarised in Table 4-4. The proposed belt buckle antenna achieves relatively stable performance in terms of both bandwidth and radiation pattern across the family of human body models. The realised gain values with Donna and Child model are slightly reduced compared to those for Gustav. This is mainly because the impedance matching in the Gustav case is the best among the three. In terms of the realised gain, different body positions (standing versus sitting) have a more significant influence than different body model types as the reflection caused by the sitting condition (mainly at the upper thighs) is significantly larger. Despite the effect of body positions and body types, the antenna still operates well within the intended band with a good gain value compared to other published works.

Table 4-4: Simulated antenna performance with different voxel model

Model.	BW(GHz)/%	Realised Gain 2.45/5.2/5.8 (GHz/dBi)
Free space	2.19-2.52/13.4% 5.23-6.05/14.9%	4.59/1.73/0.92
Gustav stand	2.26-2.58/13.0% 5.14-6.1/17.4%	5.31/4.21/3.52
Gustav sit	2.25-2.56/12.6% 5.31-6.06/13.6%	6.54/5.33/4.74
Donna	2.28-2.57/11.8% 5.15-6.08/16.9%	4.97/3.91/3.37
Child	2.27-2.60/13.4% 5.22-6.06/15.2%	4.81/3.99/3.28

4.3.3 The effect of bending on the structure

Performance of the belt buckle antenna under various bending conditions used to simulate real life use has been studied. As shown in Figure 4-9, the antenna was bent onto cylinders with radii of 200 mm and 250 mm in simulation. This level of bending is more severe than the antenna would commonly experience on an actual human body estimated based on typical body size. A frequency shift can be seen as a result of the bending. The frequency shift is more severe in the 2.45 GHz band (108 MHz in 2.45 GHz band vs. 3 MHz in 5GHz band). For on-body measurements, the antenna was attached tightly to the human body to experience the actual level of bending. In both cases, the antenna performance can be considered stable and fit for the application in 2.45 GHz and 5 GHz ISM band.

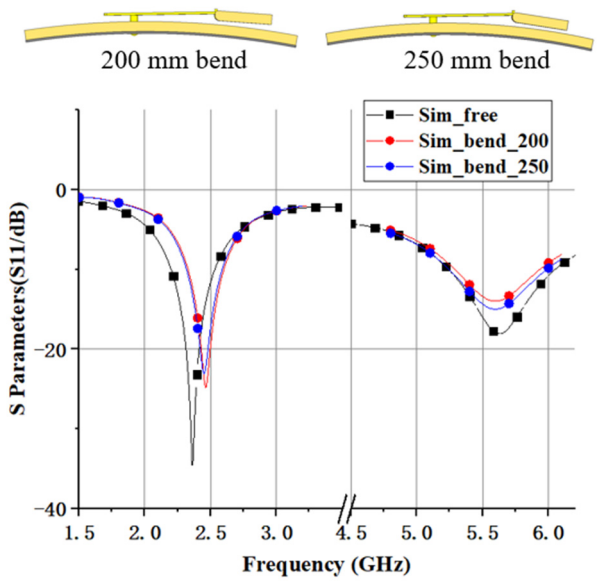

Figure 4-9：The simulated frequency shift of the belt antenna under bending towards cylinders with radii of 200 mm and 250 mm.

4.3.4 The measured bandwidth and radiation pattern

The proposed belt antenna was fabricated and tested. For ease of production, the metal structure was 3D printed with brass. The thickness of the printed buckle is 1 mm.

The resulting belt prototype is shown in Figure 4-10 (a). The off-body radiation pattern of the belt antenna was measured in an anechoic chamber as shown in Figure 4-10 (b). A holder with similar curvature of the human waist was 3D printed for the test.

The measured S_{11} is shown in Figure 4-11 and Figure 4-12 for each frequency band and compared with the appropriate simulation results. A frequency shift can be observed with human presence in both simulation and measurement. A discrepancy can be found for the sitting case between simulated and measured results. This is mainly due to the upper thighs of the human body which w closely located to the direction of the radiated field in the sitting case. In our on-body measurement, the test subject was wearing trousers and the biological composition of the test subject was different from the voxel data used during simulation. A reduction in bandwidth in the 2.45 GHz band in the on-body cases can be seen in Figure 4-11. This is likely due to the bending of the cable when placing the belt antenna close to the actual human body.

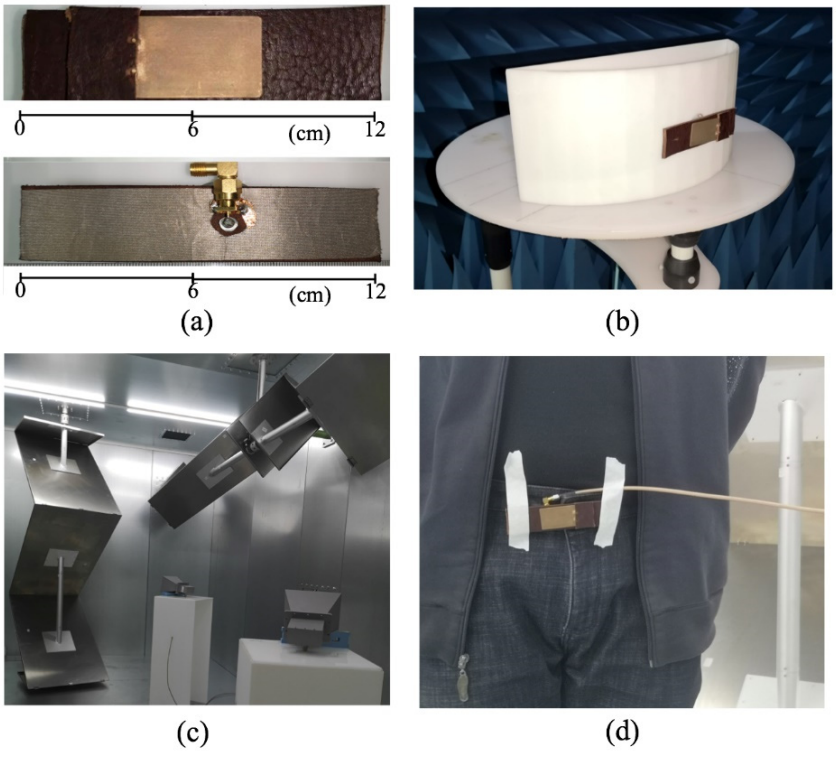

Figure 4-10：(a) Belt antenna prototype (b) Anechoic chamber measurement (c) Reverberation chamber measurement. (d) On-body measurement in reverberation chamber.

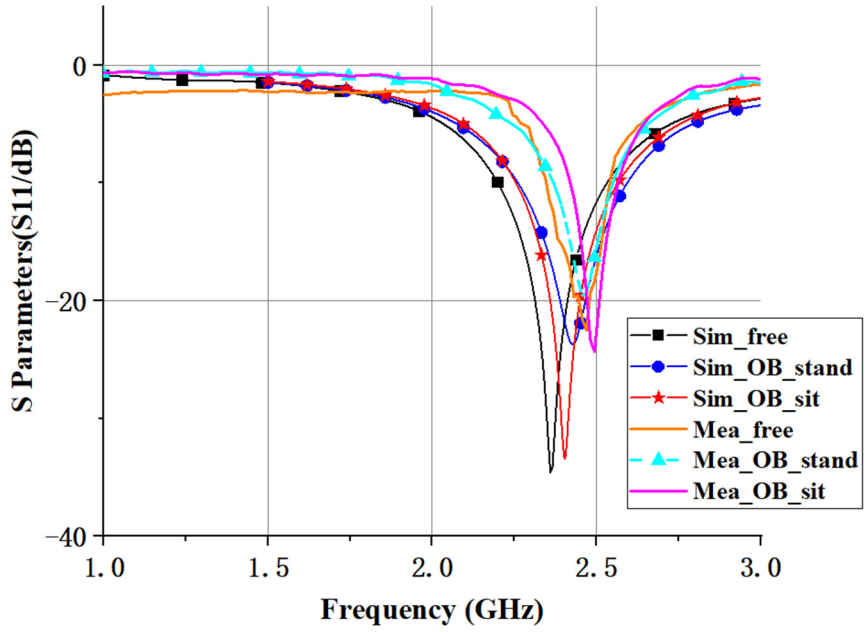

Figure 4-11：Simulated and measured S_{11} for 2.45 GHz band. (OB: on body).

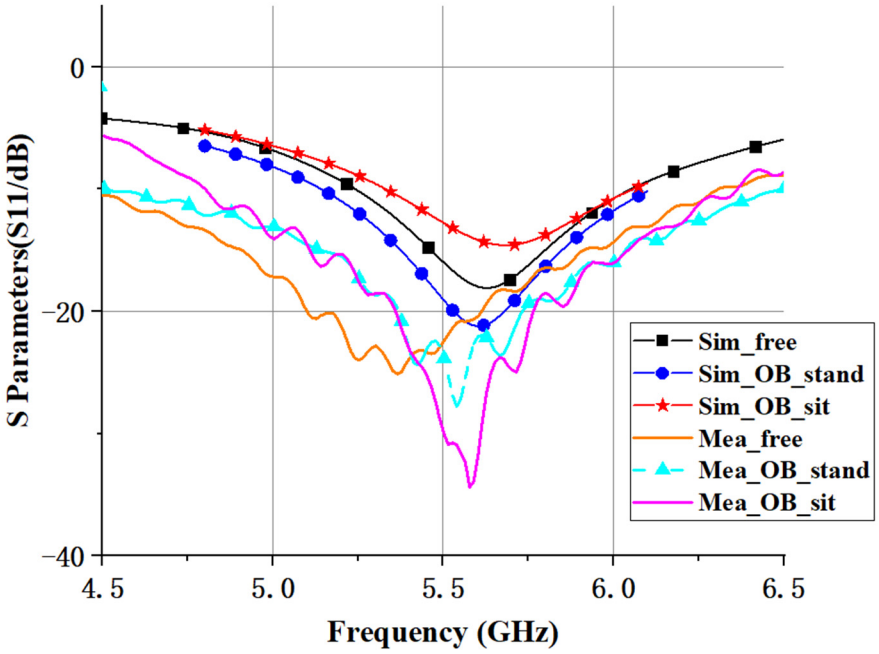

Figure 4-12：Simulated and measured S_{11} for 5 GHz band. (OB: on body).

The measured radiation patterns are shown in Figure 4-13, along with the simulated results with/without human voxel data. The measurement was performed in an in-house anechoic chamber (length: 6 m, width: 4 m, height: 3 m) with a one-dimensional rotary table. The measurement setup is shown in Figure 4-10 (b). The measured gain results

were included in Table 4-5. It should be noted that at higher frequency bands, the gain of the proposed belt antenna was lower than that of the lower bands. The nature of this TM_{30} mode (with a lower maximal gain and a wider beamwidth comparing to TM_{10}) and the higher loss at the upper frequency band both contribute to this result. Moreover, the simulated front-to-back ratio in free space is 8.275 dB at 2.45 GHz, 8.80 dB at 5.2 GHz and 4.99 dB at 5.8 GHz. The measured front-to-back ratio is 9.128 dB at 2.45 GHz, 13.31 dB at 5.2 GHz and 7.09 dB at 5.8 GHz. Due to the presence of the antenna holder in the anechoic chamber, the measured values were higher than the simulated ones. Generally, the measured results match the simulation results well.

The measured normalised radiation patterns at 2.45 GHz, 5.2 GHz and 5.8 GHz are shown in Figure 4-13. In Figure 4-13, **E_free/H_free** denotes the simulated free space radiation pattern in the E and H plane respectively for the antenna. **E_stand/H_stand** denotes the simulated radiation pattern with a standing voxel model Gustav. **E_sit/H_sit** denotes the simulated radiation pattern with the sitting voxel model Gustav. **E_meas/H_meas** denotes the measured radiation pattern results in the chamber. It should be noted that the measurement was performed in the anechoic chamber without the presence of human body due to equipment limitations. This means that the comparison of the measured results and simulation results was only fair between measured results and simulated free space radiation pattern. Comparing the free space simulation and measurement, a good agreement between simulated and measured results can be seen. When the human body was considered, the effect of the thighs in the sitting simulation can be clearly seen in the H-plane results (Figure 4-13 (b), (d) and (f)).

The SAR value was obtained by simulation according to the FCC standard and with the averaging method stated in IEEE/IEC 62704-1 [12], for an input power of 0.5 W. The results are included in Table 4-5. This input power is far in excess of that used in current Bluetooth (up to 20 dBm/100 mW for Bluetooth 5) and Wi-Fi systems (up to 20 dBm/100 mW on 2.4 GHz and 23 dBm/200 mW on 5 GHz for access points) [13].

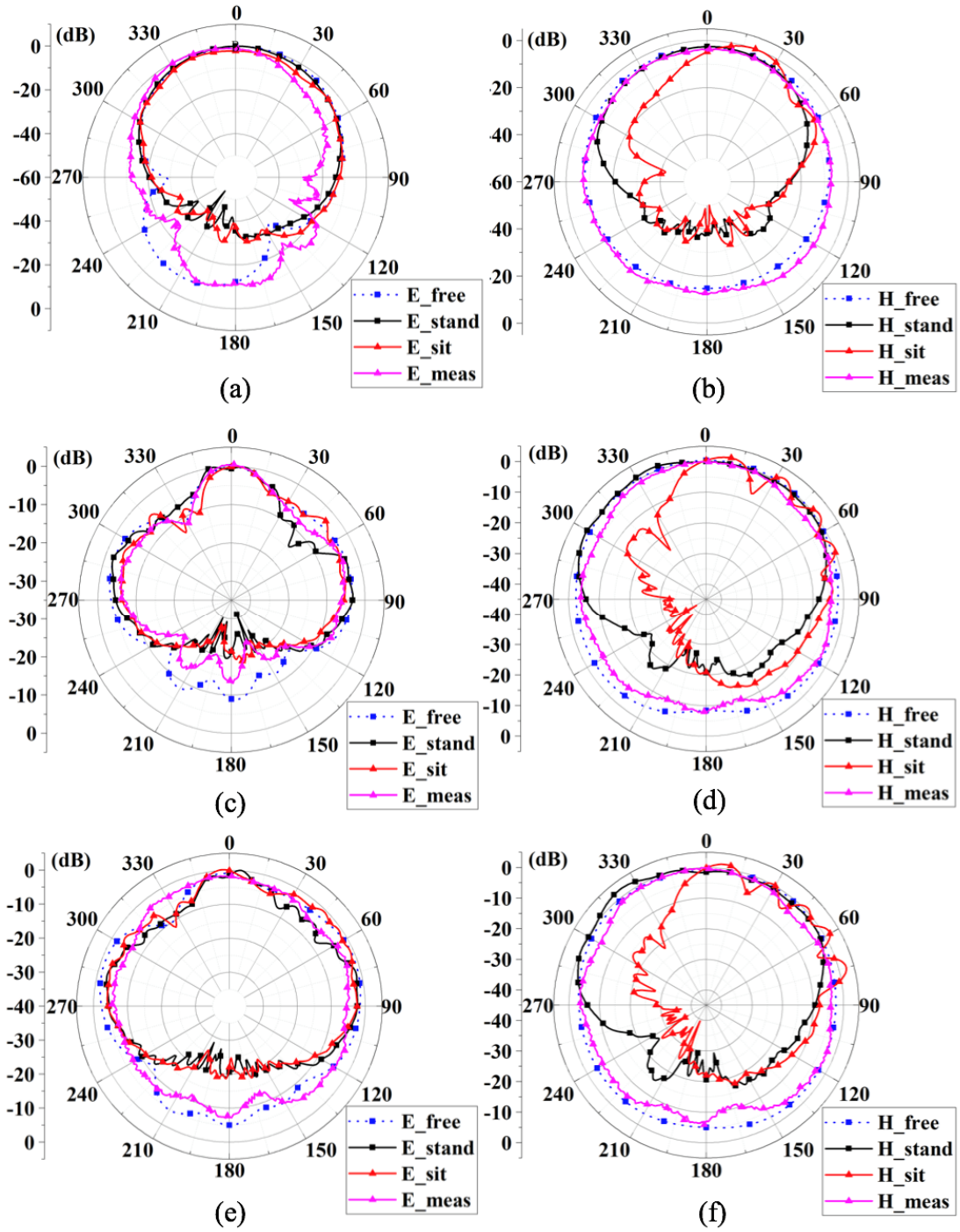

Figure 4-13：Simulated and measured radiation patterns: (a) E-plane at 2.45 GHz. (b) H-plane at 2.45 GHz. (c) E-plane at 5.2 GHz. (d) H-plane at 5.2 GHz. (e) E-plane at 5.8 GHz. (f) H-plane at 5.8 GHz.

4.3.5 The measured on-body realised gain and efficiency.

The on-body realised gain was measured in our in-house anechoic chamber with a test subject (male, 188 cm and 82 kg). The antenna was attached to the waist of the test subject with the subject standing straight during the measurement. The measured results are summarised in Table 4-5. A comparison with other state-of-the-art wearable solutions is also included in Table 4-5. It should be noted that due to the lack of original performance data, the reference [10] listed was remodelled and re-simulated in the same simulation environment as this work and data the used for comparison here came from that re-simulation.

The on-body efficiency, which is an important parameter for wearable antenna applications, was also studied with the same human subject. An in-house reverberation chamber (length: 5.4 m, width: 3.0 m, height: 2.8 m), as discussed in Chapter 3, was used to enclose both the human subject and the proposed belt antenna. The chamber has one vertical and one horizontal stirrer. The lowest usable frequency (LUF) of the chamber is 300 MHz. For on-body measurement, the belt antenna was fixed at the waist of the test subject, as shown in Figure 4-10 (d). The measurement of the on-body efficiency follows the method presented in Chapter 3. The human subject has a severe loading effect on the chamber. Thus, calibration with the human subject in the chamber is required prior to measurement. During each measurement, the dressing of the test subject was kept constant, including the contents in the subject's pockets. The stirring sequence in this experiment included mechanical stirring (2 degrees, 180 measurements), polarisation stirring (two orthogonal linear polarisations) and position stirring (4 receiver positions). A total of 1440 measured sample points were taken for each frequency point. A large number of samples were required to keep the uncertainty of the measurement to an acceptable level. Meanwhile, the number of mechanical stirs in each run was limited so that the test subject did not have to stay in the chamber for a prolonged period of time. For position stirring, in each run, the receiving antenna in the chamber was spaced by a half wavelength to the previous location, in order to create

independent samples. The resulting radiation efficiency is shown in Figure 4-14. In both frequency bands, an efficiency degradation of approximately 20 % can be seen when the belt antenna is closely attached to the human subject. Generally, the measured radiation efficiency is lower than the simulated value except for in several narrow frequency bands. This is mainly because the dielectric properties of the leather used for design and optimisation was taken at one specific frequency point (2.45 GHz in this case). The varying property of the leather will induce impedance mismatch at a wide frequency band.

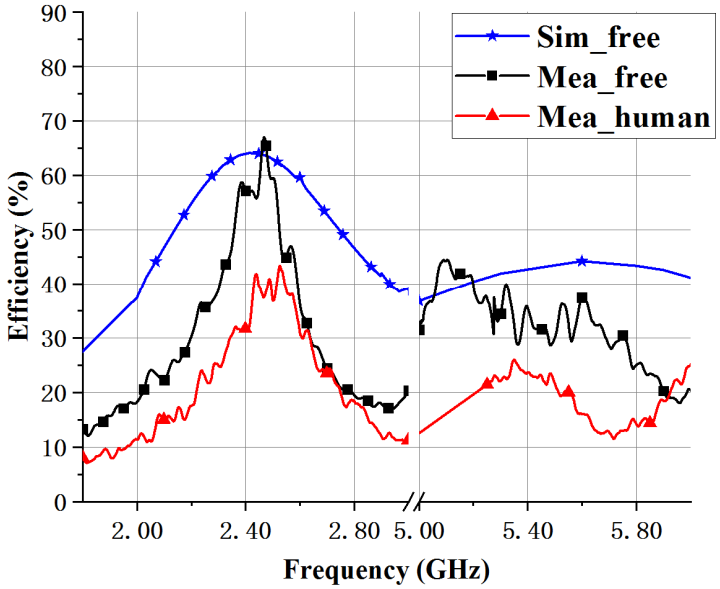

Figure 4-14：Simulated and measured radiation efficiency.

Table 4-5: Comparison of antenna performance with other systems

Ref.	BW(GHz)/%	Realised Gain (dBi)	SAR (10g)
[3] (button)	2.38-2.52/6% 4.92-6.9/36%	0.24 (2.45 GHz) 4.73 (5.2 GHz) 4.29 (5.8 GHz)	0.18 (2.45 GHz) 0.12 (5.2 GHz) 0.13 (5.8 GHz)
[6] (watch)	2.33-2.60/11%	-0.89 (2.45 GHz)	N/A
[7] (zipper)	2.37-2.49/4.92%	5 (2.45 GHz)	N/A
[8] (shoelace)	2.43(center)/11 %	9.73 (2.45 GHz)	N/A
[9] (belt)	2.45 (center)/22.8%	2.8 (2.45 GHz) 4.5 (5.25 GHz)	N/A
[10] (belt)	0.7-1.2/55.56% 1.69-2.63/38.37%	-4.16 (0.9 GHz) -8.61 (1.8 GHz) -8.61 (2.45 GHz)	1.90 (0.9 GHz) 1.63 (1.8 GHz) 1.00 (2.45 GHz)
Proposed	2.28-2.53/10.2% 4.88-6.15/23.1%	5.10 (2.45 GHz) 4.05 (5.2 GHz) 3.31 (5.8 GHz)	0.87 (2.45 GHz) 0.83 (5.2 GHz) 0.13 (5.8 GHz)

4.4 Summary

In this chapter, a dual-band belt buckle antenna based on the pin buckle belt was proposed that does not require any dedicated low-loss RF substrates. The antenna designed achieved an on-body realised gain of 5.10 dBi and radiation efficiency of approximately 40 % at 2.45 GHz. A snap-on button and pin structure was used as the feeding structure. This structure provided a sufficient level of fixture for the antenna to have a stable on-body performance. A TM_{10} and a quasi-TM_{30} mode similar to a microstrip patch antenna were formed for the two resonant frequencies. Unlike a conventional loop-based belt buckle structure, this design limits the radiation towards the inside of the human body and ensures that the specific absorption rate in both bands was well within standard safety limits [14]-[15]. The belt antenna maintains stable performance for both on and off-body communication. It is a low-cost, highly efficient, reliable solution for wearable body area network applications.

The belt buckle antenna presented in this chapter was based on a pin buckle. A

single tongue buckle with a loop style structure, when used as an antenna, typically result in an omnidirectional radiation pattern, and hence reduces on-body efficiency. However, a possible modified single tongue buckle structure is designed to overcome this drawback for a loop style belt buckle in the following chapter.

4.5 Reference

[1] X. Y. Zhang, H. Wong, T. Mo, and Y. F. Cao, "Dual-Band Dual-Mode Button Antenna for On-Body and Off-Body Communications," *IEEE Trans. on Biomed. Circuits Sys.,* vol. 11, pp. 933-941, 2017.

[2] H. Xiaomu, S. Yan, and G. A. E. Vandenbosch, "Wearable Button Antenna for Dual-Band WLAN Applications With Combined on and off-Body Radiation Patterns," *IEEE Trans. Antennas Propag.,* vol. 65, pp. 1384-1387, 2017.

[3] B. Sanz-Izquierdo, J. C. Batchelor, and M. I. Sobhy, "Button antenna on textiles for wireless local area network on body applications," *IET Microwaves, Antennas & Propagation,* vol. 4, pp. 1980-1987, 2010.

[4] S. J. Chen, T. Kaufmann, D. C. Ranasinghe, and C. Fumeaux, "A Modular Textile Antenna Design Using Snap-on Buttons for Wearable Applications," *IEEE Trans. Antennas Propag.,* vol. 64, pp. 894-903, 2016.

[5] G. Li, G. Gao, J. Bao, B. Yi, C. Song, and L. Bian, "A Watch Strap Antenna for the Applications of Wearable Systems," *IEEE Access,* vol. 5, pp. 10332-10338, 2017.

[6] S. Su and Y. Hsieh, "Integrated Metal-Frame Antenna for Smartwatch Wearable Device," *IEEE Trans. Antennas Propag.*, vol. 63, pp. 3301-3305, 2015.

[7] G. Li, Y. Huang, G. Gao, X. Wei, Z. Tian, and L. Bian, "A Handbag Zipper Antenna for the Applications of Body-Centric Wireless Communications and Internet of Things," *IEEE Trans. Antennas Propag.,* vol. 65, pp. 5137-5146, 2017.

[8] G. Li, Z. Tian, G. Gao, L. Zhang, M. Fu, and Y. Chen, "A Shoelace Antenna for the Application of Collision Avoidance for the Blind Person," *IEEE Trans. Antennas Propag.*, vol. 65, pp. 4941-4946, 2017.

[9] B. Sanz-Izquierdo and J. C. Batchelor, "A Dual Band Belt Antenna," in *2008 International Workshop on Antenna Technology: Small Antennas and Novel Metamaterials*, pp. 374-377, 2008.

[10] D. Gaspar and A. A. Moreira, "Belt antenna for wearable applications," in *2009 IEEE Antennas and Propagation Society International Symposium*, pp. 1-4, 2009.

[11] Hiren. (2017). *23 Types of Belt Buckle to Play Everyday's Style Game Perfectly.* Available: https://www.looksgud.in/blog/types-of-belt-buckle-design-men/

[12] I. Guideline, "Guidelines for limiting exposure to time-varying electric, magnetic, and electromagnetic fields (up to 300 GHz)," *Health phys,* vol. 74, pp. 494-522, 1998.

[13] M. Collotta, G. Pau, T. Talty, and O. K. Tonguz, "Bluetooth 5: A Concrete Step Forward toward the IoT," *IEEE Commun. Mag.,* vol. 56, no. 7, pp. 125-131, Jul. 2018.

[14] C. a. G. Affairs. (2016). *Specific absorption rate (SAR) for cellular telephones*. Available: https://www.fcc.gov/general/specific-absorption-rate-sar-cellulartelephones

[15] R. E. Fields, "Evaluating compliance with FCC guidelines for human exposure to radiofrequency electromagnetic fields," *OET bulletin,* vol. 65, pp. 1-52,1997.

[16] S. J. Boyes, P. J. Soh, Y. Huang, G. A. E. Vandenbosch, and N. Khiabani, "Measurement and Performance of Textile Antenna Efficiency on a Human Body in a Reverberation Chamber," *IEEE Trans. Antennas Propag.*, vol. 61, pp. 871-881, 2013.

Chapter 5 Loop Style Belt Buckle Antenna Design with Characteristic Mode Analysis

In addition to the pin buckle antenna presented in the previous section, further research on the more commonly seen single tongue buckle type is also conducted in this study. A single tongue belt buckle antenna designed with the aid of characteristic mode analysis and modified to direct radiation away from the body is proposed in this chapter. This proposed belt buckle antenna works at 2.45 GHz in the Industrial, Scientific and Medical Radio Band (ISM band) for Bluetooth Low Energy (BLE) communications. During the design process, characteristic mode analysis (CMA) was used to explore the underlying design and further optimize antenna performance.

This chapter is mainly based on work published in:

R. Pei, M. P. Leach, E. G. Lim, Z. Wang, C. Song, J. Wang, W. Zhang, Z. Jiang and Y. Huang, "Wearable EBG-Backed Belt Antenna for Smart On-Body Applications," *IEEE Transactions on Industrial Informatics*, vol. 16, no. 11, pp. 7177-7189, 2020.

5.1 Introduction

A belt with a metal buckle is an ideal platform to integrate wearable electronics not only due to its metal sections, but also its popularity in daily life. The idea of a belt buckle antenna has been considered in the previous chapter as well as in previous studies [1]-[2]; however, the previous studies did not consider the effect of the human body in detail. In this work, the effect of the body has been investigated in detail.

Characteristic mode analysis (CMA) has been applied to the structural design of the belt's metal fixtures to achieve a desirable current distribution. CMA offers two advantages in the design of such antennas, firstly, there are typically restrictions in belt

buckle shape and size which can be used to provide an initial structure for the Eigencurrent analysis required by the CMA. Secondly, since the field distribution and hence the radiation pattern is closely related to the current modes, by analysing and selecting a specific current mode, the radiation pattern of the wearable antenna can be carefully designed to be steered away from the human body. This helps to reduce the specific absorption rate (SAR) in the body as well as the effect of the human body on antenna performance.

5.2 Characteristic Mode Analysis

Developed by Garbacz and refined by Harrington and Mautz in 1971 [3]-[4], the Theory of Characteristic Modes (TCM) was initially applied to the analysis of slots in perfect electric conductors (PEC) [5], but also showed the potential to provide current model solutions for conductors with arbitrary shapes. The theory was extended to include objects with dielectric and magnetic materials as described in [6]. TCM was revisited in 2007 with specific attention drawn to the application of antenna design [7], for which it has been used extensively, for example in [8]-[10], often because it provides a physical interpretation of the antenna radiation.

For thoroughness, some key concepts and mathematics formulation are included here. The characteristic modes can be obtained as the eigenfunctions of the eigenvalue equation $\boldsymbol{X}\boldsymbol{J}_n = \lambda_n \boldsymbol{R}\boldsymbol{J}_n$ [7] where matrices $\boldsymbol{R}$ and $\boldsymbol{X}$ are the real and imaginary Hermitian parts of the impedance operator $\boldsymbol{Z}=\boldsymbol{R}+j\boldsymbol{X}$ [7]. The characteristic modes or characteristic currents $\boldsymbol{J}_n$ here can be interpreted as the real currents flowing on the conducting body. Being independent to any source or excitation, the characteristic currents only depend on the shape and size of the conductor itself. The eigenvalue term λ_n is always real and has a magnitude which describes how well the n^{th} characteristic mode radiates. When a mode resonates, the absolute value of λ_n is 0. The absolute value used as the eigenvalue can be either positive (storing magnetic energy) or negative (storing electric energy). The total current denoted by $\boldsymbol{J}$ can be expressed by (5-1)

$$\boldsymbol{J}=\sum \frac{V_n^i \boldsymbol{J}_n}{1+j\lambda_n} \tag{5-1}$$

$$\left|\frac{1}{1+j\lambda_n}\right| \tag{5-2}$$

From this formula, it can be found that the total current $\boldsymbol{J}$ is inversely dependent on the eigenvalue λ_n. Thus, the term (5-2) is more commonly used to characterize the current distribution and evaluate how well a mode resonates. This term is called the model significance (MS) which has a range between 0 and 1 and is independent of any sources or excitations. When MS is 1, the model is resonant and will radiate most efficiently. $\boldsymbol{V}_n^i$ in Equation (5-1), is the model-excitation coefficient and is defined as,

$$V_n^i=\langle J_n, E^i \rangle = \oint_n J_n \bullet E^i ds \tag{5-1}$$

This term quantifies how the excitation influences the contribution of each current mode to the total current. The term $\boldsymbol{V}_n^i \boldsymbol{J}_n$ denotes the coupling of the excitation (could be antenna feed or incident field) and the n^{th} current mode determines whether a specific mode is properly excited by the excitation source. This term also provides a conceptual guideline for placing the excitation, which should induce an electrical field or current with strong coupling to the desired model current.

5.3 Antenna Structure Design

Characteristic mode analysis was used to test the feasibility of the initial design and provide a range for further parametric study. Intuitively, the basic shape of the belt buckle will lead to a current distribution and radiation pattern similar to that of a loop antenna. However, if the belt antenna follows the radiation pattern of a conventional one-wavelength loop, a considerably large portion (up to half) of the energy will be directed towards the human body leading to a relatively low radiation efficiency and limitations on output power due to SAR regulations. Also, antenna performance would be particularly sensitive to the condition of the human body behind it (clothing, fat to

muscle ratio, etc.). Utilising a metal cap in the structure, as seen in Figure 5-1 (a), commonly used to hold the end of the belt in place, radiation can be better directed away from the body.

The characteristic modes for the shape of the belt buckle and holding cap were analysed. To save computational complexity, only the metal parts are considered, the leather belt, which is essentially a lossy dielectric material, was not included initially. The analysis at this stage did not include an excitation source. The meshed radiating element and the corresponding model significance are shown in Figure 5-1. The model significance illustrates that at 2.45 GHz there are two near-resonant modes, mode 1 and mode 4. The specific current distribution for these two modes and their associated radiation patterns are illustrated in Figure 5-2.

The current distribution of mode 1 has current maximums concentrated on each of the two sides of the buckle (along the *x*-axis), along the same two sides of the cap and in the corner of the cap connecting arms. The resulting radiation pattern is shown in Figure 5-2 (c). The pattern is almost omnidirectional in the yoz plane. In real-life scenarios, the human body will be located directly behind the metal buckle, in the negative *z* direction. The omnidirectional property of mode 1 would mean that approximately half of the radiation would be directed towards the human body. This would result in a low radiation efficiency and a high specific absorption rate.

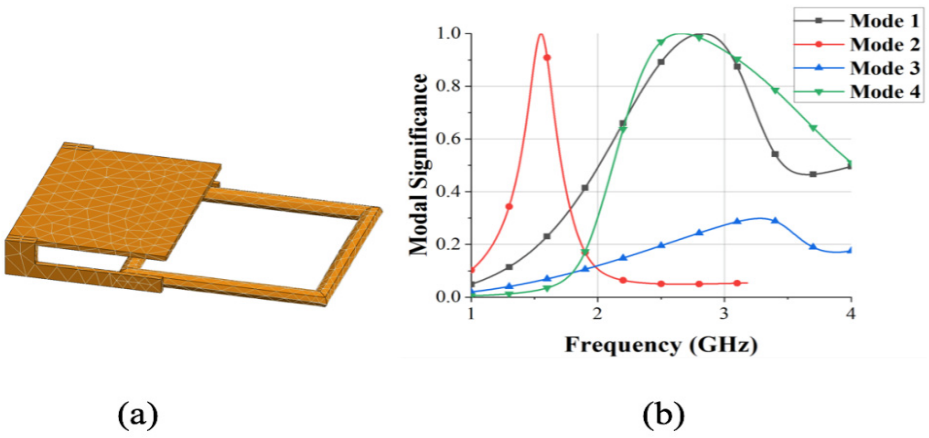

Figure 5-1：CMA anlysis of the belt. (a) The meshed metal structure of the belt buckle. (b) Model Significance.

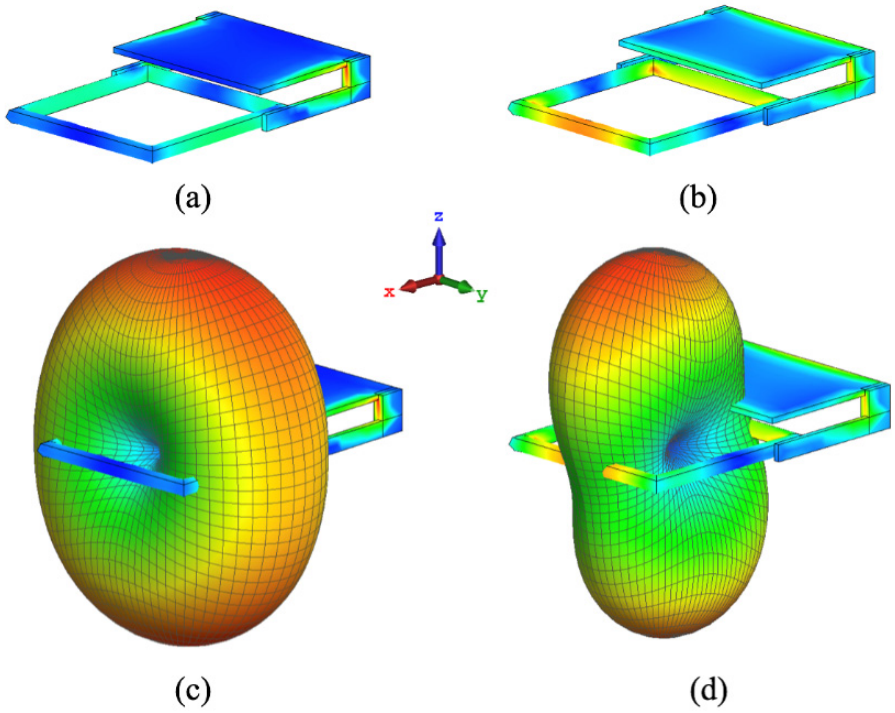

Figure 5-2：The current distribution and corresponding radiation pattern for different characteristic modes. (a) The current distribution of mode 1. (b) The current distribution of mode 4. (c) The radiation pattern for mode 1. (d) The radiation pattern for mode 4.

Meanwhile, for mode 4, the current maximums are concentrated on the belt buckle arms aligning with the *y*-axis. The main benefit of this mode is that there is a significant amount of current flow on the metal cap. The radiation pattern of this mode is bidirectional as shown in Figure 5-2 (d). This offers the potential to increase the radiation in the positive *z*-direction, away from the human body. To achieve this, the aim is to increase the current intensity on the cap and to make sure the current flow on the cap is in the same direction as the current flow on the buckle legs. In other words, the current flow on the cap and the buckle legs should be in phase to create an additive effect towards the positive *z*-direction and an out-of-phase cancelling effect towards the negative *z*-direction. By placing the feed and tuning the dimensions of the design, the intended current distribution on the metal cap can be achieved, resulting in more radiation directed away from the body. The optimal feed point was found to be at the buckle arm below the metal cap.

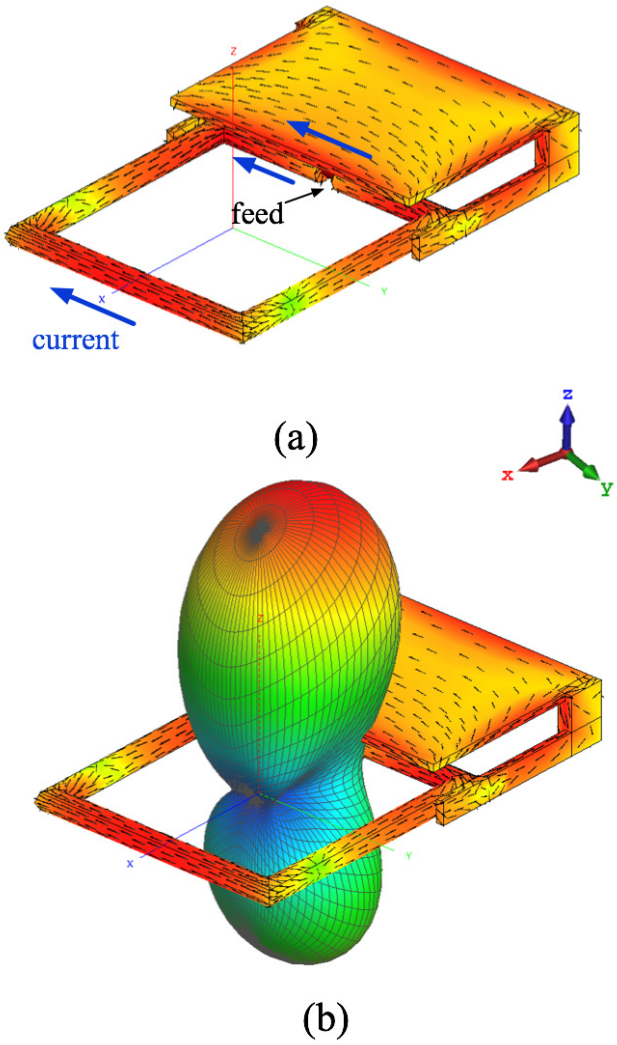

Figure 5-3：The current distribution and corresponding radiation pattern for the characteristic mode 4 with size tuning and feed added. (a) The current distribution. (b) The 3D radiation pattern.

In Figure 5-3 (a), the coupling between the excitation and the current flow, labelled with blue arrows, is maximised. With the excitation added, the radiation pattern, shown in Figure 5-3 (b), exhibits an uneven distribution as more radiating energy is guided away from the body. With the metal radiating structure determined, other essential parts of the belt, the leather and the pin were added to the model. Further optimisation of the structure parameters was required after these dielectric materials were added.

The optimised belt antenna design with all features added is shown in Figure 5-4. The metal parts include the belt buckle, the metal cap and two holding arms for the

metal cap. The material selected for these parts is brass. For ease of manufacturing, the belt pin was 3D printed from non-conducting high strength ABS material. In the belt buckle, a small gap was left to fit an SMA connector as a feed. The relative dielectric constant of the leather was measured to be 2 using a Keysight N1501 probe with the same method as described in Section 3.3. The loss tangent of the leather was measured to be 0.16.

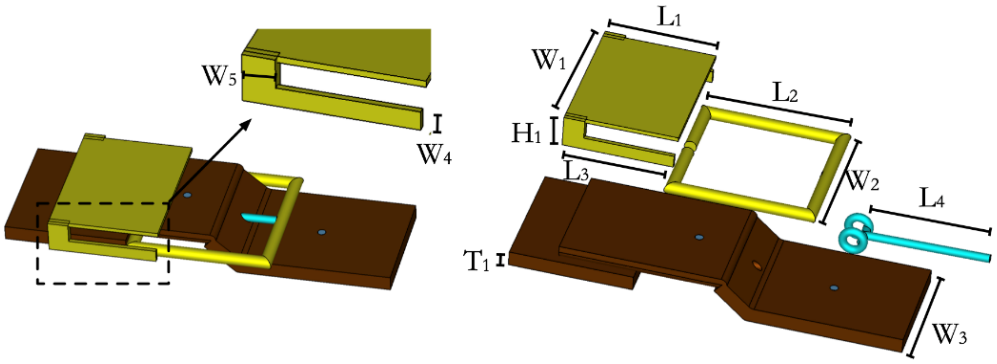

Figure 5-4：The geometry and key parameters of the belt antenna.

The final dimensions of the design are summarised in Table 5-1.

Table 5-1: The belt antenna geometry parameters

Symbol	Quantity	Value (mm)
W_1	width of the metal cap	31
W_2	width of the belt loop	31
W_3	width of the leather	25
W_4	width of the cap holding arm	3
W_5	width of the cap holding arm	5
L_1	length of the metal cap	27
L_2	length of the belt loop	30
L_3	length of the holding arm	16
L_4	length of the belt pin	25.5
H_1	height of the holding arm	7.6
T_1	thickness of the leather	3.6

The full belt antenna model was simulated in free space using Computer Simulation Technology (CST) Microwave Studio; and the 3D radiation pattern is shown in Figure 5-5 (a). The *yoz*-plane cut of the normalised radiation pattern is shown in Figure 5-5 (b).

It can be seen from the figure that a 3-dB front-to-back ratio is obtained with this belt structure. This means that a much larger portion of the radiated energy is now towards the outside of the human body. Further simulations using the CST human voxel model were performed to check the response of the structure in its proposed operating environment, around the waist of the model and the results will be discussed in the following section.

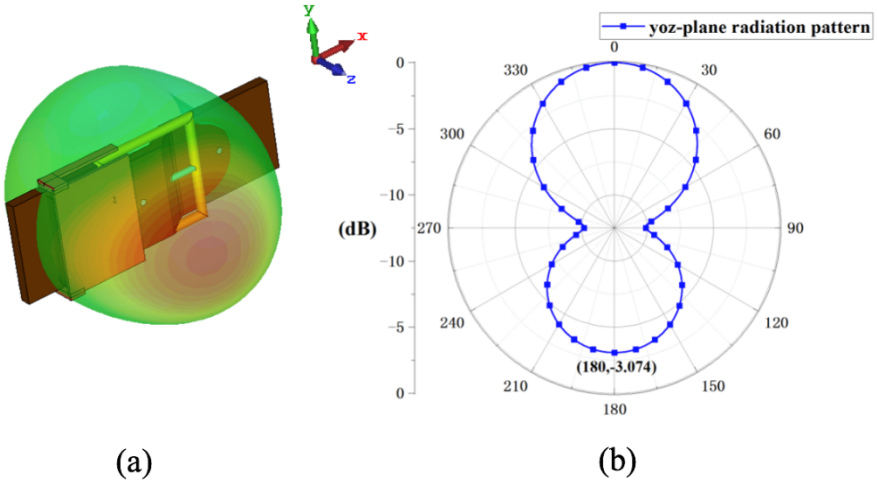

Figure 5-5：The radiation pattern for the final belt design with all features added. (a) The 3D radiation pattern. (b) The *yoz* plane cut.

5.4 Antenna Performance

5.4.1 The effect of human body on the antenna

When the belt antenna is placed close to the human body using the CST voxel human body model Gustav, a frequency shift is observed in comparison to the free space case. In the simulation, the belt leather is closely attached to the voxel model, leaving a gap of 3.6 mm (the thickness of the leather) between the radiating belt buckle and the human body model. As this situation reflects the principal usage of such an antenna, the parameters are further optimised to compensate for the on-body frequency shift; and the resulting antenna parameters are those in Table 5-1.

The main beamwidth of the belt antenna has been considered in two common body positions, standing straight and sitting down. The reflection coefficient (S_{11}) of the antenna for each of these positions is shown in Figure 5-6. In the sitting position, a greater level of absorption from the thigh causes a decrease in S_{11} and a slight frequency shift.

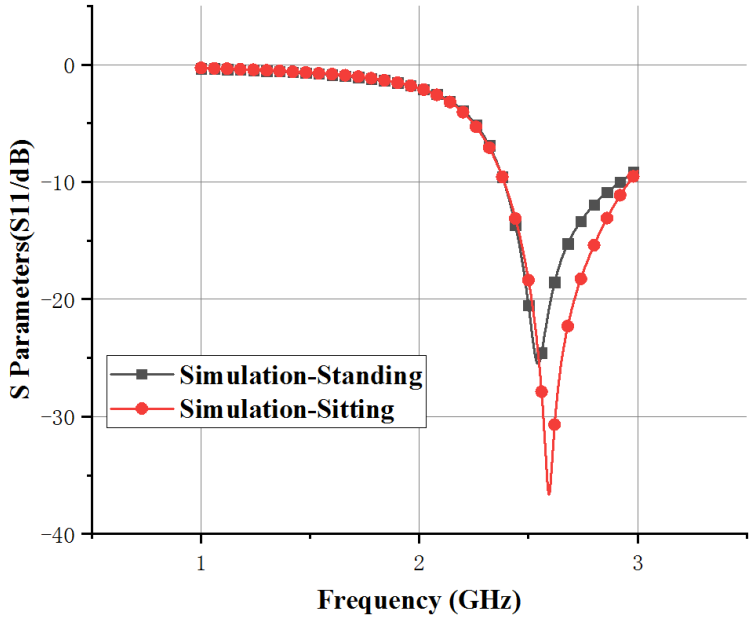

Figure 5-6：The simulated S_{11} of the belt antenna including voxel human model with two common postures.

For wearable applications, antenna radiation efficiency is a crucial indicator of antenna performance. Using the lossy voxel human body model, the resulting radiation efficiency for each body position at 2.45 GHz is given in Table 5-2. Despite more radiation being guided away from the body due to the belt cap, (recall the 3-dB front-to-back ratio in the previous section), the radiation efficiency is still only around 50%. The radiation efficiency is slightly lower for the sitting scenario as there is more absorption from the thighs, which is consistent with the S_{11} results. The realised gain, including the mismatch loss as shown in Table 5-2 confirms that the sitting position reduces the gain by almost 0.4 dB. The 3D in-situ radiation patterns for the two poses are shown in Figure 5-7 with normalised 2D E-plane and H-plane cuts shown in Figure 5-8.

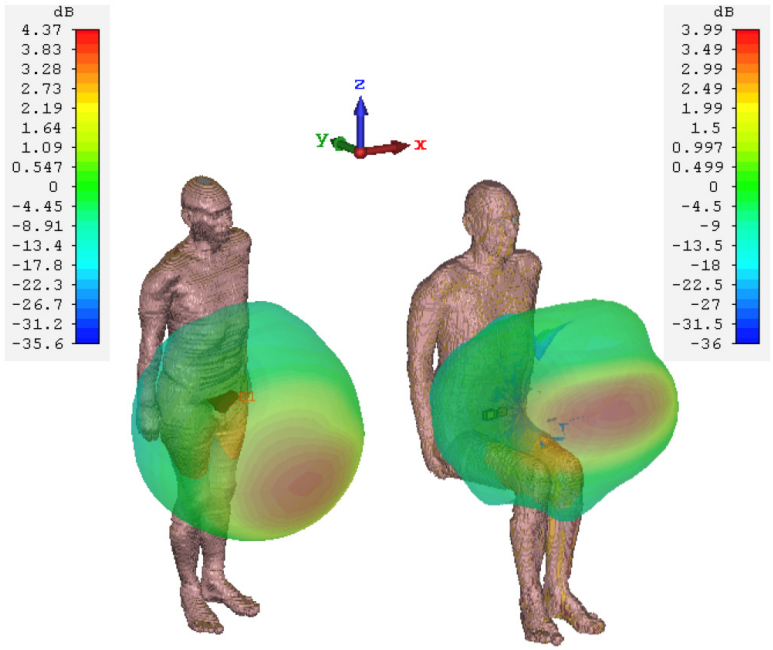

Figure 5-7：The simulated realised gain (dB) of the belt antenna including voxel human model with two common postures at 2.45 GHz.

Table 5-2: Radiation performance of the antenna at 2.45 GHz

Postion	Radiation Efficiency (%)	Realised Gain (dB)
Standing	54.36	4.373
Sitting	46.78	3.989

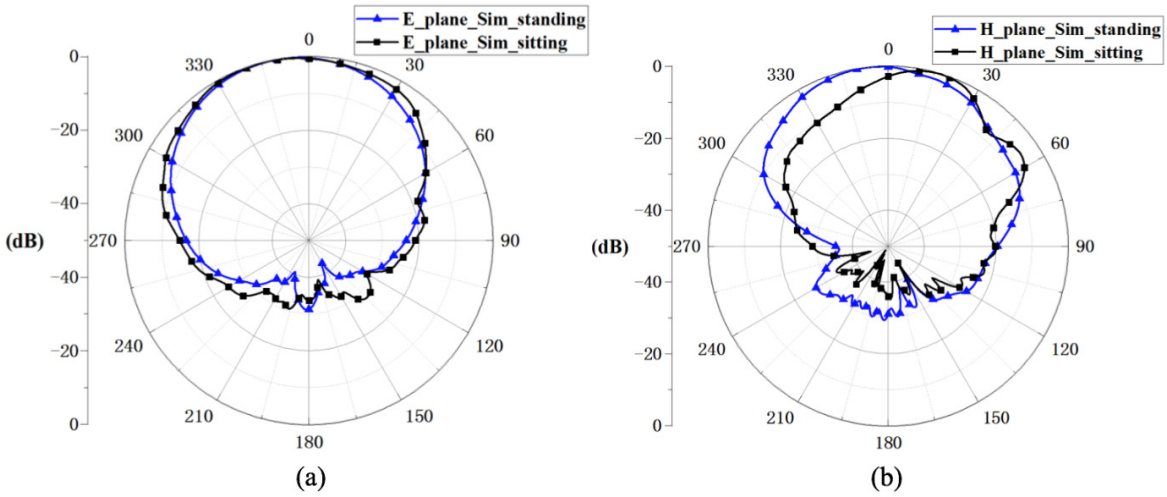

Figure 5-8：The simulated E-plane and H-plane for including voxel human model with two common postures at 2.45 GHz. (a) E-plane. (b) H-plane.

Due to the proximity of the antenna to the human body, SAR regulations must be considered. There are two common regulatory values for SAR on human body tissues, the first is imposed by the International Commission on Non-Ionizing Radiation Protection (ICNIRP) [11], which generally requires a maximum SAR value of 2 W/kg averaged over every 10 g of tissue. The second standard is from the Federal Communications Commission (FCC), which requires a maximum SAR of 1.6 W/kg averaged over each 1 g of tissue [12].

In Table 5-3, the SAR value was obtained by simulation according to the FCC standard and with the averaging method stated in IEEE/IEC 62704-1 [13], for an input power of 0.5 W. Simulated input power limitations for the antenna based on the ICNIRP and FCC standards are shown in Table 5-4. This input power is far in excess of that used by the BLE system proposed in this study, which would have a maximum output power of 0 dBm (i.e. 1 mW) [14]. The SAR distribution averaged over 10 g is shown in Figure 5-9. In both sitting and standing conditions, the maximal SAR was concentrated beneath the centre of the belt buckle loop.

Table 5-3: SAR value of the antenna at 2.45 GHz (0.5 W input power)

Postion	SAR (1g)	SAR (10g)
Standing	8.03 W/kg	2.71 W/kg
Sitting	3.16 W/kg	1.67 W/kg

Table 5-4: Maximum input power to meet SAR regulations

Postion	ICNIRP (2W/kg for 10g)	FCC (1.6W/kg for 1g)
Standing	370 mW	100 mW
Sitting	600 mW	190 mW

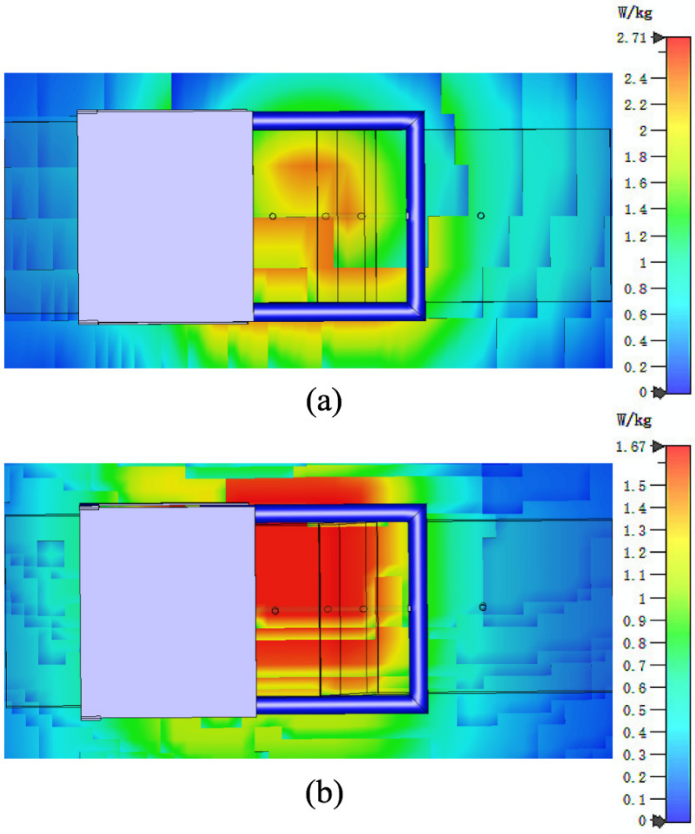

Figure 5-9：The SAR distribution of the belt antenna without the EBG. (a) The distribution with the standing model averaged over 10 g tissue. (b) The distribution with the sitting model averaged over 10 g tissue.

5.4.2 A comparison with conventional loop-like belt antenna

In this section, the antenna performance with the presence of the human body was studied. In order to determine the performance enhancement of this design quantitatively, the structure presented in [2] was used as a comparison. Since the radiation pattern and accurate efficiency data were not provided in the original paper, the design was re-modelled and simulated in the same simulation environment used here. At its design frequency, 1.8 GHz, the radiation pattern is similar to a one-wavelength loop antenna, omnidirectional in the vertical plane, resulting in almost half of the radiated energy being directed towards the human body. The simulation of the antenna showed a radiation efficiency of 3.61 % and a realised gain of -8 dBi when applied to the same voxel human body model used in the previous section. The belt

buckle antenna proposed here achieved a radiation efficiency of 54.35 % and a realised gain of 4.37 dBi under the same conditions. This numerical comparison demonstrates the effectiveness of this novel belt buckle structure design presented.

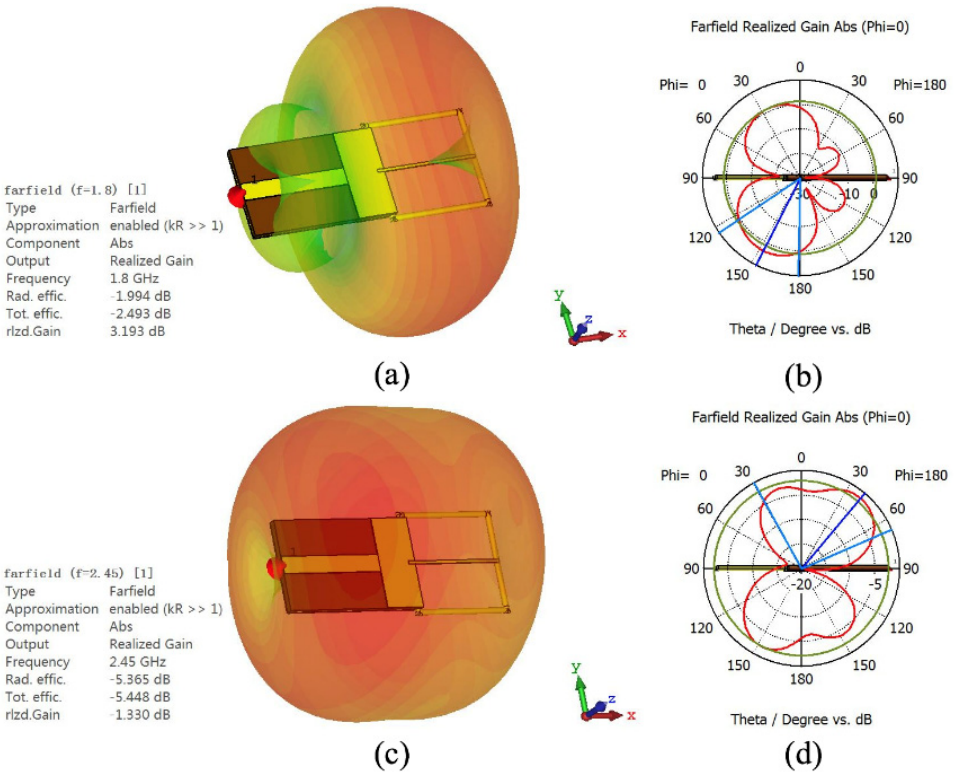

Figure 5-10：The radiation pattern of the loop belt structure proposed in [1] re-simulated.

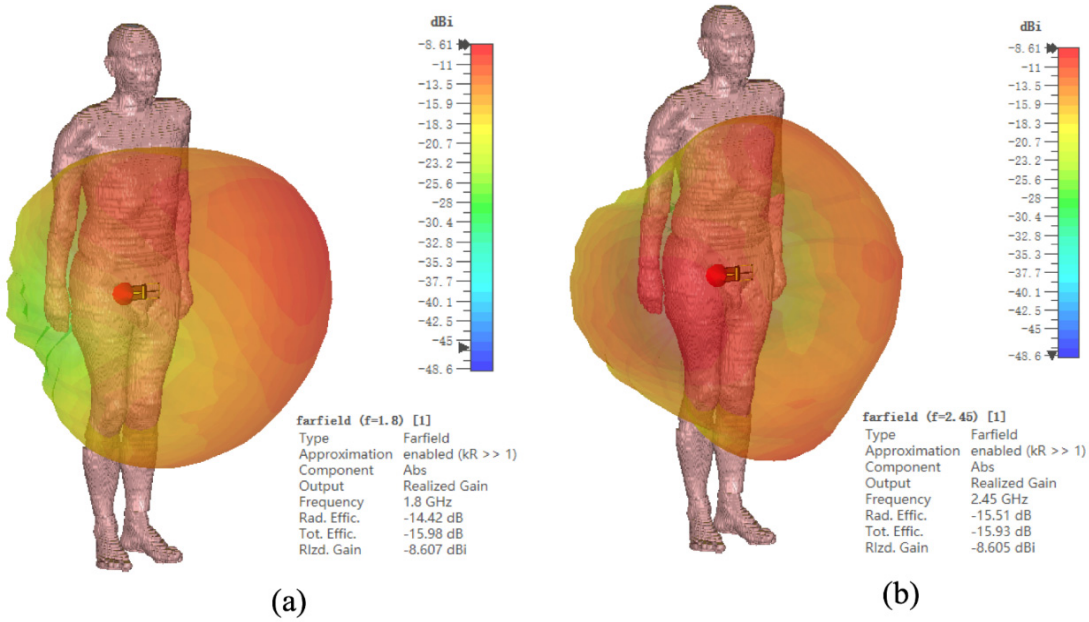

Figure 5-11：The radiation pattern of the loop belt structure proposed in [1] re-simulated with voxel human body model.

5.5 Summary

In this section, a novel belt buckle antenna developed with the aid of characteristic mode analysis and able to direct more radiation away from the human body through the use of a raised cap section was presented. The advantages of the proposed antenna structure and the effectiveness of CMA in wearable antenna designs are shown with analysis of the antenna performance with voxel human body models and a comparison with another proposed belt antenna. The proposed antenna can achieve an on-body radiation efficiency of over 50 %. The antenna can be considered safe for BLE systems which have a maximum output power of 0 dBm.

5.6 Reference

[1] B. Sanz-Izquierdo and J. C. Batchelor, "A Dual Band Belt Antenna," in *2008 International Workshop on Antenna Technology: Small Antennas and Novel Metamaterials*, pp. 374-377, 2008.

[2] D. Gaspar and A. A. Moreira, "Belt antenna for wearable applications," in *2009 IEEE Antennas and Propagation Society International Symposium*, pp. 1-4, 2009.

[3] R. Garbacz and R. Turpin, "A generalized expansion for radiated and scattered fields," *IEEE Transactions on Antennas and Propagation*, vol. 19, pp. 348-358, 1971.

[4] R. Harrington and J. Mautz, "Theory of characteristic modes for conducting bodies," *IEEE Transactions on Antennas and Propagation*, vol. 19, pp. 622-628, 1971.

[5] A. EI-HajJ, and K. Y. Kabalan, "Characteristic Modes of a Rectangular Aperture in a Perfectly Conducting Plane," *IEEE Transactions on Antennas and Propagation*, vol. 42, pp. 1447-1450, 1994

[6] R. F. Harrington, J. R. Mautz, and Y. Chang, “Characteristic modes for dielectric and magnetic bodies,” *IEEE Transactions on Antennas and Propagation*, vol. 20, pp.

194–198, 1972.

[7] M. Cabedo-Fabres, E. Antonino-Daviu, A. Valero-Nogueira, and M. F. Bataller, "The Theory of Characteristic Modes Revisited: A Contribution to the Design of Antennas for Modern Applications," *IEEE Antennas and Propagation Magazine*, vol. 49, pp. 52-68, 2007.

[8] F. H. Lin and Z. N. Chen, "Low-Profile Wideband Metasurface Antennas Using Characteristic Mode Analysis," *IEEE Transactions on Antennas and Propagation*, vol. 65, pp. 1706-1713, 2017.

[9] X. Yang, Y. Liu, and S. Gong, "Design of a Wideband Omnidirectional Antenna with Characteristic Mode Analysis," *IEEE Antennas and Wireless Propagation Letters*, vol. 17, pp. 993-997, 2018.

[10] Q. Zhang, R. Ma, W. Su, and Y. Gao, "Design of a Multimode UWB Antenna Using Characteristic Mode Analysis," *IEEE Transactions on Antennas and Propagation*, vol. 66, pp. 3712-3717, 2018.

[11] ICNIRP, "Guidelines for limiting exposure to time-varying electric, magnetic, and electromagnetic fields (up to 300 GHz)," *Health phys*., vol. 74, pp. 494-522, Apr. 1998.

[12] FCC (2016). *Specific absorption rate (SAR) for cellular telephones* [online].Available: https://www.fcc.gov/general/specific-absorption-rate-sar-cellular-telephones.

[12] K. Chan, R. F. Cleveland, D. L. Means, "Evaluating compliance with FCC guidelines for human exposure to radiofrequency electromagnetic fields," *OET bulletin*, vol. 65, Dec. 1997.

[13] C. Gomez, J. Oller, and J. Paradells, "Overview and Evaluation of Bluetooth Low Energy: An Emerging Low-Power Wireless Technology," *Sensors*, vol. 12, 2012

Chapter 6 Textile EBG Ground Plane for the Belt Antenna

A textile ground plane has been designed to be integrated into trouser fabric behind the belt buckle antenna of Chapter 5 to provide isolation from the body and simultaneously improve antenna radiation characteristics. Through the application of the ground plane, the belt buckle antenna achieves a maximum realised gain of 7.94 dBi and a minimum specific absorption rate (SAR) of 0.04 W/kg at 0.5 W input power at 2.45 GHz. Two EBG structures were designed and analysed in detail for this application scenario. The suspended transmission line method was used to evaluate EBG performance variations when the textile ground plane was bent. A prototype of the system was fabricated and tested. Experimental results showed that the belt antenna, together with the textile EBG ground plane, is an excellent candidate for a smart belt system with desirable radiation pattern, efficiency, and safety limit.

This chapter is mainly based on the following publication:

R. Pei, M. P. Leach, E. G. Lim, Z. Wang, C. Song, J. Wang, W. Zhang, Z. Jiang and Y. Huang, "Wearable EBG-Backed Belt Antenna for Smart On-Body Applications," *IEEE Transactions on Industrial Informatics*, vol. 16, no. 11, pp. 7177-7189, 2020.

6.1 Motivation for the Ground Plane Design

From Chapter 5, the performance of the belt antenna can be considered appropriate for establishing a BLE link for a smart belt application. However, the efficiency of the antenna is still significantly influenced by the human body. Also, if the belt antenna was to be used in applications requiring a higher antenna input power level, for example, the latest Bluetooth 5 protocol which has a maximal output power of 20 dBm [1], SAR limitations could still present a problem. In real-life applications, a belt is commonly

worn with pants or trousers located between the belt and the human body. The utilisation of this material area offers the potential to further improve antenna performance. For example, by placing a ground plane between the antenna and the human body, the efficiency and gain of the on-body antenna can be increased. A conventional metallic ground would need to be located at a distance of around a quarter of the operating wavelength from the radiating element, otherwise, the mirrored currents due to the ground plane would interfere destructively with currents in the radiating element, reducing radiation efficiency. For the belt antenna scenario, leaving a quarter wavelength distance or using high dielectric constant materials to reduce the distance is not realistic.

Using an electromagnetic bad-gap (EBG) structure as a ground plane woven into the garment worn between belt and body would allow the ground plane to be placed directly beneath the radiating element. It should be noted that the EBG structures in this study have been denoted as high impedance surfaces (HIS) or artificial magnetic conductors (AMC) in other literature [2]-[5]. In previous studies, EBG substrates and ground plane layers have been applied to loop antennas and planar slot antennas to achieve low profile, high gain antenna performance [2]-[5]. In this study, the EBG structure is situated separately from the radiating element, thus acting more like a reflector located very close to the radiating element. Unlike the rigid belt structure, the textile EBG structure will experience a level of mechanical bending in-situ. Also, effects like stretching make it difficult to model the textile EBG in simulation accurately. The process of textile EBG design is discussed in the following sections.

6.2 Analysis of Two Basic EBG Unit Cell Structures

Two EBG structures suitable for loop-style linear polarised antennas [3]-[5], square patches with vias (also named mushroom-like structures) and concentric squares, have been analysed according to this specific application scenario. The unit cell designs of the two types of EBG are shown in Figure 6-1 (a) and (b). Each unit cell consists of a

conductive upper layer, a dielectric substrate, and a conductive ground plane. For mushroom-like structures, a conductive shorting via is located at the centre of the patch. Concentric square designs can provide dual band gap properties and are commonly applied with dual-band antenna though in this design only a single band was targeted.

The simplified equivalent circuits of the two structures are shown in Figure 6-1. The conducting loop of the square structure is characterised as inductance L_1 and the inter-element capacitance is characterised as capacitance C_1. For the concentric square structure, the conducting central loop is characterised by inductance L_2, the outer loop by inductance L_3 and the ground plane by inductance L_4. The gap between the outer and inner loops gives rise to capacitance C_2 and the inter-element capacitance is denoted by capacitance C_3. The resonant frequency of each structure can be determined from the capacitances and inductances of the equivalent circuits.

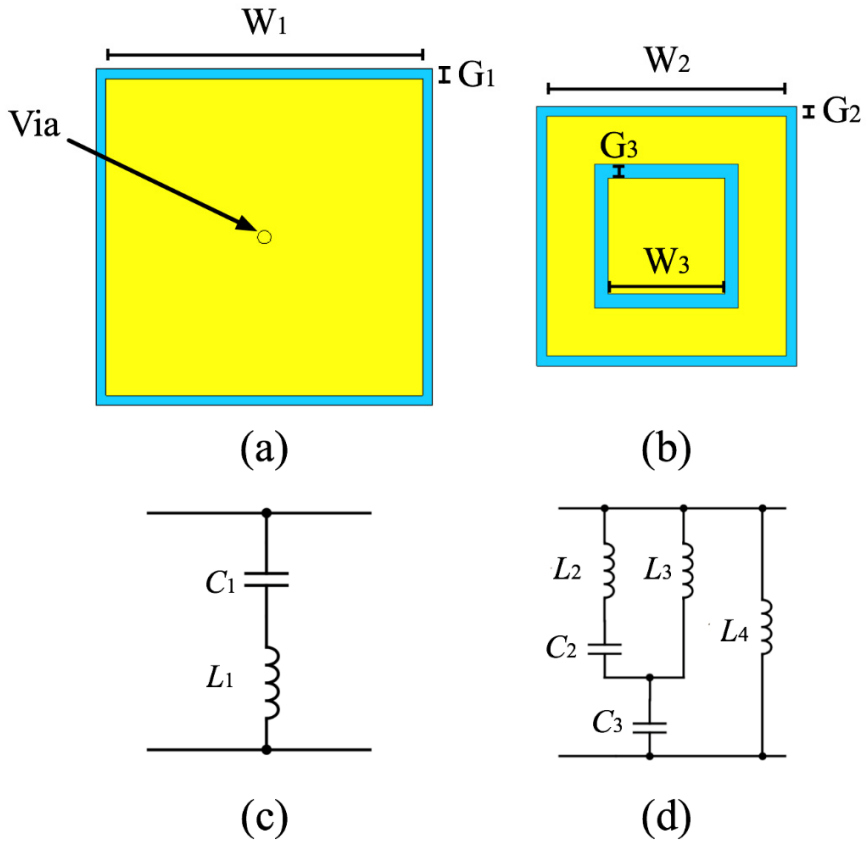

Figure 6-1：The unit cell structure of two types of EBG structure and their equivalent circuits. (a) The square patches with vias. (b) The concentric squares. (c) The simplified equivalent circuit of square patches. (d) The simplified equivalent circuit for concentric squares structure.

6.3 Application of the Textile EBG with the Belt Antenna

For an EBG plane to be used as a ground plane, a resonant cavity model previously developed for a planar antenna with an EBG surface can be used [6]. The main difference between other planar EBG ground plane designs and this textile EBG ground plane with the belt antenna is that the radiating element here is not on a flat plane, which leads to different distances between the partial reflective surface and the main radiating sections. This relationship is illustrated in Figure 6-2, in which 3 radiating sub-elements are labelled for detailed analysis. The upper layer of the textile EBG is denoted as a partial reflective surface (PRS) and the bottom layer is denoted as a perfect electric conductor (PEC). The PRS has two significant parameters, the reflection phase coefficient ϕ_R and the transmission phase coefficient ϕ_T. The phase shift introduced by the PEC surface is π. Ray optics analysis, which has been used for high gain planar antennas with PRS [6], has been applied to analyse this scenario.

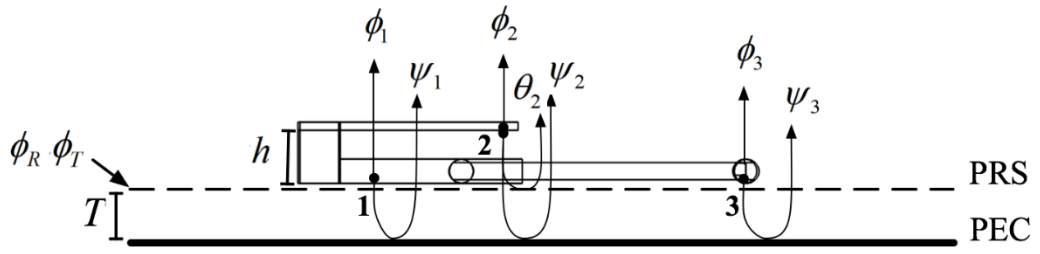

Figure 6-2：Cavity model with ray analysis for the EBG ground plane and the belt antenna (PRS: partial reflective surface. PEC: perfect electric conductor).

For sub-elements located at a distance h from the PRS (example point 2 in Figure 6-2), the phase difference between the radiating wavefront (ϕ_i) and the reflected wave through the EBG cavity (ψ_i) is:

$$\phi_i - \psi_i = 2\phi_T - \frac{4\pi(h+T)}{\lambda} - \pi \qquad (6\text{-}1)$$

The term T here denotes the height of the cavity, which is the thickness of the textile material in this case. Once the type of textile material is determined, this value is fixed for the design.

For a micro radiating element placed very close to the EBG ground plane (example points 1 and 3), the previous formula can be simplified to,

$$\phi_i - \psi_i = 2\phi_T - \frac{4\pi T}{\lambda} - \pi \tag{6-2}$$

When the radiating element is located a distance above the EBG plane, an additional wave reflected from the PRS needs to be considered. The phase difference between these two waves can be calculated using (6-3)

$$\phi_i - \theta_i = \phi_R - \frac{4\pi h}{\lambda} \tag{6-3}$$

The structural design of this antenna and the EBG structure should be optimised with respect to the following boundary conditions to avoid cancelation between the original outgoing wave and the reflected wave by consideration of:

$$-\frac{\pi}{2} \leq \phi_i - \psi_i \leq \frac{\pi}{2} \tag{6-4}$$

$$-\frac{\pi}{2} \leq \phi_i - \theta_i \leq \frac{\pi}{2} \tag{6-5}$$

The wavefront created by the i^{th} subvolume element can then be denoted by,

$$E_i = a_{i,1} e^{j(2\pi f_0 t_i + \phi_i)} + a_{i,2} e^{j(2\pi f_0 t_i + \theta_i)} + a_{i,3} e^{j(2\pi f_0 t_i + \psi_i)} \tag{6-6}$$

where a_i is the attenuation factor for a certain reflected wave from the i^{th} subvolume and f_0 is the resonant frequency. The term ϕ_i denotes the directly radiated wave. The terms θ_i and ψ_i are the reflected wave from the PRS and the PEC respectively. A graphical representation of these terms can be found in Figure 6-2.

The total wavefront can be expressed as a superposition of all the subvolume element waves by

$$E = g_k(E_1, E_2, E_3 \ldots, E_k) \tag{6-7}$$

where g_k represents the superposition.

This theoretical analysis provides a guideline for the optimisation of the EBG design parameters. The phase of the reflected waves at each plane, one closely attached to the PRS and one elevated by a distance *h*, should be considered in the simulation. The reflected phase can be obtained in CST by adding a thin layer of air between the PRS and a floquet port located in the unit cell simulation. The ideal reflected phase is 0 degrees from both planes. However, for a certain EBG design with fixed parameters, the reflected phase would change with the distance between the floquet port, the PEC and the PRS. Thus, a middle ground where the reflected phase at the two planes were both very close to zero was selected. Detailed dimensions of the concentric square EBG unit cell are listed in Table 6-1. For the square patches with vias, the optimised dimension for the edge is 50 mm long and the gap between patches is 6 mm.

Comparing the two types of EBG design, the square patches with vias design is almost 4 times larger in size than the concentric square design. Moreover, the via structure used to suppress the surface wave is much more difficult to fabricate with textile materials.

Table 6-1: The EBG geometry parameters

Symbol	Quantity	Value (mm)
W_1	outer width of the square	50
W_2	outer width of the square	26
W_3	inner width of the square	8
G_1	gap between two unit cells	6
G_2	gap between two unit cells	4
S_1	width of the inner square track	2

6.4 Suspended Transmission Line Method and Bending

EM wave suppression is a characteristic for EBG structures. As discussed in section 2.4, the EBG structure can stop EM wave transmission in its band gap frequency. This property can be used together with a transmission line to evaluate the band gap of the EBG structure.

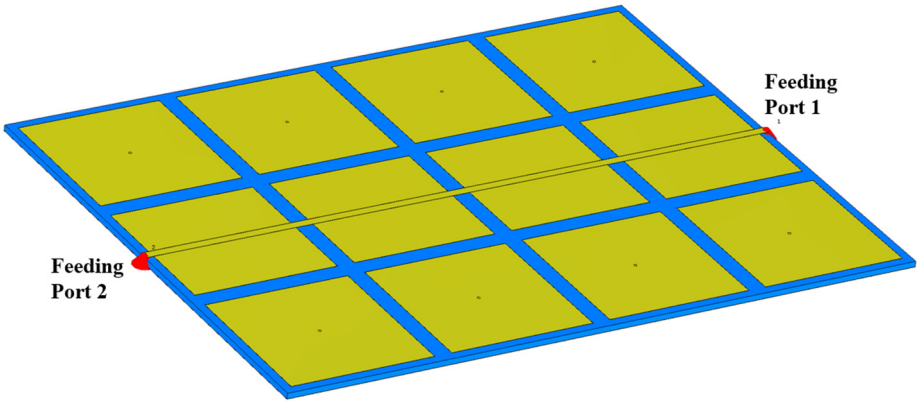

Figure 6-3：An illustration of the suspended transmission line method.

The method places a suspended strip line across the EBG surface and evaluates the transmission coefficient (S_{21}) of the line. The S_{21} value can be measured directly by placing two feeding points at the two terminals of the transmission line; the simulation setup is illustrated in Figure 6-3. This method has been used in previous studies to determine the resonating frequency for EBG/AMC structures [7].

Figure 6-1 shows that the capacitance formed by the gap between unit cells or within each unit cell is crucial in determining the resonant frequency of the EBG structure. When the textile EBG is applied on the human body, the bending of the material may cause changes especially in this capacitance and influence the resonant frequency, therefore this influence must be evaluated. The reflected phase can be obtained through simulation using the CST unit cell boundary condition; however, it is difficult to either perform the reflection phase simulation over the entire textile ground or perform actual measurements of the reflected phase, especially under bending conditions. Therefore, the suspended transmission line method has been used to evaluate the performance of the entire EBG structure under bending conditions. To the best knowledge of the author, this is the first time that such a method has been applied in the evaluation of bending effects for textile EBG material. In the experimental condition, the S_{21} value can be directly obtained using a calibrated network analyser. The actual experimental setup is shown in Figure 6-10 (c).

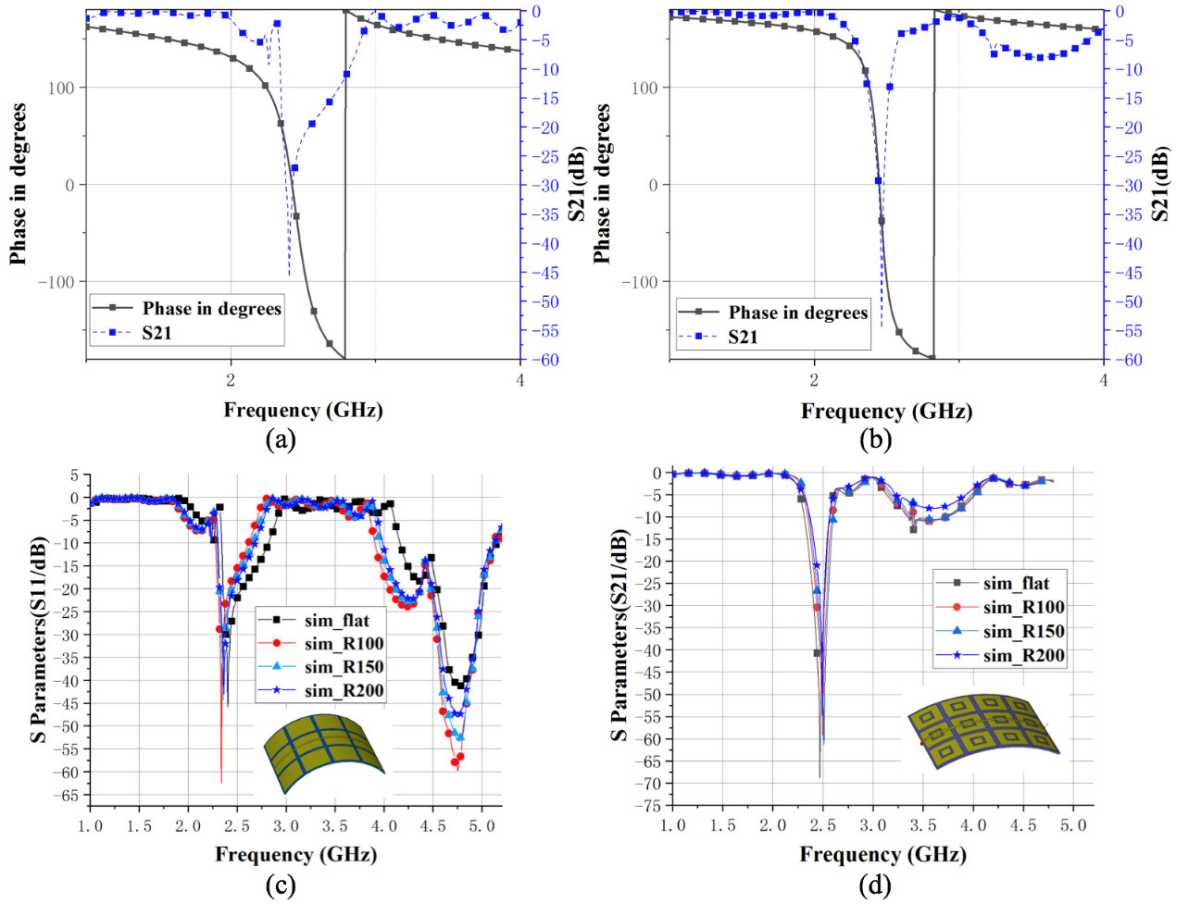

Figure 6-4：Comparison between the reflected phase of the EBG structure and the S_{21} of the corresponding suspended transmission line. (a) The reflected phase and band gap for square patches with vias EBG structure. (b) The reflected phase and band gap for concentric squares EBG structure. (c) The band gap of the square patches with vias EBG structure when bent. (d) The band gap of the concentric squares EBG structure when bent.

Figure 6-4 (a) and (b) show the simulation results characterising the relationship between the reflected phase and EBG band gap for each EBG type, square and concentric square respectively. The band gap of each design was determined from the S_{21} of the suspended transmission line experiment. The ideal reflected phase of 0 degrees was located approximately at the centre of the band gap. From both the reflected phase and the band gap, it can be seen that the square patches with vias structure would provide a wider bandwidth compared to the concentric squares structure. This is the main benefit of the square patches structure.

Figure 6-4 (c) and (d) show the effects of bending on the band gap of the two EBG structures evaluated using suspended transmission line simulation. The structures were

bent towards a cylinder with radii of 100 mm, 150 mm and 200 mm.

From the figures, it can be seen that for both structures the bending leads to a slight reduction in bandwidth. The square patches structure has a larger bandwidth, however, for the targeted BLE application, the concentric squares structure provides sufficient bandwidth and is preferable due to its smaller size and fabrication simplicity.

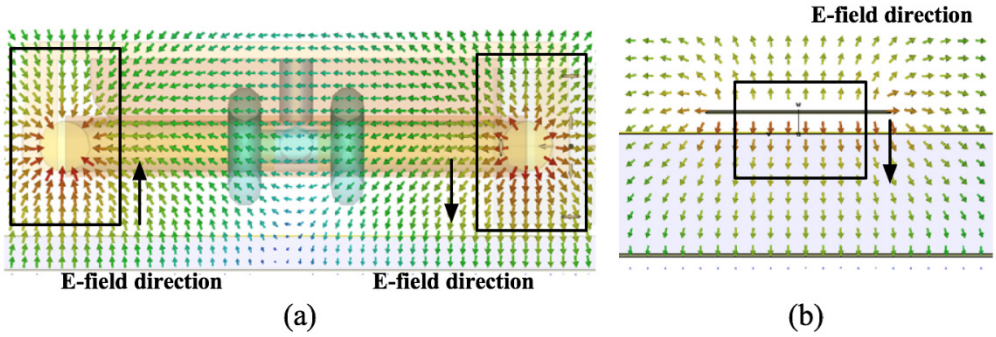

Figure 6-5：Comparison between fields. (a) The E field of the belt antenna over the EBG plane. (b) The E field of the suspended transmission line.

Figure 6-5 supports the use of the suspended transmission line method in determining the properties of the EBG ground plane. The E-field cross-section plots show that the main radiating fields towards the EBG in the case of both the belt antenna and the suspended transmission line are perpendicular to the EBG. Thus, the band gaps seen by the radiated field in these two cases are similar.

6.5 Antenna Performance Analysis

6.5.1 The radiation pattern, efficiency and SAR value

The belt antenna with textile concentric square EBG ground plane has been simulated using the voxel model Gustav in CST with two different postures. The 3D far-field results are shown in Figure 6-6. The radiation pattern is very similar to that observed without the textile EBG. However, the maximum realised gain significantly increases from 4.37 dBi to 7.70 dBi with the help of the textile EBG.

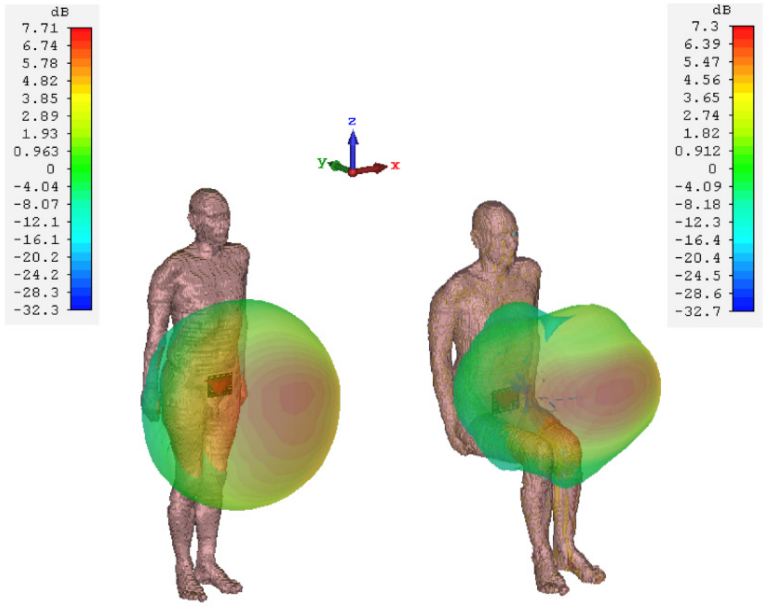

Figure 6-6：The simulated radiation pattern and realised gain of the belt antenna with EBG ground plane.

One-dimensional polar radiation patterns are shown in Figure 6-7. In the E plane, antenna boresights in both the standing and sitting case are almost aligned. The effect of the upper thighs can be clearly seen in the H plane with the sitting model.

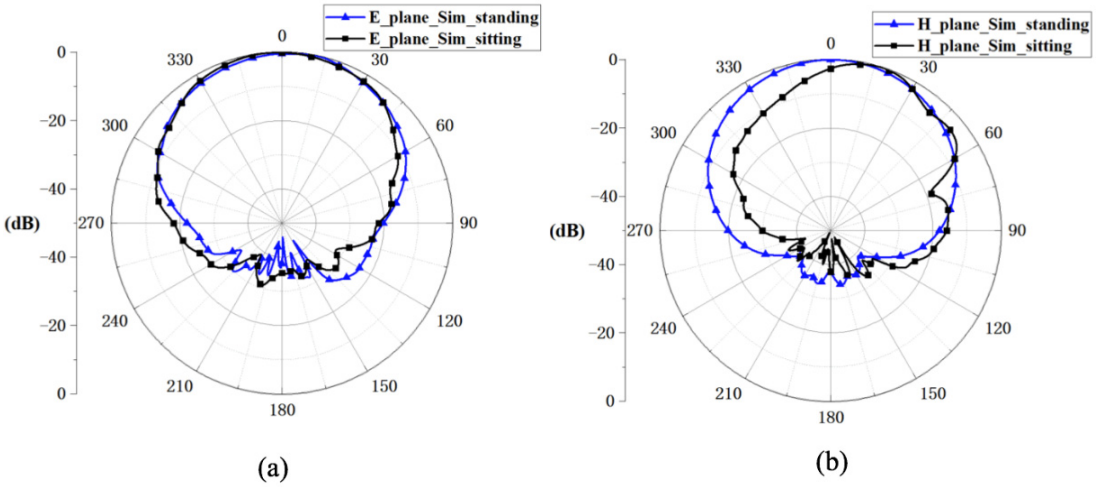

Figure 6-7：The simulated radiation pattern of the belt antenna with textile EBG ground plane. (a) E plane. (b) H plane.

Aside from the radiation pattern, the radiation efficiency and SAR values are two very important figures for wearable antenna applications. The application of the textile EBG plane has improved the belt antenna performance in these two aspects, as shown

by Table 6-3. An increase in radiation efficiency and a reduction in SAR value can be achieved due to the isolation and reflection of the textile EBG ground plane. The SAR value distribution is shown in Figure 6-8. It should be noted that, due to the isolation of the textile EBG, the maximal SAR in the sitting condition was located at the right thigh close to the belt metal cap. The SAR values in both cases are below the ICNIRP (2W/kg) and FCC (1.6W/kg) requirement used in this study.

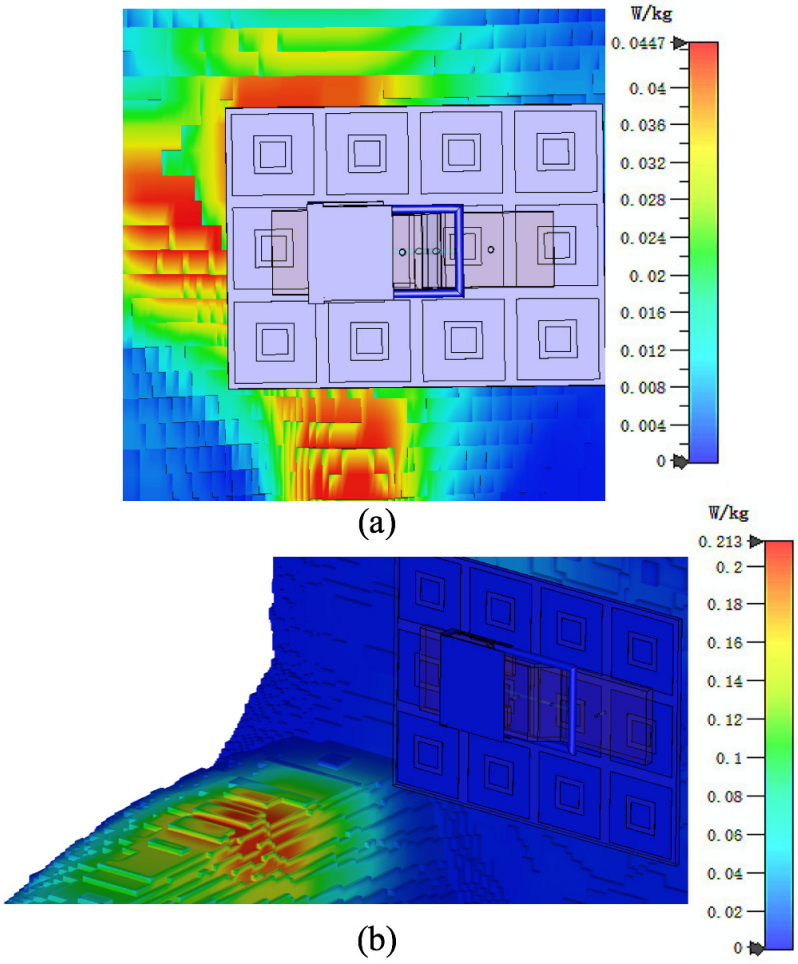

Figure 6-8：The SAR distribution of the belt antenna with the EBG. (a) The distribution with the standing model averaged over 10g tissue. (b) The distribution with the sitting model averaged over 10g tissue.

6.5.2 The effect of different human body

The simulation process in the previous sections used only the Gustav model in the CST voxel family, which is a model of a 38-year-old male (176 cm, 69 kg). With different body shapes, the tissue composition would vary and thus result in different electrical properties. To evaluate the effect of different body shapes on antenna performance, two other body models from the CST voxel family, Donna (40-year-old female, 176 cm, 79 kg) and Child (7-year-old female, 115 cm, 21.7 kg), were also used in the simulation. The reflection coefficients for different body models are shown in Figure 6-9 and the radiation parameters are summarised in Table 6-2. Without the textile EBG, frequency shifts and changes in radiation efficiency and gain can be observed with different human body models. When the textile EBG is used, the effect of the human body was significantly reduced. The belt antenna backed with the textile EBG offers stable performance when applied to people with different body compositions and shapes.

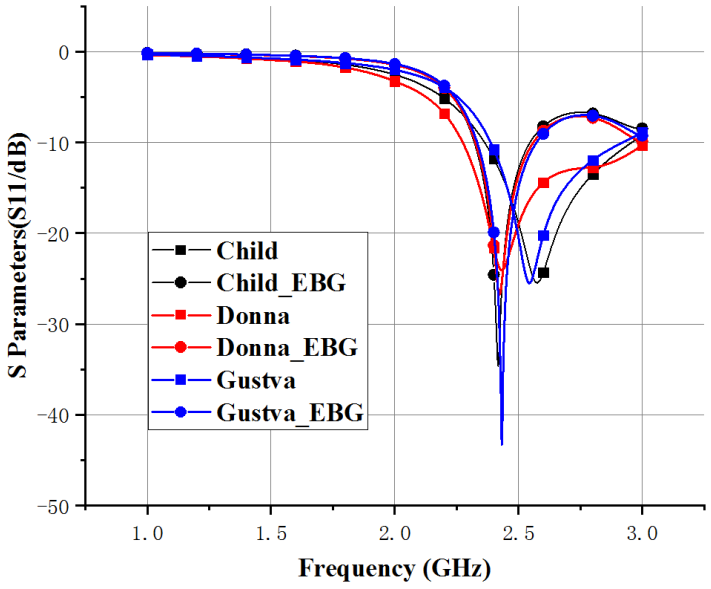

Figure 6-9：*S* parameters of the antenna with/without textile EBG on different voxel human models.

Table 6-2: Comparison of the antenna performance with different human body model

Model	Radiation Efficiency (%)	Realised Gain (dBi)
Gustav	54.36	4.37
Gustav_EBG	84.11	7.70
Donna	49.56	1.87
Donna_EBG	83.96	7.57
Child	47.78	2.06
Child_EBG	84.24	7.59

6.5.3 The fabricated antenna and performance comparison

The metal part of the belt antenna was fabricated by 3D printing brass while the belt pin was 3D printed from high-intensity ABS material. Three part-cylinders were also made by 3D printing from ABS to provide mounting structures to allow the band gap of the textile EBG to be measured under bending conditions. The fabricated antenna and EBG, along with the testing conditions, are shown in Figure 6-10. Before being applied to the belt buckle antenna, the textile EBG was firstly evaluated with a suspended transmission line and the results are shown in Figure 6-11.

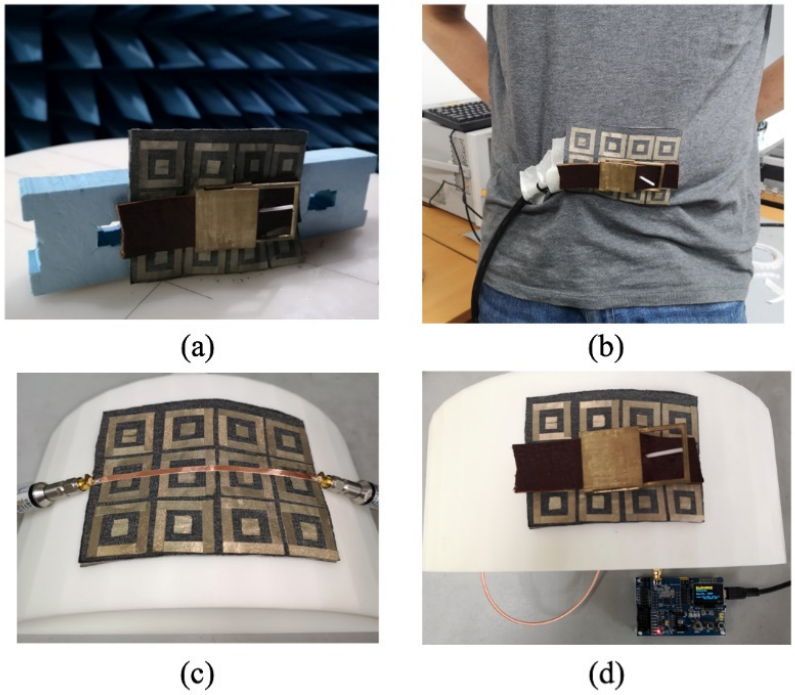

Figure 6-10：The fabricated prototype and measurement setup. (a) The radiation pattern measurement in the anechoic chamber. (b) The testing on the real human body. (c) The suspended transmission line test for textile EBG. (d) The prototype integrated with the BLE module.

In all cases, the measured results indicate a slight frequency shift (shift down by 0.15-0.21 GHz) and a larger bandwidth in comparison to the simulation result. This is mainly due to the inability to accurately model the electrical properties of the conducting fibre, especially under the effects of bending and stretching. Also, the measured results show that the band gap of the fabricated EBG covers the desired band and can be applied with the belt buckle antenna.

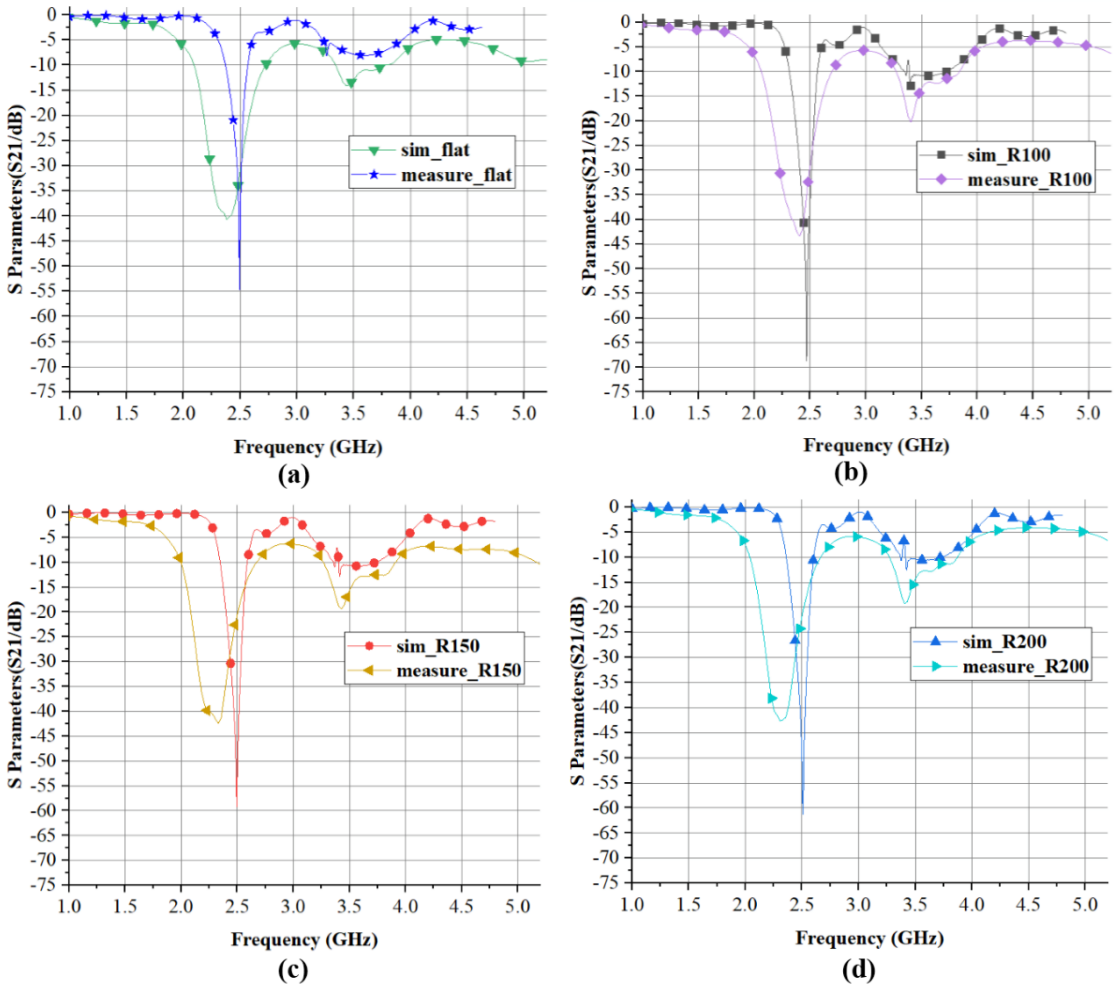

Figure 6-11：The simulated and measured band gap for the suspended transmission line over concentric square textile EBG ground plane: (a) Flat. (b) Bent towards cylinder with a radius of 100 mm. (c) Bent towards cylinder with a radius of 150 mm. (d) Bent towards cylinder with a radius of 200 mm.

The measured S_{11} and radiation patterns are shown in Figure 6-12(a), Figure 6-13 (a) and Figure 6-13 (b) respectively. The measured maximal realised gain versus frequency is shown in Figure 6-12 (b). The measurements were performed in our in-house anechoic chamber. A low permittivity foam was used as the support structure on the rotary table. Generally, the measured results match the simulations well. Some discrepancies occurred in the radiation pattern measurement at 90° and 270° in both the E- and H-planes. This was due to the slight curvature of the lossy belt leather and the textile EBG when they are closely attached. The measured radiation pattern matches the simulated radiation pattern with the sitting/standing voxel human model well in the direction of the main lobe. However, a larger back lobe can be observed due to the lack

of body tissue absorption.

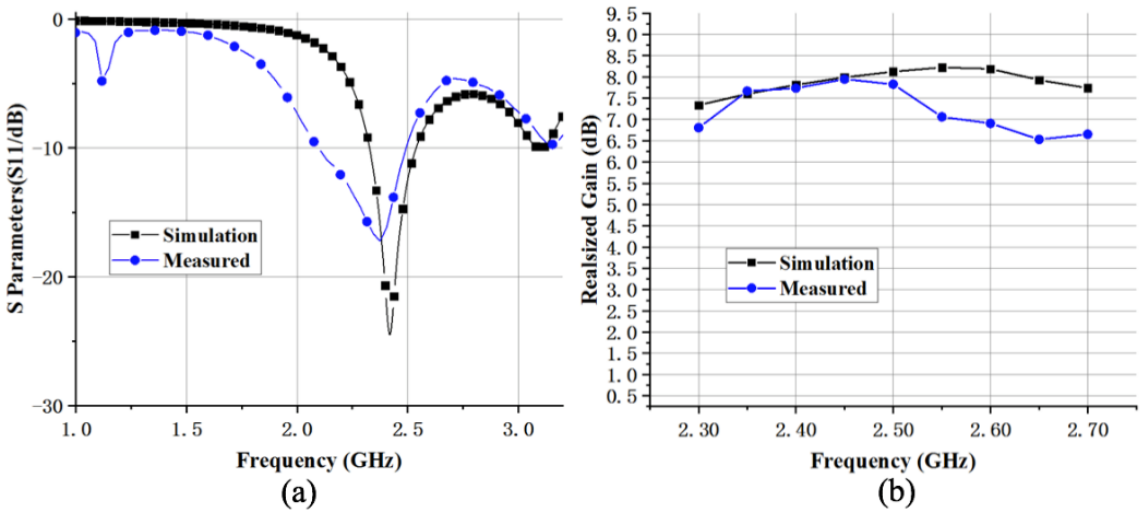

Figure 6-12：The simulated and measured results. (a) S11 for the belt antenna with the textile EBG ground plane. (b) Realised gain over frequency.

Both free space and on-body realised gains were measured. The antenna was attached to the waist of a human subject (188 cm, 81 kg) in the chamber to measure the on-body realised gain. The measured maximal realised gain of the belt antenna with textile EBG at 2.45 GHz was 7.94 dBi without human presence and 7.15 dBi when the antenna was attached to the human waist.

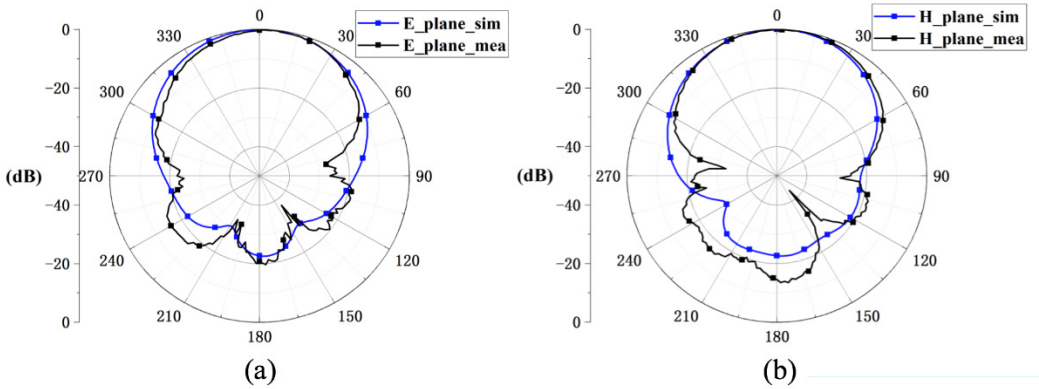

Figure 6-13：The simulated and measured radiation pattern for the belt antenna with textile EBG ground plane (a) E plane (b) H plane.

Table 6-3: Comparison of Antenna Performance with/without EBG and with Other Systems

Ref.	Antenna Type	Radiation Efficiency (%)	Realised Gain (dBi) (sim/mea)	SAR (10g, with 0.5 W input) (W/kg)
This Work	Standing with EBG	84.11	7.70/7.15	0.04
	Standing without EBG	54.36	4.37/4.01	2.71
	Sitting with EBG	67.77	7.30/-	0.21
	Sitting without EBG	46.78	3.98/-	1.67
	Free space with EBG	86.25	7.98/7.94*	N/A
[8]	Replicated belt antenna design	19.01	-1.33/-	N/A
[4]	Textile antenna with EBG structure	61.30	5.20/-	0.37
[9]	Button with textile ground	72.10	5.16/1.1*	0.176 (32 mW input)
[10]	Smart watch frame antenna	26.00	-0.89/3.8*	N/A
[11]	Loop over high impedance surface	40.00	4.20/3.00	0.55 (100 mW input)

* The gain measured is free space gain, without actual human or phantom presence,

A comparison between the proposed belt antenna and some related state-of-the-art wearable antenna solutions is included in Table 6-3. The results with/without the textile EBG on different voxel model structures (standing model and sitting model) are all included. It should be noted that in this study, CST voxel models were used to evaluate the human body effect on the antenna performance and the value of SAR was calculated according to IEEE/IEC 62704-1 with a 0.5 W input power [12]. The simulation condition for [8] and [4] in Table 6-3 was identical to the condition used in this study.

In [9], a partial uniform human body model was employed whilst the SAR was evaluated with the same standard but with an input power of 32 mW. In [10], a one-layer wrist model was used for evaluation. In [11], a four-layer human tissue model was used. The SAR was evaluated with the same standard whilst the input power was set to be 100 mW. Moreover, a noticeable difference in the simulated and measured realised gain values can be seen for [9] and [10] in Table 6-3. This is because the provided simulated value was with the human body model whilst the measurements were

performed in a free space scenario. For the design in [9], the human body would have a significant reflecting effect and hence the on-body gain would be higher. Meanwhile in [10], the effect of body tissue absorption was more significant than the reflection. Therefore, the on-body realised gain was lower. For the proposed belt buckle antenna with EBG, the measured free space and on-body realised gain is consistent due to the textile EBG structure.

Measurements were performed in the XJTLU in-house anechoic chamber (length: 6 m, width: 4 m, height: 3 m) and the antenna was attached to a human subject (188 cm, 81 kg) for on-body measurements. Generally, all evaluations of the results in Table 6-3 and this work were performed under similar experimental conditions and therefore the results are comparable and promising. Overall, the proposed belt buckle antenna achieves a higher realised gain and a lower SAR value due to the structural design and the isolation/reflection provided by the textile EBG.

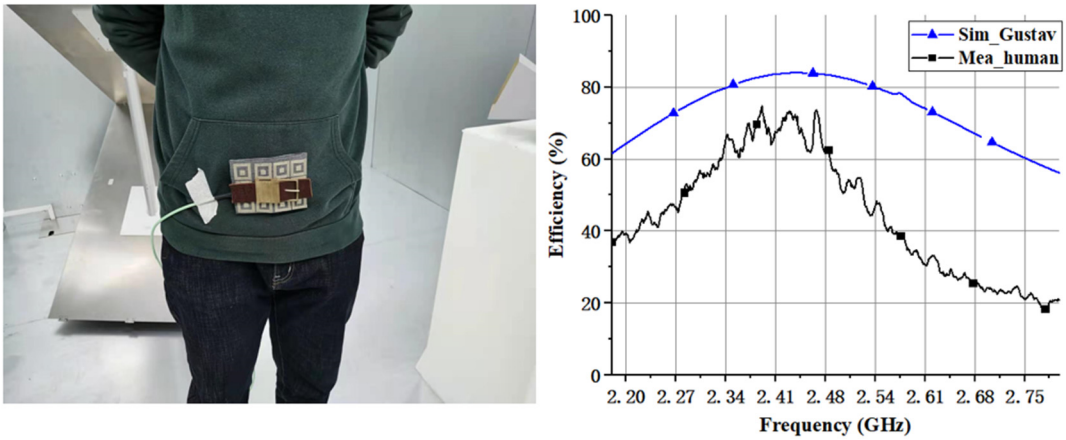

Figure 6-14：The measurement of the on-body antenna radiation efficiency. (a) The measurement setup. (b) The measured result compared with simulation with voxel model Gustav.

The on-body efficiency was studied with the same human subject using the same in-house reverberation chamber (length: 5.4 m, width: 3.0 m, height: 2.8 m) as discussed in Chapter 3. Figure 6-14 (a) shows the experimental setup. The belt antenna, along with the textile EBG ground plane, was fixed at the waist of the test subject. The measurement of the on-body efficiency follows the method presented in section 3.3.

The calibration with the human subject in the chamber is performed prior to measurement. During each measurement, the dressing of the test subject was kept constant, including the contents in the subject's pockets. The stirring sequence in this experiment included mechanical stirring (2 degrees, 180 measurements), polarisation stirring (two orthogonal linear polarisations) and position stirring (4 receiver positions). A total of 1440 measured sample points were taken for each frequency point. A large number of samples were required to keep the uncertainty of the measurement to an acceptable level. Meanwhile, the number of mechanical stirs in each run was limited so that the test subject did not have to stay in the chamber for a prolonged period of time. The position of the receiving antenna in the chamber was spaced by a half wavelength for each run to create independent samples. The resulting radiation efficiency is shown in Figure 6-14 (b). An approximately 70 % radiation efficiency is achieved in the measurement.

6.5.4 Smart Belt System Prototype

A smart belt prototype system was developed using a Texas Instrument CC2401 BLE chip and a developer board obtained from AMO MCU as shown in Figure 6-10 (d), as proof of concept. A link between the smart belt and an Android cellphone was set up and the output power for the chip was set to be -10 dBm. The relationship between the received signal strength indicator (RSSI) and line-of-sight distance in the lab is shown in Figure 6-15 (a). The raw data was not enough to provide accurate distance measurement and was largely influenced by the surrounding multipath environment. The data can still be used to make sure the cell phone stays in Bluetooth range of the belt and the range can be changed by setting the input power.

An onboard gyroscope was integrated into the smart belt prototype. In Figure 6-15 (b), data from 40 seconds of walking and a simulated falling over was recorded. The simulated falling over happened at the 26^{th} second on the timeline and a sharp increase in the acceleration in the *z*-direction can be observed at that moment. The smart belt

system could provide a fall alarm for the elderly.

The belt antenna with the textile EBG ground plane has a high efficiency when placed in close proximity with the human body and a low SAR value towards the body. When applied in the smart belt system, it can reduce requirements on system power use and hence prolong battery life.

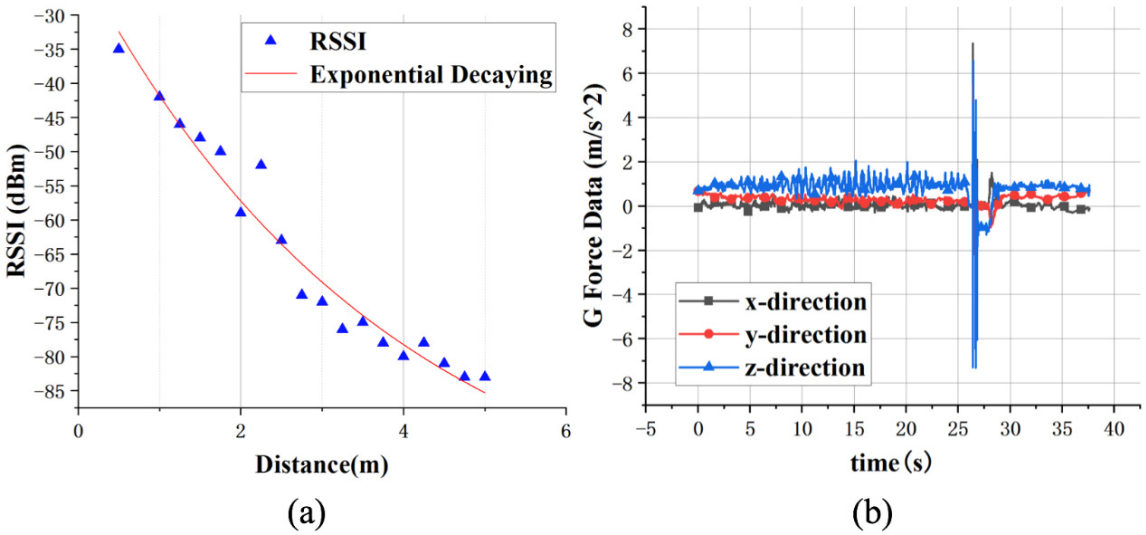

Figure 6-15：The smart belt prototype. (a) The BLE received signal strength index (RSSI) on the cellphone at different distances. (b) The data from the gyroscope onboard the smart belt system.

6.6 Summary

The belt antenna proposed in Chapter 5 can satisfy the BLE transmission requirement on its own. However, considering that the belt antenna could be operating for long periods of time and that the available battery size for typical wearable systems is limited, further improvements should be made regarding SAR and radiation efficiency.

In this chapter, a textile EBG ground plane is designed to work together with the belt buckle antenna proposed in the previous section. The effect of the human body with/without the EBG ground plane was closely evaluated. The separate textile EBG ground plane can be integrated into the trousers behind the belt antenna. A set of wave

propagation equations for designing the EBG with non-planar wearable antennas were proposed. Also, for the first time, the suspended transmission line method was proposed in this case to accurately determine the band gap of the textile EBG under bending conditions. The belt antenna together with the textile EBG forms a highly efficient and safe transmission mechanism for a smart belt system.

6.7 Reference

[1] M. Collotta, G. Pau, T. Talty, and O. K. Tonguz, "Bluetooth 5: A Concrete Step Forward toward the IoT," *IEEE Commun. Mag.,* vol. 56, no. 7, pp. 125-131, Jul. 2018.

[2] S. Yan, P. J. Soh, and G. A. E. Vandenbosch, "Low-Profile Dual-Band Textile Antenna With Artificial Magnetic Conductor Plane," *IEEE Trans. Antennas Propag.,* vol. 62, no. 12, pp. 6487-6490, Dec. 2014.

[3] S. Zhu and R. Langley, "Dual-Band Wearable Textile Antenna on an EBG Substrate," *IEEE Trans. Antennas Propag.,* vol. 57, no. 4, pp. 926-935, Apr. 2009.

[4] M. Wang, Z. Yang, J. Wu, J. Bao, J. Liu, L. Cai*, et al.*, "Investigation of SAR Reduction Using Flexible Antenna With Metamaterial Structure in Wireless Body Area Network," *IEEE Trans. Antennas Propag.,* vol. 66, no. 6, pp. 3076-3086, Jun. 2018.

[5] A. Alemaryeen and S. Noghanian, "On-Body Low-Profile Textile Antenna with Artificial Magnetic Conductor," IEEE Trans. Antennas Propag., vol. 67, no.6, pp. 3649-3656, Jun 2019.

[6] A. P. Feresidis, G. Goussetis, W. Shenhong, and J. C. Vardaxoglou, "Artificial magnetic conductor surfaces and their application to low-profile high-gain planar antennas," *IEEE Trans. Antennas Propag.,* vol. 53, no. 1, pp. 209-215, Jan. 2005.

[7] S. Zhu and R. Langley, "Dual-Band Wearable Textile Antenna on an EBG Substrate," *IEEE Trans. Antennas Propag.,* vol. 57, no. 4, pp. 926-935, Apr. 2009.

[8] D. Gaspar and A. A. Moreira, "Belt antenna for wearable applications," in *2009 IEEE Antennas and Propagation Society International Symposium*, Charleston, SC, 2009, pp. 1-4.

[9] S. Yan and G. A. E. Vandenbosch, "Design of Wideband Button Antenna Based on Characteristic Mode Theory," *IEEE Trans. on Biomed. Circuits Sys.,* vol. 12, no, 6, pp. 1383-1391, Dec. 2018.

[10] S. Su and Y. Hsieh, "Integrated Metal-Frame Antenna for Smartwatch Wearable Device," *IEEE Trans. Antennas Propag.*, vol. 63, no. 7, pp. 3301-3305, Jul. 2015.

[11] D. Wen, Y. Hao, M. O. Munoz, H. Wang, and H. Zhou, "A Compact and Low-Profile MIMO Antenna Using a Miniature Circular High-Impedance Surface for Wearable Applications," *IEEE Trans. Antennas Propag.*, vol. 66, no.1, pp. 96-104, Jan. 2018.

[12] K. Chan, R. F. Cleveland, D. L. Means, "Evaluating compliance with FCC guidelines for human exposure to radiofrequency electromagnetic fields," *OET bulletin,* vol. 65, Dec. 1997.

[13] S. J. Boyes, P. J. Soh, Y. Huang, G. A. E. Vandenbosch, and N. Khiabani, "Measurement and Performance of Textile Antenna Efficiency on a Human Body in a Reverberation Chamber," *IEEE Trans. Antennas Propag.*, vol. 61, pp. 871-881, 2013.

Chapter 7 Conclusion and Future Work

7.1 Conclusions

Motivated by the burst in the development of wearable electronic products and their high level of adoption by consumers, the need for ergonomic, high efficiency, low SAR value antennas has been increasing. The main constraints on wearable antenna design include the usage of non-standard RF materials that are lossy, the shape and size limit to ergonomically fit within the wearable device or on a daily item of clothing or common accessory and the effect of the lossy human body on antenna performance.

This thesis focused on the development of high efficiency wearable belt buckle antennas, with the goal of addressing the aforementioned research constraints. Two novel antennas have been proposed. A reverberation chamber was constructed at Xian Jiaotong-Liverpool University to allow antenna efficiency to be practically evaluated. A textile EBG ground plane was proposed to provide necessary isolation to the human body for one of the belt buckle antennas, which loosely based on a loop structure had significant radiation directed towards the body. The EBG provided an to improved realised gain and efficiency for the antenna.

A brief history and basic information on wireless communications and antennas was provided in Chapter 1, along with the motivation and aims of this study.

In chapter 2, a review on wearable antennas was provided. Planar wearable antennas using soft substrates and accessory-like antennas were discussed in detail with state of the art designs presented. The challenges to be addressed in designing wearable antenna were then summarised.

In chapter 3, some basic information on the use of electromagnetic reverberation chambers was provided. The specifications and performance analysis of the chamber

built during this project were detailed for future reference and a test procedure was set out for efficiency testing of a wearable device.

In Chapter 4, the first belt antenna based on a pin buckle belt was presented. The proposed belt antenna utilised a TM_{10} mode and a quasi-TM_{30} mode to achieve dual operational bands. The proposed antenna was able to achieve an on-body realised gain of 5.10 dBi and radiation efficiency of approximately 40 % at 2.45 GHz without using any materials dedicated for RF applications and a separated large ground plane.

Another belt antenna designed with the aid of characteristic mode analysis was presented in Chapter 5. It was found during the design process that CMA was of great significance to determining the design parameters and placing the feed. This belt antenna design was able to direct more radiated energy towards the outside of the human body through the use of a cap in comparison to a simple loop type belt buckle antenna. Thus, the radiation efficiency is increased whilst the SAR value is reduced.

A textile EBG ground plane design was presented in Chapter 6. This separate textile EBG ground plane is designed to be integrated into the garment worn behind the belt antenna. A set of wave propagation equations for designing the EBG with non-planar wearable antennas was proposed. The suspended transmission line method was proposed in this case to accurately determine the band gap of the textile EBG especially in bending conditions. The loop type belt buckle antenna together with the textile EBG forms a highly efficient and safe transmission mechanism for a smart belt system.

7.2 Key Contributions

This work provided a study of wearable antennas. With the help of techniques including CMA and the suspended transmission line method, two high efficiency belt antennas were proposed. The main outcomes of the research are summarised in two published journal papers and one published conference paper, as listed in the preface of this thesis on page V.

There are three key contributions in this project,

1. Two novel belt antenna structures were presented; both can achieve high on-body radiation efficiency.

2. An in-house reverberation chamber was constructed and commissioned during this project. Test procedures were developed allowing wearable antenna efficiency measurements to be made. On body radiation efficiency measurement can now be performed on campus.

3. A textile EBG ground plane working together with a loop type belt antenna was proposed. Analysis of textile EBG material with circuit model and elevated transmission line method were performed. A smart belt prototype with demonstrative functionality was developed and connectivity via BLE link was established to a smartphone.

7.3 Future work

In this project, the effect of the textile properties on the antenna has not been investigated in detail. In 2020, state-of-the-art works have shown that antennas using conductive textile threads fabricated with computer-aided embroidery techniques can achieve similar radiation efficiencies as similar PCB solutions. With this achievement, wearable energy harvesting antenna arrays with conductive fibres have been proposed. There are two possible future research directions:

1. To explore the effect of textile EBG ground planes fabricated with embroidery techniques. The embroidery techniques would increase the conductivity of the conductive squares in each unit cell. It is unclear how this would increase the overall performance of the belt buckle antenna.

2. To explore the possibility of high radiation efficiency for an all textile antenna. In this study, the idea of the belt buckle antenna was initially chosen for its high-

conductivity metallic nature. The limitation in shape, size and the necessity for a lossy substrate (leather) limit the performance of belt buckle antennas. With embroidered conductive threads reaching similar conductivity, it is possible that an all textile high-efficiency wearable antenna can do the job better. To come to this conclusion, more detailed work needs to be done.